

# Analysis of Whitianga, Tararu, Kawhia and Manu Bay sea-level records to July 2024.

ISSN 2230-4363 (Online)  
[waikatoregion.govt.nz](http://waikatoregion.govt.nz)



Prepared by	Glen Reeve
For	Waikato Regional Council Private Bag 3038 Waikato Mail Centre HAMILTON 3240
Publication date	February 2024
Document ID	32499163

	Name	Date
Peer Reviewer	Stephen Hunt & Celeste Davie-Calway	August 2025
Approving Manager	Mike Scarsbrook	November 2025

### **Disclaimer**

This technical report has been prepared for the use of Waikato Regional Council as a reference document and as such does not constitute Council's policy.

Council requests that if excerpts or inferences are drawn from this document for further use by individuals or organisations, due care should be taken to ensure that the appropriate context has been preserved, and is accurately reflected and referenced in any subsequent spoken or written communication.

While Waikato Regional Council has exercised all reasonable skill and care in controlling the contents of this report, Council accepts no liability in contract, tort or otherwise, for any loss, damage, injury or expense (whether direct, indirect or consequential) arising out of the provision of this information or its use by you or any other party.

# Analysis of Whitianga, Tararu, Kawhia, Raglan and Manu Bay sea- level records to July 2024

*Prepared for Waikato Regional Council*

*February 2024*



Prepared by:  
Glen Reeve

For any information regarding this report please contact:


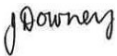

Glen Reeve  
Principal Technician  
Coastal and Estuarine Processes Group  
+64 7 856 1782  
glen.reeve@niwa.co.nz

National Institute of Water & Atmospheric Research Ltd  
PO Box 11115  
Hamilton 3251

Phone +64 7 856 7026

NIWA CLIENT REPORT No: 2024304HN  
Report date: February 2024  
NIWA Project: EVW25201

Revision	Description	Date
Version 1.0	Draft in preparation/in review	October 2024
Version 1.1	Final	February 2025
Version 1.2	Final	March 2025

Quality Assurance Statement		
	Reviewed by:	Scott Stephens
	Formatting checked by:	Jo Downey
	Approved for release by:	Michael Bruce



## Contents

<b>Executive summary .....</b>	<b>9</b>
<b>1 Introduction .....</b>	<b>11</b>
1.1 Background .....	12
1.2 Scope of the project.....	14
<b>2 Components and definitions of sea level .....</b>	<b>16</b>
2.1 Tides.....	18
2.2 Quality assurance.....	19
2.3 Sea level analysis methods .....	20
<b>3 Data .....</b>	<b>22</b>
3.1 Drift and offset in the Kawhia Gauge.....	25
3.2 Drift and offset in the Manu Bay Gauge .....	27
3.3 Meteorological data.....	27
<b>4 Mean sea level and local vertical datum .....</b>	<b>29</b>
4.1 Sea-level rise detrending .....	32
4.2 Annual mean sea-level trends .....	33
<b>5 MHWS and tide exceedance curves .....</b>	<b>38</b>
5.1 Mean high-water springs in the Waikato region .....	42
<b>6 Skew Surge .....</b>	<b>44</b>
6.1 Descriptive analysis of the largest skew surge events.....	48
<b>7 Storm tide extreme-value analysis.....</b>	<b>86</b>
7.1 Skew-surge joint-probability analysis .....	86
7.2 Breakdown of the largest storm-tide events.....	91
7.3 Seasonality of storm tides .....	94
<b>8 Sea level anomaly .....</b>	<b>99</b>
<b>9 Whitianga and Tararu Tsunami.....</b>	<b>104</b>
<b>10 Review of sea-level gauge network .....</b>	<b>105</b>
<b>11 Conclusions .....</b>	<b>107</b>
<b>12 Glossary of abbreviations and terms .....</b>	<b>109</b>

<b>13</b>	<b>References.....</b>	<b>112</b>
<b>Appendix A</b>	<b>MHWS elevations from tide model .....</b>	<b>115</b>
<b>Appendix B</b>	<b>Vertical Datums .....</b>	<b>118</b>
<b>Appendix C</b>	<b>Tide, storm tide and projected sea-level rise tables.....</b>	<b>120</b>
<b>Appendix D</b>	<b>Data Processing and Quality Assurance.....</b>	<b>123</b>

## Tables

Table 2-1:	The main components and causes of sea-level variability at various timescales longer than 2 minutes, some of which overlap. FIG=far infragravity waves; ENSO=El Niño–Southern Oscillation; IPO= Inter-decadal Pacific Oscillation.	18
Table 3-1:	Listing of the data available for the Waikato Regional Council sea-level.	22
Table 3-2:	Listing of the vertical offsets applied during the QA process to correct Waikato Regional Council sea-level records.	22
Table 3-3:	Source of meteorological data used for storm surge descriptive analysis.	28
Table 4-1:	Sea-level gauge-zero offsets to local vertical datum.	30
Table 4-2:	MSL offsets to MVD-53 datum at Auckland, Moturiki, Whitianga, Tararu, Kawhia and Raglan.	31
Table 4-3:	Linear fits for sea level detrend.	33
Table 4-4:	Estimated years when absolute sea-level rise (SLR) thresholds may be reached based on recommended projections for a central location in Aotearoa New.	33
Table 5-1:	Analysis of high waters at Whitianga, Kawhia and Tararu relative to MSL = 0.	42
Table 6-1:	Frequency–magnitude distribution of extreme skew-surges.	48
Table 6-2:	The top five skew surges on record at Tararu.	50
Table 6-3:	The top five skew surges on record at Whitianga. Measurements denoted by an asterisk (*) signify that these values are deduced from meteorological weather maps.	59
Table 6-4:	The top five skew surges on record at Kawhia.	68
Table 6-5:	The top three skew surges on record at Raglan.	77
Table 6-6:	The top three skew surges on record at Manu Bay.	80
Table 7-1:	Extreme storm-tide distribution at Whitianga.	87
Table 7-2:	Extreme storm-tide distribution at Kawhia.	88
Table 7-3:	Extreme storm-tide distribution at Tararu.	89
Table 7-4:	Extreme storm-tide distribution at Raglan.	90
Table 7-5:	Extreme storm-tide distribution at Manu Bay.	91
Table 8-1:	Minimum, mean and maximum SLA for each month of the year at Whitianga.	101
Table 8-2:	Minimum, mean and maximum SLA for each month of the year at Tararu.	101
Table 8-3:	Minimum, mean and maximum SLA for each month of the year at Kawhia.	102
Table 8-4:	Minimum, mean and maximum SLA for each month of the year at Raglan.	102
Table 8-5:	Minimum, mean and maximum SLA for each month of the year at Manu Bay.	103
Table 9-1:	There largest Tsunami event measured at Whitianga.	104

Table 9-2:	There largest Tsunami event measured at Tararu.	104
------------	---	-----

## Figures

Figure 1-1:	Location of sea-level gauges and meteorological stations. Red dots show Tararu, Whitianga, Kawhia, Manu Bay and Raglan, sea level gauges. Pink triangles show the Taharoa, Firth of Thames, Paeroa, Whitianga and Slipper Island meteorological stations.	13
Figure 3-1:	Quality assured Tararu sea level data.	23
Figure 3-2:	Quality assured Whitianga sea level data.	23
Figure 3-3:	Quality assured Kawhia sea-level data.	24
Figure 3-4:	Quality assured Raglan sea-level data.	24
Figure 3-5:	Quality assured Manu Bay sea-level data.	25
Figure 3-6:	Sea level at Kawhia.	26
Figure 3-7:	Annual mean sea levels at Kawhia compared to other sites.	26
Figure 3-8:	Annual mean sea levels at Manu Bay compared to other sites.	27
Figure 4-1:	Relationships and conversions between LVDs: Auckland (AVD-46), Moturiki (MVD-53), Tararu (TVD-52) and New Zealand Vertical Datum (NZVD2016).	30
Figure 4-2:	A comparison between the annual mean sea level of seven tide gauges.	32
Figure 4-3:	Annual mean sea level measurements from Auckland, Moturiki, Tararu, and Whitianga, normalized to a zero datum in 2005, alongside five projected sea-level rise trajectories.	35
Figure 4-4:	Whitianga annual mean sea-level in Moturiki Vertical Datum (MVD).	36
Figure 4-5:	Tararu annual mean sea-level in Moturiki Vertical Datum (MVD).	37
Figure 5-1:	High-tide markers at Whitianga relative to MSL=0.	39
Figure 5-2:	High-tide markers at Kawhia relative to MSL=0.	40
Figure 5-3:	High-tide markers at Tararu relative to MSL=0.	40
Figure 5-4:	High-tide markers at Raglan relative to MSL=0.	41
Figure 5-5:	High-tide markers at Manu Bay relative to MSL=0.	41
Figure 6-1:	Skew-surge illustration.	44
Figure 6-2:	Tararu extreme value analysis of skew surges using a GPD fitted to skew surges over a high threshold.	45
Figure 6-3:	Whitianga extreme value analysis of skew surges using a GPD fitted to skew surges over a high threshold.	46
Figure 6-4:	Kawhia extreme value analysis of skew surges using a GPD fitted to skew surges over a high threshold.	46
Figure 6-5:	Raglan extreme value analysis of skew surges using a GPD fitted to skew surges over a high threshold.	47
Figure 6-6:	Manu Bay extreme value analysis of skew surges using a GPD fitted to skew surges over a high threshold.	47
Figure 6-7:	Mean sea-level pressure map at 5 am, 13-Feb-2022 around the time of the largest measured skew surge at Tararu.	51
Figure 6-8:	Measured sea-level and its components during 13 February 2022 surge Tararu.	51
Figure 6-9:	Mean sea-level pressure map at 10 am, 05-Jan-2018 around the time of the largest measured skew surge at Tararu.	52

Figure 6-10:	Measured sea-level and its components during 05 January 2018 surge Tararu.	53
Figure 6-11:	Mean sea-level pressure map at 12 pm, 02-Oct-1992 around the time of the largest measured skew surge at Tararu.	54
Figure 6-12:	Measured sea-level and its components during 02 October 1992 skew surge Tararu.	54
Figure 6-13:	Mean sea-level pressure map at 7 am, 18-Sep-2005 around the time of the largest measured skew surge at Tararu.	56
Figure 6-14:	Measured sea-level and its components during 18 September 2005 skew surge Tararu.	56
Figure 6-15:	Mean sea-level pressure map at 6 am, 11-Jun-2014 around the time of the largest measured skew surge at Tararu.	57
Figure 6-16:	Measured sea-level and its components during 11 June 2014 skew surge Tararu.	58
Figure 6-17:	Monthly boxplot of the 5 largest skew surge events per year at Tararu.	58
Figure 6-18:	Measured sea-level and its components during 14 February 2023 skew surge Whitianga.	60
Figure 6-19:	Mean sea-level pressure map at 1 am, 14-Feb-2023 around the time of the largest measured skew surge at Whitianga.	60
Figure 6-20:	Mean sea-level pressure map at 11 pm, 10-Jan-2023 around the time of the largest measured skew surge at Whitianga.	61
Figure 6-21:	Measured sea-level and its components during 10 January 2023 skew surge Whitianga.	62
Figure 6-22:	Mean sea-level pressure map at 9 pm, 24-Sep-2013 around the time of the largest measured skew surge at Whitianga.	63
Figure 6-23:	Measured sea-level and its components during 24 September 2013 skew surge Whitianga.	63
Figure 6-24:	Tsunami signal in measured at Whitianga on 12 March 2011.	64
Figure 6-25:	Mean sea-level pressure map at 2 am, 27-Jul-2008 around the time of the largest measured skew surge at Whitianga.	65
Figure 6-26:	Measured sea-level and its components during 27 July 2008 skew surge Whitianga.	65
Figure 6-27:	Measured sea-level and its components during 11 June 2014 skew surge Whitianga.	66
Figure 6-28:	Monthly boxplot of the 5 largest skew surge events per year at Whitianga.	67
Figure 6-29:	Mean sea-level pressure map at 8 am, 6-May-2013 around the time of the largest measured skew surge at Kawhia..	69
Figure 6-30:	Measured sea-level and its components during 24 May 2013 skew surge Kawhia.	69
Figure 6-31:	Mean sea-level pressure map at 7 pm, 10-Apr-2018 around the time of the largest measured skew surge at Kawhia.	70
Figure 6-32:	Measured sea-level and its components during 10 April 2018 skew surge Kawhia.	71
Figure 6-33:	Mean sea-level pressure map at 8 pm, 20-Jun-2013 around the time of the largest measured skew surge at Kawhia.	72
Figure 6-34:	Measured sea-level and its components during 20 June 2013 skew surge Kawhia.	72

Figure 6-35:	Mean sea-level pressure map at 3 pm, 17-Apr-2013 around the time of the largest measured skew surge at Kawhia.	73
Figure 6-36:	Measured sea-level and it's components during 17 April 2013 skew surge Kawhia.	74
Figure 6-37:	Mean sea-level pressure map at 6 am, 7-Jun-2010 around the time of the largest measured skew surge at Kawhia.	75
Figure 6-38:	Measured sea-level and its components during 7 June 2010 skew surge Kawhia.	75
Figure 6-39:	Monthly boxplot of the 5 largest skew surge events per year at Kawhia.	76
Figure 6-40:	Measured sea-level and its components during 6 May 2013 skew surge Raglan.	77
Figure 6-41:	Mean sea-level pressure map at 1 pm, 13-Feb-2022 around the time of the largest measured skew surge at Raglan.	78
Figure 6-42:	Measured sea-level and its components during 13-Feb-2022 skew surge Raglan.	78
Figure 6-43:	Mean sea-level pressure map at 1 pm, 31-Jul-2008 around the time of the largest measured skew surge at Raglan.	79
Figure 6-44:	Measured sea-level and its components during 31 July 2013 skew surge Raglan.	80
Figure 6-45:	Measured sea-level and its components during 10 April 2018 skew surge Manu Bay.	81
Figure 6-46:	Mean sea-level pressure map at 1 pm, 14-Aug-2018 around the time of the largest measured skew surge at Manu Bay.	82
Figure 6-47:	Measured sea-level and its components during 14 August 2018 skew surge Manu Bay.	82
Figure 6-48:	Mean sea-level pressure map at 4 pm, 17-Jul-2021 around the time of the third largest skew surge measured at Manu Bay.	83
Figure 6-49:	Measured sea-level and its components during 17 July 2021 skew surge Manu Bay.	84
Figure 7-1:	Extreme storm tide prediction levels, and annual maximum sea levels for Whitianga.	87
Figure 7-2:	Extreme storm tide prediction levels, and annual maximum sea levels for Kawhia.	88
Figure 7-3:	Extreme storm tide prediction levels, and annual maximum sea levels for Tararu.	89
Figure 7-4:	Extreme storm tide prediction levels, and annual maximum sea levels for Raglan.	90
Figure 7-5:	Extreme storm tide prediction levels, and annual maximum sea levels for Manu Bay.	91
Figure 7-6:	The contributions of tide, skew surge and MSLA to the 10 largest storm tides recorded at the Kawhia sea-level recorder.	92
Figure 7-7:	The contributions of tide, skew surge and MSLA to the 10 largest storm tides recorded at the Tararu sea-level recorder.	93
Figure 7-8:	The contributions of tide, skew surge and MSLA to the 10 largest storm tides recorded at the Whitianga sea-level recorder.	93
Figure 7-9:	The contributions of tide, skew surge and MSLA to the 10 largest storm tides recorded at the Raglan sea-level recorder.	94

Figure 7-10:	The contributions of tide, skew surge and MSLA to the 10 largest storm tides recorded at the Manu Bay sea-level recorder.	94
Figure 7-11:	Monthly boxplot of the five largest storm tide events per year at Whitianga.	95
Figure 7-12:	Frequency of the five largest storm-tides each year sorted by month at Whitianga.	95
Figure 7-13:	Monthly boxplot of the five largest storm tide events per year at Tararu.	96
Figure 7-14:	Frequency of the five largest storm-tides each year sorted by month at Tararu.	96
Figure 7-15:	Monthly boxplot of the five largest storm tide events per year at Kawhia.	97
Figure 7-16:	Frequency of the five largest storm-tides each year sorted by month at Kawhia.	97
Figure 7-17:	Seasonal distribution of sea-level components associated with extreme storm-tide and skew-surge events around NZ (source, Stephens et al. 2020).	98
Figure 8-1:	Mean, minimum and maximum monthly sea-level anomaly.	100



## Executive summary

Waikato Regional Council (WRC) operates sea-level gauges at Tararu, Whitianga, Kawhia, Raglan and Manu Bay. Digital sea-level records began at Tararu in 1990 and at Whitianga in 1999, with the other gauge records beginning 2008. WRC engaged NIWA to analyse the sea-level records. The primary focus was on examining mean sea level change, tidal heights, and extreme events within the sea-level records to elucidate the localized dynamics of storm-tides in relation to tides and meteorological conditions. This report offers diverse sea-level analyses pertinent to coastal planning, regulatory efforts, hazard assessment, and is applicable across the five sea-level records.

All five sea-level gauges are currently collecting high-quality data, allowing for accurate extraction of various sea-level components, determination of mean sea level, and computation of extreme sea-level values. There are historical data gaps in the Raglan and Manu Bay records. WRC periodically surveys all the gauges relative to LINZ benchmarks, which has enabled us to obtain a good understanding of how mean sea level is tracking. For example, at Kawhia, a datum offset correction of 0.2698 m has been applied to the analysis in this report for the period June 2021 to present, and we recommend incorporating this correction into the WRC data feed. Similarly, datum offsets of 0.177 m and 0.126 m have been applied to Manu Bay and Raglan records, respectively, for data from 2018 onward (the offsets at Manu and Raglan have been incorporated into the WRC live feed). The long-term datum control at these sites is robust, allowing us to understand historical inconsistencies, particularly at Kawhia, where gauge drift was detected. These issues have been addressed in the analyses within this report using linear detrending, and we recommend that these corrections be applied to the WRC data feed. We were unable to resolve datum offset issues in the sea-level data from Manu Bay prior to 2018, so that part of the record was not analysed in this report.

Mean sea levels (MSL), relative to the Moturiki vertical datum, were computed for various locations: Auckland, Moturiki, Whitianga, Tararu, Kawhia and Raglan. MSL for the 2009–2023 epoch was 0.20, 0.14, 0.18, 0.19, 0.20 and 0.21 m MVD-53 respectively.

The measurements indicate that relative sea-level rise rates are tracking lower than the SSP5-8.5H<sup>+</sup> scenario but slightly above the other projections (SSP1-2.6M – SSP5-8.5M), to date.

Mean high-water spring (MHWS) elevations were derived from the gauge records, and MHWS elevations were estimated at other locations along the Waikato region's coastline using NIWA's tide model validated against the gauge records. MHWS elevations are tabulated in this report.

The distribution of skew surge events in terms of frequency and magnitude was computed for each gauge. Whitianga, Tararu, Kawhia, Raglan and Manu Bay yielded 1% Annual Exceedance Probability (AEP) skew surge estimates of 0.67 m, 0.73 m, 1.07 m, 1.18 and 0.6 respectively. These reported values are from the medians of the extreme-value analyses – 95<sup>th</sup> percent confidence intervals are also presented in the report. We recommend caution when using the skew surge and storm tide extreme value analyses at Manu Bay and Raglan, because of the short sea level record durations and large amount of missing data. Distinct surge drivers were observed between the eastern (Whitianga) and western (Kawhia, Raglan) coastlines of New Zealand. The east coast gauges have a proportionately larger inverse barometer (MSLP) component compared to the west coast gauges where surge is strongly dominated by wind setup. The east coast surges tend to be driven by tight, fast moving low-pressure weather systems, whereas the largest west coast surges are driven by prolonged strong north-westerly winds generated by weather fronts. These persistent winds have

resulted in surges nearly twice the magnitude of those observed at Whitianga, with some exceeding 1 m in recent decades.

Extreme storm-tide distributions were fitted at Tararu, Whitianga and Kawhia – Raglan and Manu Bay were omitted due to their short record durations. The median 1% annual exceedance probability (AEP) storm tide estimates were 1.47 m for Whitianga, 2.37 m for Tararu, and 2.65 m for Kawhia. Higher-than-normal high tides were the predominant component within the largest storm tides, though some instances featured a pronounced sea-level anomaly in addition. All of the largest storm tides included a moderate surge component.

There was a clear annual cycle in the sea-level anomaly at all sites with mean sea-level anomaly (SLA) peaking between March and May, minimum in October, and lagging the sea-surface temperature (SST) cycle by around 2 months. Investigation of storm tide seasonality was conducted for Whitianga Tararu and Kawhia.

The analyses are generally based on recorded sea levels without adjustment for vertical land motion (VLM), meaning the reported long-term trends represent relative sea-level rise (RSLR). An exception is the Tararu site, where VLM corrections derived from GNSS data were applied to the mean sea level record. All other analyses (e.g., extreme sea levels and anomalies) were conducted on detrended data. Derivation of absolute SLR would require vertical land motion to be recorded at the gauge sites through co-location of GNSS recorders. This could also help to identify any stability/subsidence issues with the gauge infrastructure.

In summary, the sea-level gauges have collected reliable data, and with ongoing maintenance, these records will remain valuable for forthcoming analyses of sea-level trends, skew surges, and storm-tide anomalies. The historical records from Tararu (33-years) and Whitianga (24- years) are especially significant and warrant continued investment to enhance extreme sea level estimations, assess shifting mean sea levels, and gauge rates of sea-level rise. While the Kawhia gauge's record is relatively short (15-years), its long-term value can be substantial if maintained. The Raglan (15-years but with a ~3-year gap) and Manu Bay (~6-years total) records are both short and contain large periods of missing data but have still contributed meaningfully to our understanding of sea level behaviour and will grow in value with time. The Whitianga gauge is influenced quite strongly by morphological change in the harbour entrance, so it is not an ideal representation of the east coast open-water environment. This could be mitigated by expanding the network to include at least one open-coast locations on the east coast of the Waikato region.

## 1 Introduction

Sea level measurements are important because they provide invaluable information about the local effects of global climate change. Sea level is an important indicator of global warming associated with climate change because it is directly affected by the temperature of the ocean, which is in turn affected by the amount of greenhouse gases in the atmosphere. Sea level rise reflects thermal expansion of waters in the ocean, as well as direct increase in sea level caused by melting of glaciers and polar ice sheets. By measuring sea level at different locations and times, researchers can gain insight into the effects of global warming and make informed decisions about how to best manage the environment. Sea level measurements also play a key role in understanding the impact of coastal erosion, storm tides, and other natural disasters. Furthermore, understanding the current sea level is important when predicting likely future sea level rise, which is essential for developing policies on managed retreat and the protection of coastal communities and infrastructure.

The accuracy of coastal planning frameworks that assess risks is heavily influenced by the boundary conditions of water levels, which encompass mean sea level, astronomical tides, and storm surges (Brown et al. 2018).

Sea-level records serve several purposes:

- Calculating tide heights and mean high-water springs (MHWS) elevations that define the legal boundary between land and sea.
- Determining the present-day MSL, which serves as a reference for extreme sea-level analyses and MHWS calculations.
- Monitoring long-term sea-level rise.
- Comparing relative MSL among different sites along the coastline.
- Understanding how sea level responds to tide, weather, and climate.
- Conducting extreme sea-level analyses to inform coastal inundation hazard assessments.
- Calibrating or providing boundary information for coastal hydrodynamic models.
- Verifying the quality of collected sea-level information.

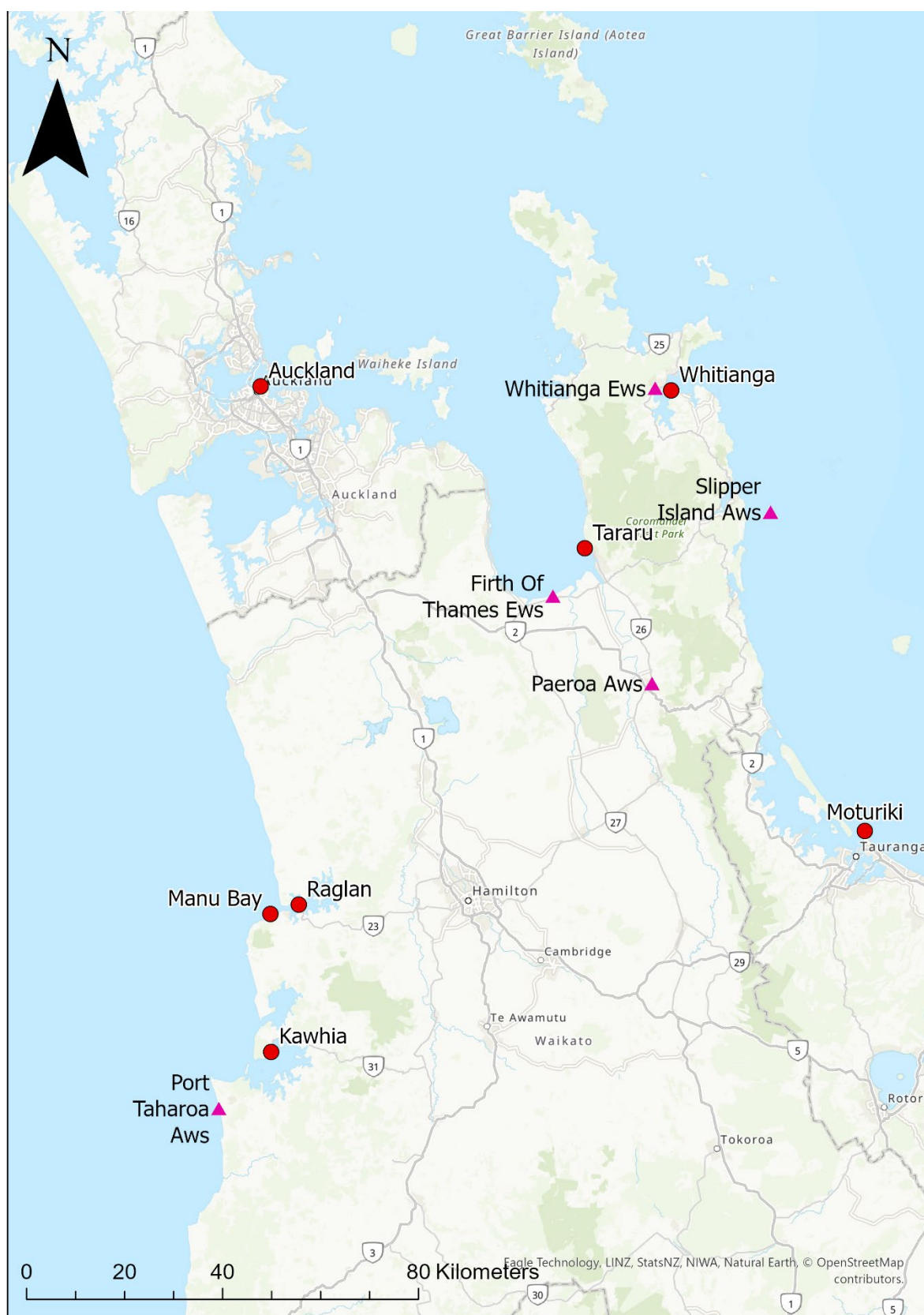
**We urge caution in the use of the skew surge and storm tide extreme value analysis results at Manu Bay and Raglan, because of the short sea level record durations.**

## 1.1 Background

Waikato Regional Council (WRC) commissioned NIWA to analyse the sea-level gauges operating in the Waikato region. These gauges are located at Whitianga, Tararu, Raglan, Kawhia, and Manu Bay (Figure 1-1). This report builds on previous analyses and updates the earlier study by Stephens et al. (2015). The current report has been revised to include data from recent large storms, specifically Tropical Cyclones Hale and Gabrielle, that occurred after the 2023 analysis. A key focus is the analysis of extreme sea-level events, aiming to provide insight into the local response of sea level to tides, weather, and wave action during storms, as well as to monitor trends in mean sea level

This report presents a range of sea-level analyses that are valuable for coastal planning, regulation, and hazard assessment at the five tide gauge locations. An additional improvement to the analyses made in 2015 (Stephens, S. A. et al. 2015) is the quality analysis of the gauges to National Environmental Monitoring Standards (NEMS) standards.

The report is accompanied by electronic tables in Excel format. To aid understanding of the technical language used, a glossary has been included in Section 12.



**Figure 1-1: Location of sea-level gauges and meteorological stations.** Red dots show Tararu, Whitianga, Kawhia, Manu Bay and Raglan, sea level gauges. Pink triangles show the Taharoa, Firth of Thames, Paeroa, Whitianga and Slipper Island meteorological stations.

## 1.2 Scope of the project

The following analyses were undertaken for each of WRC's Tararu, Whitianga and Kawhia sea-level records and where appropriate Raglan and Manu Bay:

1. Quality analysis (QA) to NEMS standards for **all** the available sea level data from the Tararu, Whitianga and Kawhia, Raglan and Manu Bay sea-level gauges.
2. Undertake tidal harmonic analysis, decomposition and detrending as required for subsequent analyses. This splits the sea-level record into components of tide, mean sea-level anomaly (MSLA), storm-surge (SS), and skew-surge. Storm-surge is evaluated hourly, whereas skew-surge is the storm-tide peak minus the high-tide peak (one for every high tide).
3. Whitianga, Kawhia, Tararu, Raglan and Manu Bay tide Gauge 'Fit for Purpose' review: Assess the Whitianga, Kawhia, Tararu, Raglan and Manu Bay Tide Gauge equipment/instrumentation in terms of providing the required information to appropriately assess water levels currently and into the foreseeable future. All equipment/instrumentation information was to be supplied by staff at WRC.
4. Tidal harmonic analysis including tidal exceedance curve and tables with tide marks relative to datums. The seasonal  $S_a$  and  $S_{sa}$  tides were omitted as the seasonal cycle was treated as part of the non-tidal residual (NTR).
5. Annual and monthly mean sea-level analysis and inter-gauge MSL comparison (including sea level records from Moturiki and Auckland to the limits of available data). A MSL datum was calculated for the duration of the sea-level gauge records. All water levels were provided in the relevant local vertical datum, and in NZVD2016.
6. Monthly boxplot of largest 5 storm-tide and skew-surge events per year. These plots reveal seasonal patterns in storm-tide and skew-surge hazards.
7. Mean seasonal sea-level cycle plot and table: mean, minimum and maximum MSLA per month of the year.
8. Calculate epoch-averaged MSL consistent with the latest MFE sea level rise guidance, for those sea-level records that span the required epoch. Calculate MSL for a common recent epoch so that all gauges can be directly compared.
9. Extreme skew-surge analysis (annual exceedance probability and magnitude) undertaken for skew-surge using Generalised Pareto Distribution fitted to peaks-over-threshold data (Coles 2001). The extreme-value and maxima data were plotted and included in tables.
10. Extreme storm-tide (total sea-level) analysis (frequency and magnitude) using the skew-surge joint-probability technique (Batstone et al. 2013; Stephens, S. A. et al. 2020). Table of top 10 storm-tide events and list of contributing component elevations (MSLA, tide, skew-surge). The extreme-value and maxima data were plotted and were included in tables.

11. A descriptive analysis of largest 3–5 skew surges at Whitianga, Kawhia, Tararu, Raglan and Manu Bay tide gauges. Those events were identified as large outliers from the earlier extreme sea-level analyses. The descriptive analyses include synoptic weather maps, situational weather analysis, and inverse barometer (IB) response.
12. An analysis for evidence of tsunami from the Whitianga and Tararu sea level records. While all gauges now record at 1-minute intervals following a 2021 review, Whitianga and Tararu have been recording at this resolution for a longer period, making them particularly well-suited for capturing the peaks of long tsunami waves (Greer et al. 2017).
13. An appendix including data tables that update the levels used in the [WRC coastal inundation tool](#), as currently specified on pages 4–9 of the [Tool user guide](#).
14. Tables of MHWS–10 and HAT elevations extracted from the NIWA tide model at similar locations to Stephens et al. (2015) - these were supplied in excel format and included in the report.
15. A schematic is provided for each tide gauge showing the conversions between MSL, local datum (MVD-53 or TVD-52 depending on gauge) and NZVD2016.
16. Recommendations are made in Section 10 to assist the long-term usefulness of the sea-level gauge network.



## 2 Components and definitions of sea level

There are several meteorological and astronomical components contributing to sea-level variability. These contributions can occasionally combine to inundate low-lying coastal land, cause beach or cliff erosion, or drive changes in groundwater levels and salinity. The following sources of sea-level variability can combine to create coastal hazards. Those relevant to this study are underlined.

- Mean sea level (MSL) – the average (mean) level of the sea, relative to a vertical datum over a defined period, usually of several years e.g., 19 years used by Land Information NZ for Standard Ports in their Nautical Almanac.
- Mean sea-level anomaly (MSLA) – the variation of the non-tidal sea level about the longer-term MSL on time scales ranging from a monthly basis to decades, due to climate variability. This includes the influence of El Niño Southern Oscillation (ENSO) and Inter-decadal Pacific Oscillation (IPO) patterns on sea level, winds and sea temperatures, and seasonal effects. MSLA is influenced by annual, interannual and interdecadal processes (Table 2-1). The abbreviation SLA is used in place of MSLA in some plots.
- High astronomical tides (high tide). The tides are caused by the gravitational attraction of solar-system bodies, primarily the Sun and the Earth’s moon, which then propagate as forced long waves in the ocean interacting in a complex way with continental shelves. In New Zealand the astronomical tides have by far the largest influence on sea level, followed by storm surge (in most locations).
- Storm surge, and skew surge – the temporary increase in sea level, induced by winds and barometric pressure associated with weather systems. Low-pressure weather systems and/or adverse winds cause a rise in water level known as storm surge. Storm surge and skew surge result from two processes: 1) low-atmospheric pressure relaxes the pressure on the ocean surface causing a temporary rise in sea-level, and 2) wind stress on the ocean surface pushes water down-wind, or alternatively, to the left of an alongshore wind (in the southern hemisphere) from a persistent wind field, piling up against any adjacent coast e.g., for the Whitianga gauge located on New Zealand’s east coast, this would occur for onshore winds (from NE quadrant) and alongshore winds from SE respectively, and for Kawhia on the west coast, onshore winds from south-west and alongshore winds from north-west. Wind setup within harbours varies according to the fetch present at various tide states, but at high tide can be several decimetres. Whereas storm surge is calculated by subtracting the predicted tide at the same sampling interval as the sea-level record, skew surge is calculated as the height difference between the nearest sea-level peak and the nearest predicted astronomical high tide. It may occur at a different time to the tide peak, hence the term skew surge—skewed in time. There is one skew-surge measurement per high tide. Thus, storm surge and skew surge are both measures of pressure- and wind-induced water level setup but are calculated (and used) differently.
- Long waves – there is typically a distinction between short waves, which are waves with periods less than approximately 25 s, and long waves, which are oscillations with periods between ~25 s and 40 min. Water-level oscillations with periods or recurrence intervals larger than around 1 hour, such as astronomical tide and storm surge, are referred to as still-water-level variations. The short waves are wind waves and swell, whereas long waves are divided into infragravity waves (surf beats), seiche and tsunamis.



- Infragravity waves – Infragravity waves are surface gravity waves with frequencies lower than the (wind generated) short waves consisting of both wind sea and swell – thus corresponding with the part of the wave spectrum lower than the frequencies directly generated by forcing through the wind. The common scientific usage is limited to gravity waves that are generated by groups of short (wind) waves. Wind waves and ocean swells are shorter, with typical dominant periods of 1 to 25 s. In contrast, the dominant period of infragravity waves is typically 80 to 300 s.
- Seiche – a standing wave in an enclosed or partially enclosed body of water. Seiches and seiche-related phenomena have been observed on lakes, reservoirs, swimming pools, bays, harbours, caves, and seas. The key requirement for formation of a seiche is that the body of water be at least partially bounded, allowing the formation of the standing wave.
- Tsunami – an ocean wave, usually caused by a submarine earthquake, an underwater or coastal landslide, or a volcanic eruption.
- Wave setup and runup – wave setup is the elevation of the mean water level at the shoreline due to wave breaking in the surf zone, resulting from the release of wave energy in the surf zone as waves break. Wave runup is the maximum onshore elevation reached by waves, relative to the shoreline position in the absence of waves—it is the maximum vertical extent of sporadic wave “up-rush” of flowing water on a beach or structure. Wave runup is only a short-term upper-bound fluctuation in water level compared to wave setup.
- Wave overtopping – occurs when the wave runup exceeds the crest elevation of the beach or berm and flows over (“overtops”) the top of the dune or seawall.

Sea-level interaction with groundwater, including:

- rising groundwater level, and
- salinization of groundwater.
- Climate change effects, including:
  - changes in the storm surge and wave climate, e.g., increased storminess, and
  - Sea-level rise (incorporating both absolute and local contributors, e.g., vertical land movement). This includes long-term (> 30-years) climate-driven trend (Table 2-1).
- Vertical land movement from tectonic processes (earthquake event and inter-seismic periods) or sedimentary-basin subsidence.

**Table 2-1: The main components and causes of sea-level variability at various timescales longer than 2 minutes, some of which overlap.** FIG=far infragravity waves; ENSO=El Niño–Southern Oscillation; IPO= Inter-decadal Pacific Oscillation.

Phenomenon	Cause	Period
long waves (meteo-tsunami, FIG)	weather	2 – 20 min
tsunami	earthquakes/landslides	5 min – 1 h
seiche	resonance and weather	20 min – 4 h
tides	astronomical	3 h – 29 h
storm surge	weather	12 h – 5 d
annual (seasonal)	temperature	1 yr
interannual	ENSO climate cycle	2 – 4 yrs
interdecadal	Pacific IPO climate cycle	20 – 30 yrs
climate trend	global warming	decades to centuries

## 2.1 Tides

Ocean tides are the rise and fall of sea levels caused by the combined effects of the gravitational forces exerted by the Moon and the Sun and the rotation of the Earth.

The times and amplitude of the tides at a given location are influenced by the alignment of the Sun and Moon, by the pattern of tides in the deep ocean and by the shape of the coastline and near-shore bathymetry that substantially modifies the tidal wave.

The Equilibrium Tide has three coefficients that characterise the main *species* of lunar tides (Pugh 2004):

- the *long-period species*, with tidal changes over a month and longer; these are due to changes in the lunar distance and declination,
- the *diurnal species* at a frequency of around one cycle per day, controlled by the lunar declination and the earth’s rotation, and
- the *semidiurnal species* at two cycles per day, controlled by the earth’s rotation.

Tidal constituents are the individual components which comprise the tides. Each constituent arises either from a specific astronomical feature or from the interaction between two or more constituents. Semi-diurnal or “twice-daily” tidal constituents dominate New Zealand tides (Walters et al. 2001) with tidal periods between 12–13 hours, e.g., the solar semi-diurnal constituent  $S_2$  (12-hour period); the lunar semi-diurnal constituent  $M_2$  (12.42-hour period); the elliptic semi-diurnal constituent  $N_2$  (12.66-hour period) that covers the elliptical nature of the Moon’s orbit around Earth each month.

In the Waikato Region there are two high tides most days with different heights (and two low tides also of different heights), a pattern resulting from the interaction of the  $M_2$ ,  $S_2$  and  $N_2$  harmonic constituents, and known as a mixed semi-diurnal tide.

In New Zealand, the largest constituent is the "principal lunar semi-diurnal", also known as the  $M_2$  tidal constituent, which results directly from the Moon's gravitational pull on the oceans ( $M$  stands for "Moon"). Its period is about 12 hours and 25.2 minutes, which is half the "lunar day" (24 hours 50 minutes) required for the Earth to rotate once relative to the Moon. The  $M_2$  tidal constituent alone represents approximately an average tide range (between spring and neap). The two other most dominant harmonics are the  $S_2$  and  $N_2$  constituents.

$S_2$ , the solar semi-diurnal constituent has a period of exactly 12-hours, and this arises because the Sun passes over the same spot on Earth every 24 hours. Spring/neap tides occur every fortnight (14.765 days to be exact) in conjunction with Moon's phase in relation to alignment with the Sun; spring tides occur just after New and Full Moon; neap tides occur just after First and Last Quarter. Spring tides have a larger tidal range than neap tides because at New and Full Moon, the Moon and Sun are lined up and they pull together upon Earth's waters; whereas at First and Last Quarter the Moon and Sun are opposed, and the pull is less. Another equivalent definition is that spring and neap tides are the result of  $M_2$  (the lunar semi-diurnal constituent) beating in and out of phase with the  $S_2$  (the solar semi-diurnal constituent). The  $S_2$  tide is quite small on the east coast of New Zealand (Walters et al. 2001) compared to the west coast, which makes the fortnightly spring/neap cycle less pronounced on the eastern coasts (especially in the central regions).

$N_2$ , the elliptic semi-diurnal constituent, arises from the elliptic orbit of the Moon around Earth. Each constituent has a unique tidal period. Perigean/Apogean tides occur every month (27.555 days to be exact) in conjunction with the position of the Moon in its elliptical orbit around Earth. When the Moon is closest to Earth, it is in its perigee and larger than normal Perigean tides occur. When the Moon is farthest from Earth, it is in its apogee and smaller than normal Apogean tides occurs. Another equivalent definition is that Perigean and Apogean tides are the result of  $M_2$  (the lunar semi-diurnal constituent) beating in and out of phase with  $N_2$  (the elliptic semi-diurnal constituent). Because the  $N_2$  tide doesn't decrease on the east coast of New Zealand as much as the  $S_2$  tide does, the main variation in tides on the east coast arises from a monthly Perigean/Apogean cycle superimposed on a smaller spring/neap cycle. This explains why the tides every second spring-tide period are higher than the previous set a fortnight earlier.

Perigean-spring combination tides peak about every 7 months (206.6 days to be exact) when New or Full Moon occurs at the same time as the Moon is in its perigee. Usually, these are the tides with the largest tidal range often referred to as "king tides". NIWA publishes annually a red-alert tide calendar<sup>1</sup> which covers the dates in New Zealand when higher Perigean-spring tides will occur and if they combine with storms, can have the potential to cause coastal inundation of low-lying areas.

While  $M_2$ ,  $S_2$  and  $N_2$  are the major harmonic constituents in the Waikato Region, there are 62 tidal constituents (albeit mostly small) resolved in most harmonic analysis techniques, depending on the sea-level record length and quality.

## 2.2 Quality assurance

Sea level quality assurance (QA) refers to the process of ensuring the accuracy, reliability, and consistency of sea level measurements and data. It involves various techniques, methodologies, and procedures to monitor and verify the quality of sea level observations. Sea level QA is essential for ensuring the accuracy and reliability of sea level measurements, facilitating climate research, and

---

<sup>1</sup> [Storm-tide red-alert days 2023 | NIWA](#)

informing coastal management, disaster preparedness, and infrastructure planning. A full description of the QA process is outlined in Appendix D.

We recommend allowing approximately 3-hours (per location) to set-up all the input files (\*.json with all the site data, filter parameters etc., Appendix D). Then allow about 2-hour for each year of sea-level record for processing. We recommend to analysing each year separately, then apply additional corrections in the form of spikes and datum shifts. Re-run the processing script for that year of data to check the corrections and move onto the next year of data.

## 2.3 Sea level analysis methods

The steps and methods used for the analysis of each sea-level record are described here:

1. Obtain and quality analyse the sea-level record data (Section 2.2), including corrections for drift and datum offsets (Sections 3.1 and 3.2).
2. Calculate the tidal component of sea level using tidal harmonic analysis, following the Unified Tidal Analysis and Prediction method, using the UTide Matlab Functions (Codiga, D.L. 2011b). The analyses fitted the standard 67 harmonics and used a signal to noise ratio of 10. The tidal predictions deliberately excluded the gravitational solstice tides, namely  $S_a$  and  $S_{sa}$ , as they were instead left in the non-tidal residual to be accounted for in the seasonal sea-level cycle. See section 5 for more details on tidal prediction.
3. Subtract the predicted tide from the quality-assured sea-level record to obtain the non-tidal residual (NTR). The annual mean sea level (MSL), mean sea level anomaly (MSLA) and long-term linear trend are calculated from the NTR.
4. Calculate annual MSL from NTR by averaging NTR for each calendar year (Section 4).
5. Calculate the long-term linear trend (see Section 4.1) in annual MSL and subtract this from the NTR before calculating skew surge, storm-tide and MSLA using the detrended NTR. To calculate the long-term linear trend, linear fits were calculated using a least-squares analysis fitted to annual MSL.
6. Calculate skew surge as the absolute difference between the maximum recorded storm tide during each tidal cycle and the predicted maximum astronomical tidal level for that cycle, irrespective of differences in timing between these (Batstone et al. 2013; Williams et al. 2016). See Section 6 for more detail.
7. Calculate an extreme skew surge distribution, using a generalised Pareto distribution (GPD) fitted to skew surge maxima selected using a peaks-over-threshold (POT) method. This is a standard methodology for extreme value fitting (Coles, 2001). See Section 6 for more details. This provides estimates of skew-surge heights for various annual exceedance probabilities.
8. Calculate storm surge and inverse barometer for the descriptive analysis of storm events—used to determine the influence of low air pressure relative to wind setup, on surge height (Section 6.1). Storm surge was calculated by subtracting the predicted tide from the measured data to form a residual and band-pass filtering the residual to remove most of the leftover tide, the high frequency noise, seiches, weekly and inter-

month to seasonal (>1 month) effects. We perform the same processing on the atmospheric pressure and subtract it from its yearly mean to estimate the inverted barometer (IB) component of storm surge. The band-pass storm-surge height (covering bands from 16 hours to 512 hours) was used only in plots for descriptive purposes and was not used in any of the tables—the tables use skew surge.

9. Use the skew-surge joint-probability method (SSJPM) to calculate an extreme storm-tide distribution (Section 6.1). This combines the detrended skew surge record with the predicted high tide record to provide estimates of storm-tide heights for various annual exceedance probabilities. The SSJPM (Batstone et al. 2013) is a best practice method for relatively short ( $\sim < 30$  years) sea level records. Joint-probability methods provide more robust low-frequency magnitude estimates for short-duration records because they overcome the main theoretical limitations of extreme value theory application to sea levels—splitting the sea level into its deterministic (predictable) tidal and stochastic (e.g., unpredictable, storm-driven) non-tidal components, and analysing the two components separately before recombining (Tawn and Vassie 1989; Haigh et al. 2010). Storm-tide return periods can be estimated from relatively short records because all skew surges are considered, not just those that lead to extreme levels.
10. Calculate MSLA by applying 31-day running average to the detrended NTR—a monthly sliding window.
11. Calculate the mean, minimum and maximum MSLA for each month of the year (Section 8). This is done by sorting the MSLA into calendar months, then calculating the mean, maximum and minimum value for each calendar month.
12. Identify tsunami (Section 9). A sampling frequency of 1-minute or less is desirable for assessing tsunami signals in sea-level data. While all gauges now record at 1-minute intervals following a 2021 review, this resolution has been available at Tararu and Whitianga for a longer period. Tsunamis were identified at Tararu and Whitianga by filtering the detrended NTR, using a fourth-order Butterworth high-pass filter to highlight sea level variability with oscillation periods within the 2–48-minute range. Activity in this range was visually obvious after filtering. We then searched internet sources for known earthquakes/tsunami generation events and were able to relate all identified tsunami evidence to known tsunami-generating events. Once identified, the tsunami amplitude at each station was calculated as the difference between the peak amplitude of the observed water level and the harmonic predicted tide.

### 3 Data

Table 3-1 presents the available data for the five Waikato Regional Council tide gauges (refer to Hunt (2021) for full site description). All datasets were analysed up to 1 July 2024, except for Tararu, where only the present record up to 14 February 2024 was used in this analysis. The Tararu record will continue at an adjacent platform beyond this date.

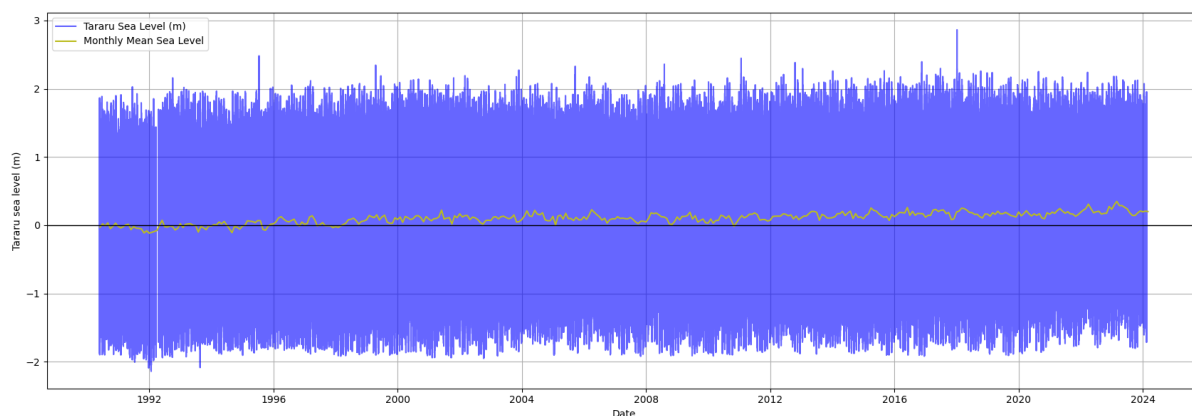
**Table 3-1: Listing of the data available for the Waikato Regional Council sea-level.** Bad data consists of gaps in the record which are longer than 24 hours, or values that were removed.

Sea Level Gauge	Site Number	Start Date	Bad data %	Number of gaps >24 hours	Longest gap length (Days)
Kawhia	41799	29 August 2008	3.99	16	108
Tararu	9415	25 May 1990	0.55	16	27
Whitianga	11599	13 July 1999	0.47	8	18
Raglan	42399	1 July 2008	30.12	6	955
Manu Bay	42799	11 July 2008	50.4	16	1624

**Table 3-2: Listing of the vertical offsets applied during the QA process to correct Waikato Regional Council sea-level records.** Data with an Asterix (\*) represent offset which have now been incorporated into the Waikato Regional Council data feed.

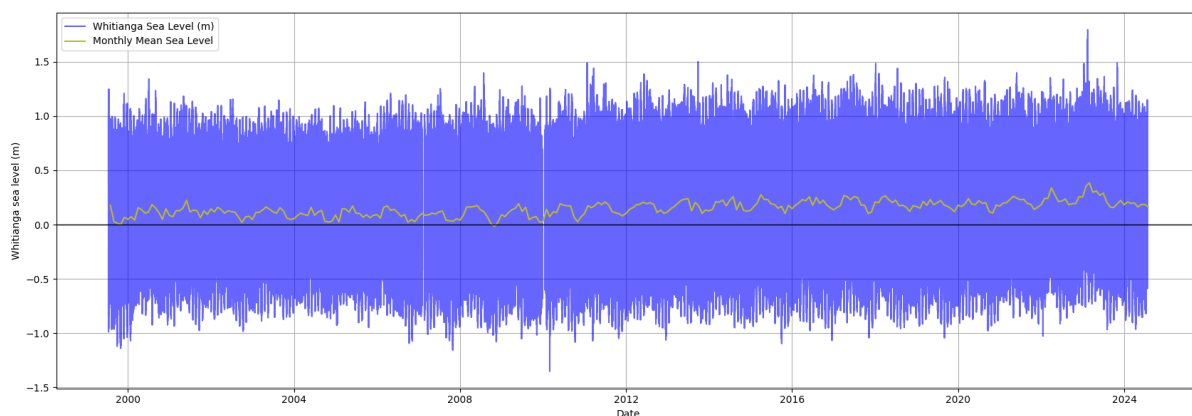
Sea Level Gauge	Correction type	Start Date	End Date	Offset (m)
Kawhia	datum offset	03/06/2021	23/07/2024	0.2698
	detrend	15/04/2019	03/03/2020	0.1567
	detrend	12/09/2021	26/09/2021	-0.462
Raglan*	datum offset	04/11/2019	23/07/2024	0.126
Manu Bay*	datum offset	17/03/2018	23/07/2024	0.177
	detrend	17/03/2018	25/01/2019	0.05

The Tararu sea level recorder was installed on 25 May 1990 and has a recording duration of 32-years until the end of 2023. Initially, the sampling interval was 7.5 minutes until 1997, then it changed to 5 minutes until 2011, and since then it has been set at 1-minute (Hunt 2021). The complete sea level record includes 16 gaps larger than 24 hours, with the longest gap spanning 27 days from 20 March 1992. The sea-level record at the present location stopped on 14 February 2024. The full QA'd (Quality Assured) Tararu sea level record in Figure 3-1 shows no apparent issues with datum or offset. However, VLM been recorded at the Tararu gauge is in the order of 3 mm/yr and is discussed further in Section 4.1. VLM may continue at the new adjacent platform.



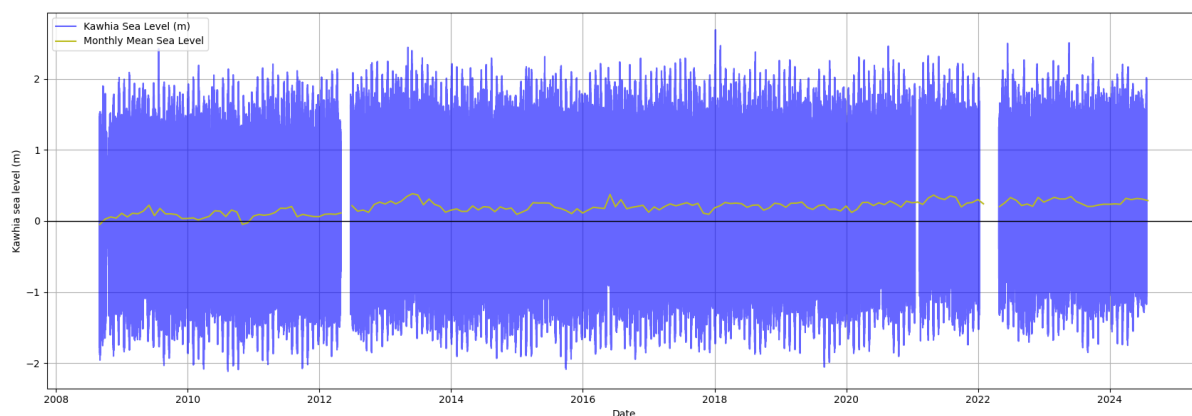
**Figure 3-1: Quality assured Tararu sea level data.** Blue line sea level (m) relative to TVD-52. Black line represents gauge zero relative to local vertical datum. Yellow line monthly mean sea level.

The sea-level recorder at Whitianga was installed on 13 July 1999 and has a recording duration of 25-years until present. The sampling interval was 5 minutes up until 2009 and has been changed to a 1-minute sample interval since then (Hunt 2021). Table 3-1 only displays the availability of data used in this report from 1999 to 2024. The largest gap in the water level records spans 22 days, starting on 27 December 2009. Figure 3-2 presents the complete QA'd Whitianga sea level record, which shows no apparent issues with datum or offset.



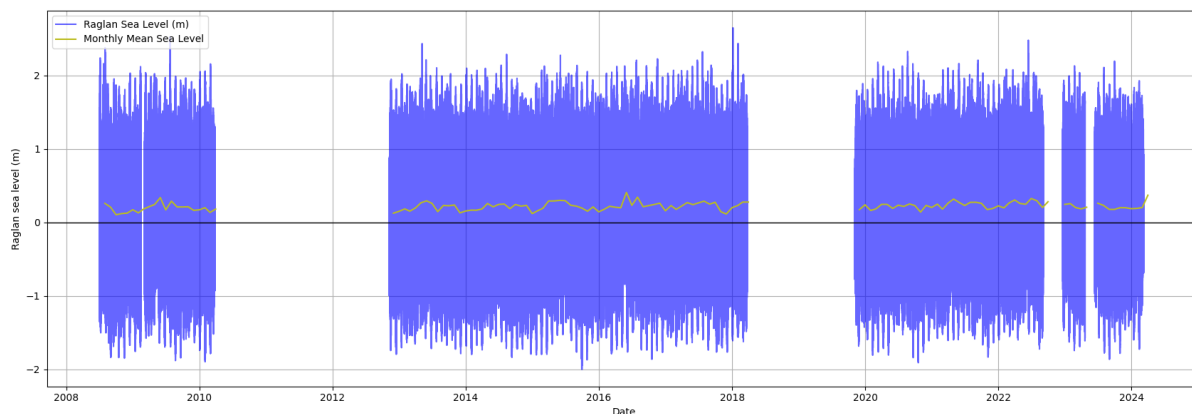
**Figure 3-2: Quality assured Whitianga sea level data.** Blue line sea level (m) relative to MVD-53. Black line zero level indicator. Yellow line monthly mean sea level.

The available data from the Kawhia sea-level recorder station are listed in Table 3-1, and Figure 3-3 displays the measured water level for the full duration of the gauge record. The sea level recorder was installed on 28 August 2008 and spans a duration of 16-years until the end of 2023. The sampling interval was initially set to 1-minute until 2012, changed to 2 minutes until mid-2021 and has been 1-minute since this time (Hunt 2021). There are 16 gaps in the data spanning more than 24 hours, with the largest gap being 108 days, starting on 8 January 2022. After adjustments were made to the vertical datum (see Section 3.1) the QA'd Kawhia sea level record, shows no apparent issues with datum or offset.



**Figure 3-3: Quality assured Kawhia sea-level data.** Blue line sea level (m) relative to MVD-53. Black line zero level indicator. Yellow line monthly mean sea level.

The available data for the Raglan sea-level recorder station are listed in Table 3-1, and Figure 3-4 displays the measured water levels. The Raglan sea-level recorder was installed on 1 July 2008 and intermittently spans a period of 15-years until the end of 2023. The sampling interval was 1-minute up until 2010, when it was changes to 2 minutes until mid-2021, like Kawhia, the sampling was set back to 1-minute. There are 6 gaps in the data spanning more than 24 hours, with the largest gap in the data occurred when the Raglan Wharf (where the gauge is installed) was destroyed by fire. This gap was 955 days and starting on 26 March 2010. Figure 3-4 presents the complete QA'd Raglan sea-level record, which shows no apparent issues with datum or offset.

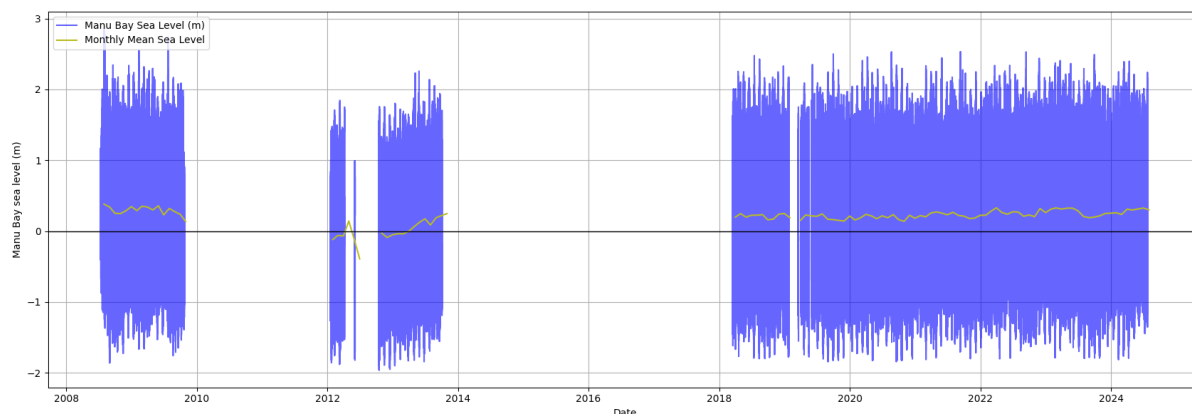


**Figure 3-4: Quality assured Raglan sea-level data.** Blue line sea level (m) relative to MVD-53. Black line zero level indicator. Yellow line monthly mean sea level.

At the Manu Bay sea-level recorder station, the available data is listed in Table 3-1, and Figure 3-5 displays the measured water level for the full duration of the gauge record. The sea level recorder was installed on 11 July 2008. Figure 3-5 illustrates that sea level measurements collected before 2018 appear to exhibit drift and inconsistent offsets of mean sea level. Consequently, only data collected after 2018 have been used in subsequent analyses. The sampling interval was initially set to 5-minutes until 2009, changed to 1-minute until 2018 when it was changed back to a 5-minute sampling interval and since October 2021 the gauge was adjust to 1-minute (Hunt 2021). There are 17 gaps in the data spanning more than 24 hours, with the largest gap being 1625 days, starting on 3 October 2013 because of a renovation to the breakwater where the gauge is situated.



As discussed by Hunt (2021) the Manu Bay sea-level record has very “noisy” sea-level record likely due to location of the gauge where wind waves, surge and infragravity waves propagating around the breakwater and up the boat ramp and including larger waves breaking over the breakwater. After adding vertical datum adjustments (see Section 3.2) the QA’d sea-level record after 2018, shows no apparent issues with datum or offset.

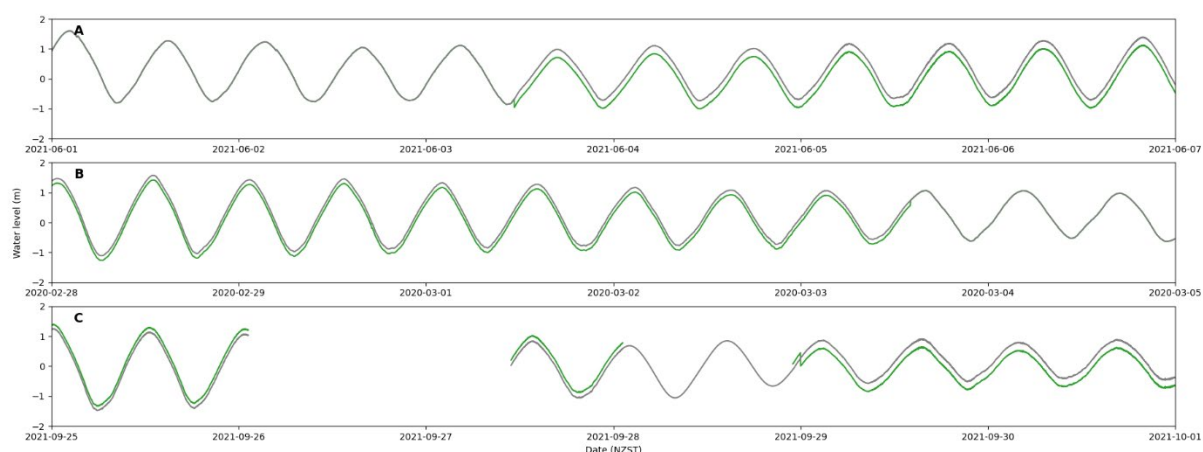


**Figure 3-5: Quality assured Manu Bay sea-level data.** Blue line sea level (m) relative to MVD-53. Black line zero level indicator. Yellow line monthly mean sea level.

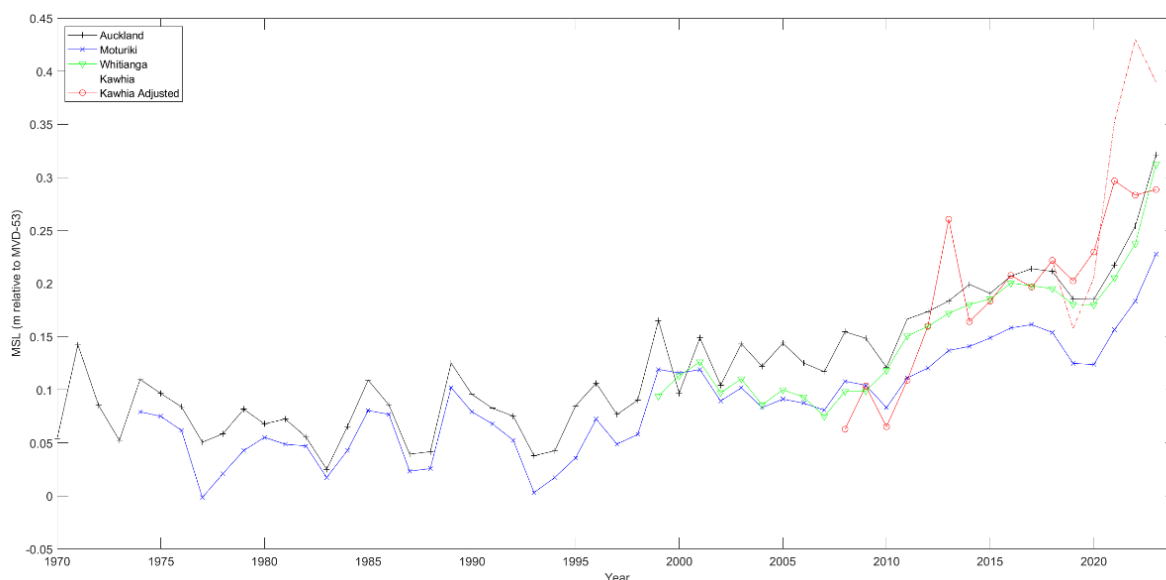
### 3.1 Drift and offset in the Kawhia Gauge

At Kawhia, a vertical correction of 0.2698 m was applied to the sea-level record from 3 June 2021 to the present (Table 3-2). This correction accounts for a step change in measured water levels following the temporary installation of a radar sensor before the upgrade from the older bubbler system on 3 June 2021. As of the time of writing, this correction had not yet been incorporated into the WRC live-feed data.

There are also three further notable deviations (jumps) in the Kawhia sea-level record (Figure 3-6). Two of the periods where these jumps occurred the sea level had a downward linear trend. Discussions with the Waikato Regional Council indicated that these periods were likely caused by sand accumulation in the bubbler orifice and the failure of the bubbler foot, leading to a temporary radar gauge being installed to keep the record going, subsequently a permanent radar unit has been installed on the wharf. These two periods were clearly identifiable, as sharp corrections were made after maintenance on 3 March 2020 and 29 September 2021 (see Figure 3-6, Table 3-2). To align the sea level data at Kawhia with the overall trend and other sites, it was necessary to detrend the record for these periods. For the earlier period starting from 3 March 2020, which is likely the result of sand accumulation, there is evidence of a slightly skewed and sawtooth tidal signal. Therefore, the start of the detrend was selected as the point when the tidal signal became skewed. In the second period (29 September 2021), associated with the loosening of the bubbler foot, it was more challenging to identify the start of the drift in the sea-level record. Here, we used the non-tidal residual (NTR) to identify a noticeable deviation at which we initiated the detrend in the sea-level record.



**Figure 3-6: Sea level at Kawhia.** Green line = measured “raw” uncorrected sea level data, grey line = corrected sea level. Panel A: sea level datum shift requiring correction which was identified by Waikato Regional Council. Panel B: drift in the sea level record. Panel C: drift in sea level gauge.

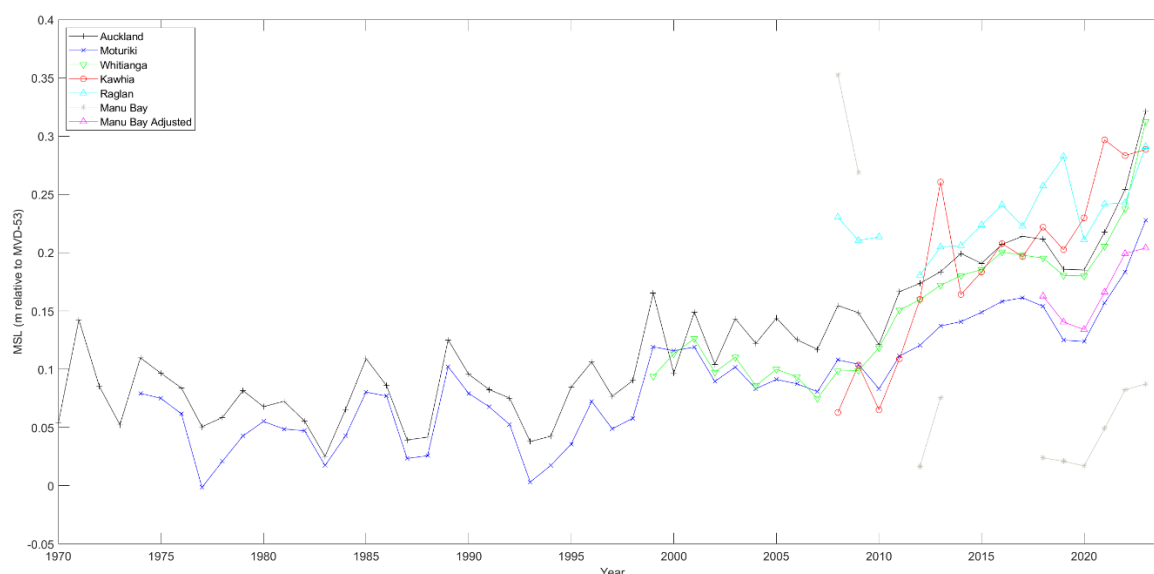


**Figure 3-7: Annual mean sea levels at Kawhia compared to other sites.** All sites show MSL relative to Moturiki vertical datum. Black line = Auckland for 1970–2023, Blue line = Moturiki for 1974–2023, Green line = Whitianga for 1999–2023, Red lines = Kawhia for 2008–2023. Dashed red line is the MSL at Kawhia before adjustment. Solid red line with circle markers is Kawhia after adjustment.

In summary, the sea level record at Kawhia exhibits three notable deviations. A datum offset issue was corrected, but the annual MSL values still increased significantly compared to other sites (Figure 3-7). Further investigation revealed two periods of sea level divergence, likely due to sand accumulation and bubbler foot failure. Detrending of the sea level data was performed, re-aligning the tide by removing the drift in the tidal signal for each period. Even with these corrections the Kawhia relative MSL is trending higher than the other WRC gauges. This could be influenced by localised land subsidence or infrastructure subsidence, which WRC could choose to investigate.

### 3.2 Drift and offset in the Manu Bay Gauge

The MSL at Manu Bay changes several times over the full deployment period 2008 to 2024. When compared to the MSL values of Moturiki, Auckland, Whitianga and Kawhia, the annual MSL for data measured before 2010 was higher than the other sites (Figure 3-8). However, after 2010 the MSL drops and the MSL becomes significantly lower when compared to other sites. In consultation with Doug Stewart from WRC a datum offset issue at Manu Bay was identified because gauge zero was set 0.177 m too high. Applying the datum offset to the Manu Bay tidal signal appears to correct the MSL for the period after 2018. This vertical offset has now been incorporated into the WRC live-feed data (Table 3-2). However, this data offset only applies to data after 2012 so data before this period remains uncorrected and has not been used in this analysis.



**Figure 3-8: Annual mean sea levels at Manu Bay compared to other sites.** All sites show MSL relative to Moturiki vertical datum. Black line = Auckland for 1970–2023, Blue line = Moturiki for 1974–2023, Red line = Kawhia for 2008–2023, Light grey line is Manu Bay before datum adjustment and pink line with triangle symbols is Manu Bay MSL after datum offset correction and removal of data before 2010.

In summary, sea level data at Manu Bay required a datum offset correction. All the available data at Manu Bay was QA'd. With this correction the annual MSL values before 2018 still appear to contain errors. Hunt (2021) identified issues pre-2018 from sediment being lodged in the aperture, this likely caused the drift pre-2018. This issue was partially corrected by modifying the aperture of the bubbler. However, due to these issues, analyses presented here were only conducted using data collected after 2018.

### 3.3 Meteorological data

In an earlier draft of this report, wind speed and direction data from NIWA Environmental Weather Stations (EWS) and MetService Automatic Weather Stations (AWS), as shown in Figure 1-1, were utilised. In this final version, we have incorporated, where possible, the wind speed and direction data supplied by WRC for the Tararu and Raglan sites. Table 3-3 outlines the sources of meteorological data used for the descriptive skew surge analysis in Section 6. The mean sea-level pressure (MSLP) measured at the Tararu gauge appears to have a sampling and offset error prior to 8 November 2011; after this date, the MSLP signal aligns well with the Firth of Thames EWS data.

Therefore, we have opted to use publicly available data from the Paeroa AWS and Firth of Thames EWS sites for the period prior to this sampling error. For the Paeroa AWS data, an offset of 0.2 hPa was applied to the MSLP to align it with the overlapping period of the Firth of Thames EWS data.

**Table 3-3: Source of meteorological data used for storm surge descriptive analysis.**

Description	Source	Distance away from sea-level gauge (km)	Latitude	Longitude
Tararu Sea level (1990-2024)	Tararu gauge	0	-37.128	175.521
Tararu MSLP (1991-2006)	Paeroa AWS	30.8	-37.373	175.684
Tararu MSLP (2006-present)	Tararu gauge	0	-37.128	175.521
Tararu Wind (2006-present)	Tararu gauge	0	-37.128	175.521
Tararu Wind (1991-2010)	Paeroa AWS	30.8	-37.373	175.684
Tararu Wind (2010-present)	Firth of Thames EWS	12	-37.2151	175.4505
Whitianga Sea level	Whitianga gauge	0	-36.833	175.709
Whitianga MSLP (2007 – 2014)	Whitianga gauge	0	-36.833	175.709
Whitianga MSLP (1999 – 2006)	Whitianga aero AWS	2.8	-36.834	175.677
Whitianga wind (1995 – 2004)	Whitianga Aero AWS	2.8	-36.834	175.677
Whitianga wind (2005 – present)	Slipper Island AWS	32	-37.052	175.943
Kawhia Sea level	Kawhia gauge	0	-38.0659	174.8232
Kawhia MSLP (2010 – present)	Kawhia gauge	0	-38.0659	174.8232
Kawhia MSLP (1990 – June 2010)	Port Taharoa AWS	15.5	-38.171	174.707
Kawhia wind (1990 – 2023)	Port Taharoa AWS	15.5	-38.171	174.707
Raglan Sea level	Raglan gauge	0	-37.795	174.8803
Raglan MSLP (2010 – Present)	Raglan gauge	0	-37.795	174.8803
Raglan Wind (2010 – Present)	Raglan gauge	0	-37.795	174.8803
Raglan MSLP (2008 – 2010)	Port Taharoa AWS	45.14	-38.171	174.707
Raglan Wind (2009 – Present)	Port Taharoa AWS	45.14	-38.171	174.707
Manu Bay Sea level	Manu Bay gauge	0	-37.8127	174.8149
Manu Bay MSLP (2011 – Present)	Manu Bay gauge	0	-37.8127	174.8149
Manu Bay Wind (1990 – Present)	Port Taharoa AWS	41.2	-38.171	174.707

## 4 Mean sea level and local vertical datum

Prior to September 2009, land heights in New Zealand were denoted using 13 local vertical datums (LVD). Within the Waikato region, two LVDs were relevant: Moturiki Vertical Datum 1953 and Tararu Vertical Datum 1952 (TVD-52). Additionally, the Auckland Vertical Datum 1946 (AVD-46) served as a nearby LVD that could be used as a point of reference. However, with the introduction of the New Zealand Vertical Datum 2009 (NZVD2009) in September 2009, these previous datums have now been superseded.

Historically, these local reference points were established by first determining Mean Sea Level (MSL) using tide-gauges, and then transferring this level to benchmarks in the surrounding inland areas through precise levelling. It is important to note that sea level varies along the coast of New Zealand, and the Local Vertical Datums (LVDs) were established at different times in the last century. As a result, the MSL levels determined at each LVD's tide-gauge differ, leading to discrepancies between adjacent datums. Additionally, in most cases, the MSL levels for these vertical datums were determined several decades ago and have not been officially updated to account for the impact of sea level rise.

MVD-53 was established as MSL at Moturiki Island from sea-level measurements between 7 February 1949 and 15 December 1952. TVD-52 was established as MSL at Tararu Point from sea-level measurements in 1922–1923 (Hannah & Bell 2012) and AVD-46 was established as MSL at Port of Auckland from 7 years of sea level measurements collected in 1909, 1917–1919 and 1921–1923 (Hannah & Bell 2012). Based on these historical measurements, the MSL for Auckland Vertical Datum-1946 (AVD-46) was set in 1946 to +1.743 m relative to the present tide gauge zero at Port of Auckland, which equals Chart Datum.<sup>2</sup>

For navigation purposes, depths on nautical charts are specified relative to Chart Datum (CD). The CD adopted usually approximates Lowest Astronomical Tide (LAT) which is the lowest tide predicted to occur under normal meteorological conditions. CD is defined with reference to permanent benchmarks ashore and the zero of the tide gauge. It is common to set the zero of the tide gauge to CD, and thus there is a local offset from CD to LVD, as shown for Auckland and Moturiki in Table 4-1.

The convention adopted for the five gauges in the Waikato region is for gauge zero = 0 m LVD. Table 4-1 and Figure 4-1 show the vertical offset between the three LVDs: Moturiki (MVD-53), Auckland (AVD-46) and Tararu (TVD-52), and NZVD2016 which can be used to convert the data to an alternative local vertical datum. The offsets are based on the LINZ survey marks described within the Table.

MSL was calculated for Auckland, Moturiki and for the WRC tide gauges relative to MVD-53, both for 2005–2023 (a full 19-year tidal epoch), and 2008–2023 (length of the Kawhia and Raglan record), and the recent decade 2013–2023 (Table 4-2). However, years with more than 31 days of missing data were excluded from the analysis to ensure accuracy. MSL at Tararu was corrected for a known land subsidence rate of –3.0 mm per year (Denys 2024). We calculated MSL over the respective epochs from annual MSL, which are plotted in (Figure 4-2). MSL appears to be tracking similarly at all locations.

---

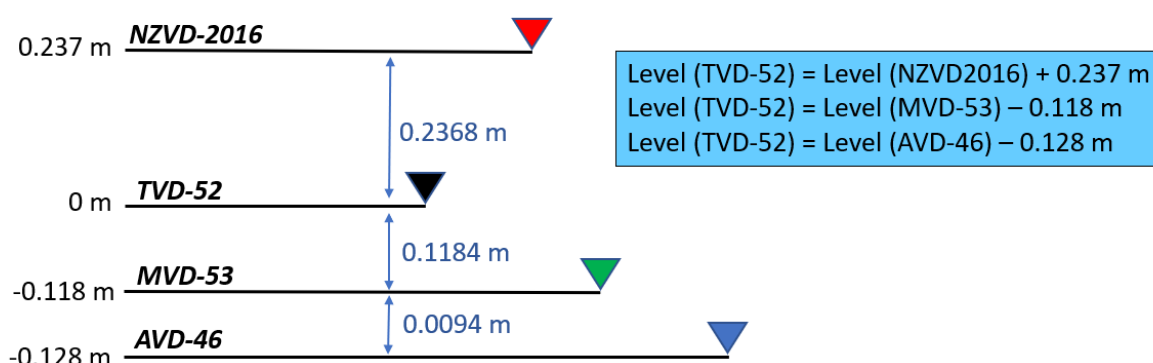
<sup>2</sup> Note: The old Auckland Harbour Board Chart Datum is 0.15 m lower prior to the present Chart Datum set in 1 Jan 1973.

MSL and MSLA at annual or longer timescales is continually changing in response to large-scale weather patterns such as El Niño–Southern Oscillation (ENSO) at 2–4 year timescales and Inter-decadal Pacific Oscillation (IPO) at longer 20–30 year timescales, as well as long-term sea-level rise. Figure 4-2 shows the annual MSL for five tide gauges. The Waikato tide gauge records are still too short to ascertain long-term sea level rise rates, but a recent rising sea-level trend can be seen in all records.

Annual MSL at Auckland and Moturiki have exhibited similar behaviour since 1974. Patterns of annual MSL at Tararu since 1990, at Whitianga since 1999, at Raglan and Kawhia since 2008 and at Manu Bay since 2018 are consistent with the Auckland and Moturiki records.

**Table 4-1: Sea-level gauge-zero offsets to local vertical datum.**

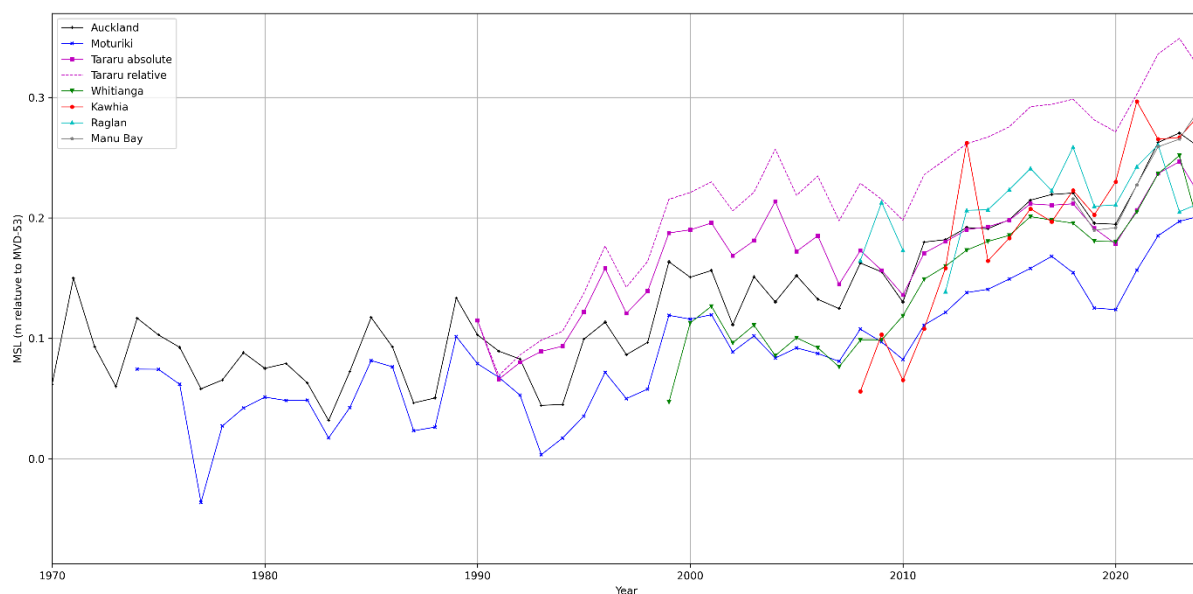
Sea-level gauge location	Local vertical datum	Gauge zero	Ref BM
Auckland	AVD-46	-1.743 m (AVD-46) -1.521 m (NZVD2016)	DD1N
Moturiki	MVD-53	-1.487 m (MVD-53)	AB5A
Whitianga	MVD-53	0 m (MVD-53) +0.291 m (NZVD2016)	BUGN
Tararu	TVD-52	0 m (TVD-52) -0.118 m (MVD-53) +0.237 m (NZVD2016)	A6BM, AF7P, AF7H
Kawhia	MVD-53	0 m (MVD-53) +0.288 m (NZVD2016)	EW67, EW68
Raglan	MVD-53	0 m (MVD-53) +0.229 m (NZVD2016)	AGE4, AGE5
Manu Bay	MVD-53	0 m (MVD-53) +0.27 m (NZVD2016)	EW6P



**Figure 4-1: Relationships and conversions between LVDs: Auckland (AVD-46), Moturiki (MVD-53), Tararu (TVD-52) and New Zealand Vertical Datum (NZVD2016).** The offsets are calculated from the LINZ survey marks in Table 4-1. NZVD2016 varies spatially so the offset shown here is specific to the tide gauge at Tararu.

**Table 4-2: MSL offsets to MVD-53 datum at Auckland, Moturiki, Whitianga, Tararu, Kawhia and Raglan.**  
MSL epoch averages were calculated from annual means.

Location	Mean sea-level offset relative to MVD-53	MSL averaging period	Description
Auckland	+0.20 m	2008–2023	Kawhia record duration
Moturiki	+0.14 m	2008–2023	
Whitianga	+0.18 m	2008–2023	
Tararu	+0.19 m	2008–2023	
Kawhia	+0.19 m	2008–2023	
Auckland	+0.18 m	1999–2023	Whitianga record duration
Moturiki	+0.12 m	1999–2023	
Whitianga	+0.15 m	1999–2023	
Tararu	+0.19 m	1999–2023	
Auckland	+0.23 m	2009–2023	Raglan record duration
Moturiki	+0.16 m	2009–2023	
Whitianga	+0.21 m	2009–2023	
Tararu	+0.21 m	2009–2023	
Kawhia	+0.25 m	2009–2023	
Raglan	+0.23 m	2009–2023	
Auckland	+0.22 m	2018–2023	Manu Bay Record duration
Moturiki	+0.21 m	2018–2023	
Whitianga	+0.15 m	2018–2023	
Tararu	+0.20 m	2018–2023	
Kawhia	+0.20 m	2018–2023	
Raglan	+0.22 m	2018–2023	
Manu Bay	+0.22 m	2018–2023	
Auckland	+0.19 m	2013–2023	Recent decade
Moturiki	+0.13 m	2013–2023	
Whitianga	+0.16 m	2013–2023	
Tararu	+0.19 m	2013–2023	
Kawhia	+0.20 m	2013–2023	
Raglan	+0.14 m	2013–2023	
Auckland	+0.18 m	2005–2023	19-year tidal epoch
Moturiki	+0.19 m	2005–2023	
Whitianga	+0.19 m	2005–2023	
Tararu	+0.18 m	2005–2023	



**Figure 4-2: A comparison between the annual mean sea level of seven tide gauges.** Tararu for 1990-2023, Whitianga for 1999-2023, Kawhia for 2008-2023, Moturiki for 1974-2023, Auckland for 1970-2023, Raglan for 2008 to 2023. All sites show relative MSL, which is the elevation relative to the local land elevation. Absolute MSL is also shown for Tararu, after correcting for a land subsidence rate of -3.1 mm/year.

## 4.1 Sea-level rise detrending

All sea-level records exhibit a rising trend in MSL. MSLA, tides and surges all ride on top of the MSL. To analyse changes in storm tides and surge through time, the underlying sea-level rise trend must first be removed. There are two main causes of rising MSL through time:

1. Absolute (or eustatic) rise in ocean levels around New Zealand.
2. Relative (or local) sea-level rise, which is the net rise from absolute, regional-sea offsets and local vertical land movement, measured relative to the local landmass.

The sea level gauges sit on the land surface, so they are recording relative sea-level rise (RSLR). It is RSLR that is observable through time in Figure 4-2. However, because the land surface is subsiding so rapidly at Tararu compared to the other gauges, we also plotted a VLM-adjusted absolute SLR comparison for the Tararu record in Figure 4-2.

To detrend the datasets, linear fits to the relative annual MSL were calculated using a least-squares analysis (Table 4-3). These linear fits were subtracted from the non-tidal residuals before undertaking further analyses.



**Table 4-3: Linear fits for sea level detrend.**

Sea Level record	Linear detrend (mm/year)	Zero axis crossing date for linear fit detrending (MVD-53)
Auckland	1.78	7 December 1921
Moturiki	2.84	13 December 1967
Kawhia	13.16	11 May 2001
Tararu	6.6	15 May 1973
Whitianga	6.28	10 December 1987
Raglan	3.69	28 November 1958
Manu Bay	16.0	15 May 2006

## 4.2 Annual mean sea-level trends

These projections use updated shared socio-economic pathways (SSPs), which incorporate socioeconomic assumptions and emissions trajectories. The updated SSPs are outlined in the Ministry for the Environment (MfE) Coastal Hazards and Climate Change Guidance (MfE 2024). The scenarios cover a wide range of plausible societal and climatic futures, from a 1.5°C ‘best-case’ low-emissions scenario (SSP1-2.6) to a high-emissions scenario (SSP5-8.5) with over 4°C of warming by 2100 (Chen et al., 2021 (Chen et al. 2021)). Even under the low-emissions scenario (SSP1-2.6), average SLR around Aotearoa could exceed 1 m shortly after 2200 (Table 6).

**Table 4-4: Estimated years when absolute sea-level rise (SLR) thresholds may be reached based on recommended projections for a central location in Aotearoa New.** Adapted from the MfE Coastal Hazards and Climate Change Guidance.

SLR (metres)	Year achieved for SSP5-8.5 H+ (83rd percentile)	Year achieved for SSP5-8.5 (median)	Year achieved for SSP3-7.0 (median)	Year achieved for SSP2-4.5 (median)	Year achieved for SSP1-2.6 (median)
0.2	2035	2040	2045	2045	2050
0.3	2050	2055	2060	2060	2070
0.4	2055	2065	2070	2080	2090
0.5	2065	2075	2080	2090	2110
0.6	2070	2080	2090	2100	2130
0.7	2080	2090	2100	2115	2150
0.8	2085	2100	2110	2130	2180
0.9	2090	2105	2115	2140	2200
1.0	2095	2115	2125	2155	>2200
1.2	2105	2130	2140	2185	>2200
1.4	2115	2145	2160	>2200	>2200

SLR (metres)	Year achieved for SSP5-8.5 H+ (83rd percentile)	Year achieved for SSP5-8.5 (median)	Year achieved for SSP3-7.0 (median)	Year achieved for SSP2-4.5 (median)	Year achieved for SSP1-2.6 (median)
1.6	2130	2160	2175	>2200	>2200
1.8	2140	2180	2200	>2200	>2200
2.0	2150	2195	>2200	>2200	>2200

Figure 4-3 shows the annual mean sea level measurements from four locations, these represent relative sea-level rise (RSLR): Auckland, Moturiki, Tararu, and Whitianga, all normalised to a zero datum of 2005. Of the Waikato Regional Council (WRC) gauge sites, only Whitianga and Tararu contain data extending back beyond 2005, making them suitable for normalisation with the sea-level rise scenarios. This allows for direct comparison with the five sea-level rise scenarios from the MfE National Coastal Guidance.

- **Auckland and Moturiki:** The sea-level measurements from these locations behave in a similar manner relative to each other. They appear to be tracking lower than the SSP5-8.5H+ scenario but slightly above the other projections.
- **Tararu:** This gauge shows good agreement with the Auckland and Moturiki measurements, despite having a shorter record.
- **Whitianga:** The relative sea-level measurements- here are tracking in alignment or slightly higher than the SSP5-8.5H+ projection. This could be caused by local land subsidence and a reliable measure of VLM is required to confirm this. Another possible influence is a regime shift in the Whitianga record that occurred in about 2006 (Stephens et al. 2015). From 2000–2006 the  $M_2$  tide had a reduced amplitude. This coincides with relatively flat MSL trajectory (Figure 3-2), which would affect the normalisation to 2005 datum, potentially causing the Whitianga record to plot higher.

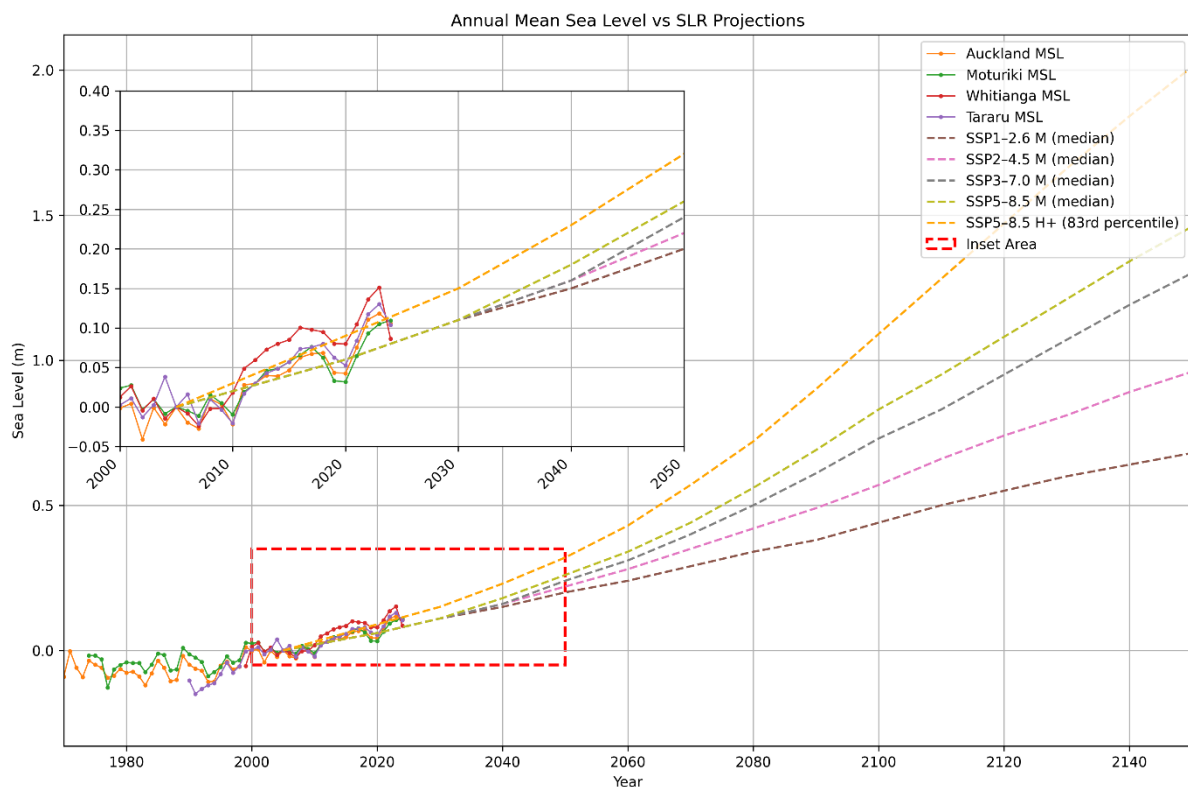
The date in Figure 4-3 has been limited to show data from 1980 to 2150 and shows both historical data and future projections under various climate change scenarios.

Figure 4-4 and Figure 4-5 show the annual mean sea levels at Whitianga and Tararu in MVD-53, along with future sea-level rise projections<sup>3</sup>. The projections have been adjusted to align with the mean sea level recorded at Whitianga and Tararu in the year 2005, referenced to MVD-53.

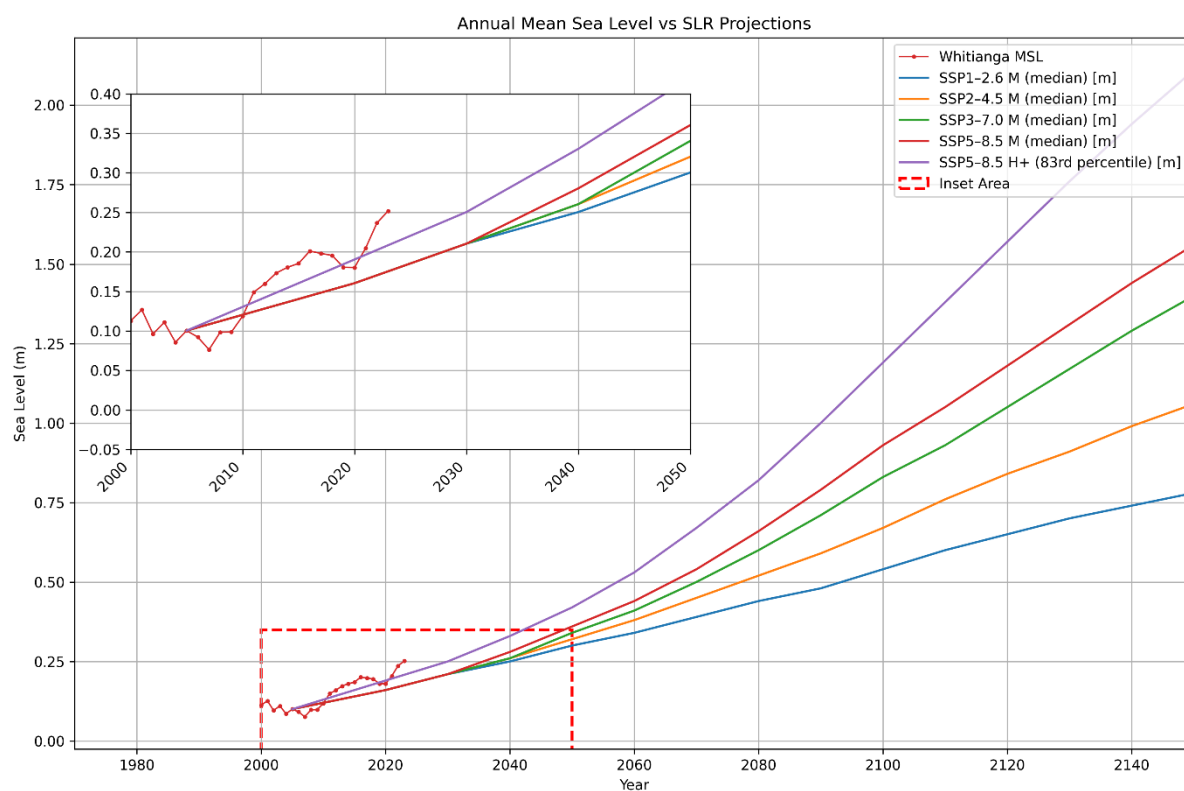
At least 50 years of record is required, due to the influence of climate variability, to determine a statistically significant historical rate of change in mean sea level. The plot overlaps historical mean sea level change measurements with sea-level rise projections. This indicates how sea level is tracking relative to projections, but the period of overlap is small and does not imply that future mean sea level will follow these projections, as it will depend on future climate change and vertical land motion.

<sup>3</sup> Note: Only the Whitianga and Tararu sea-level gauges have records extending back to 2000, allowing alignment with the sea-level projection baseline.

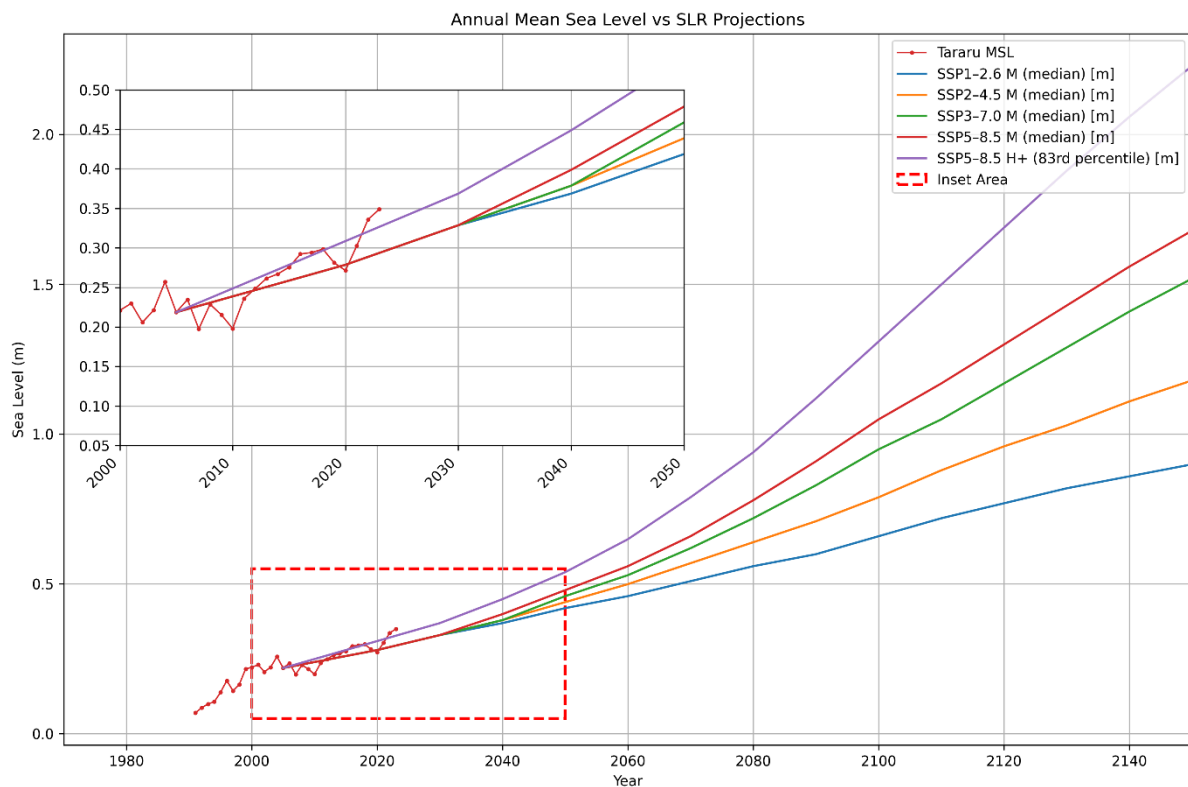
Understanding the relationship between sea-level changes and climatic patterns, such as the El Niño–Southern Oscillation (ENSO) and the Interdecadal Pacific Oscillation (IPO), requires extensive datasets due to the multi-decadal nature of these cycles. Studies have shown that ENSO and IPO significantly influence sea surface temperatures across various regions, including Australia and the southwestern United States, with the IPO exhibiting a quasi-oscillatory period of 40–60 years (Dong and Dai 2015). Given this timescale, sea-level records shorter than 30 years, such as those from the Waikato gauges, are insufficient for establishing reliable correlations. The complexity and variability of these climate systems, compounded by potential shifts due to climate change, make it challenging to predict the strength and nature of future ENSO and IPO cycles and their impact on sea levels. NIWA is currently developing a methodology to assess long-term sea-level rise trends.



**Figure 4-3:** Annual mean sea level measurements from Auckland, Moturiki, Tararu, and Whitianga, normalized to a zero datum in 2005, alongside five projected sea-level rise trajectories.



**Figure 4-4: Whitianga annual mean sea-level in Moturiki Vertical Datum (MVD-53).** Ministry for the Environment sea-level rise scenarios are shifted to align with the mean sea level at Whitianga in 2005.



**Figure 4-5: Tararu annual mean sea-level in Moturiki Vertical Datum (MVD-53).** Ministry for the Environment sea-level rise scenarios are shifted to align with the mean sea level at Tararu in 2005.

## 5 MHWS and tide exceedance curves

The mean high-water springs (MHWS) elevation is typically calculated based on tidal observations over a specific period of time. There are several methods to calculate the MHWS elevation, but one commonly used approach is the harmonic method. We undertook a tidal harmonic analysis on the quality assured sea-level gauge records from Whitianga, Kawhia, Tararu, Raglan and Manu Bay. Tide exceedance curves were then generated by predicting 100 years of high tides and plotting the cumulative exceedance of the high tides. These curves exclude weather (e.g. SS) and climate-related (SLA) effects. High-tide exceedance curves, based on the cumulative distribution function (CDF) of long-term tide predictions, allow MHWS to be consistently defined based on a common exceedance threshold that is independent of tide regime (Bell 2010; Stephens, Scott A. et al. 2014).

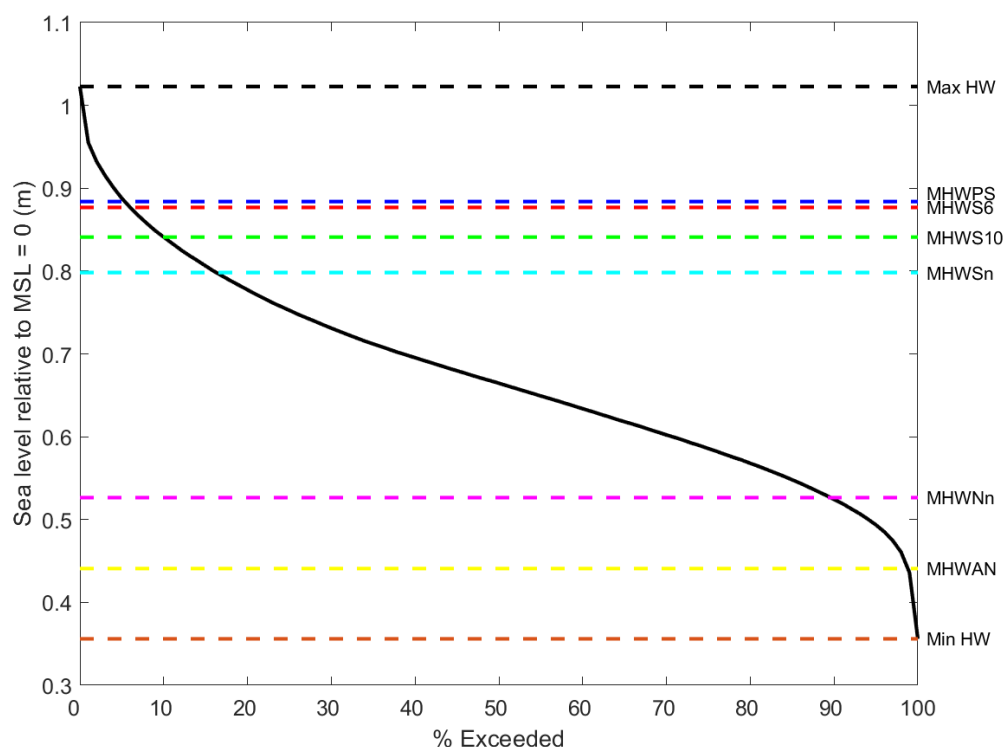
Tide predictions were undertaken using the Unified Tidal Analysis and Prediction, using the UTide Matlab Functions (Codiga, D.L. 2011b). The analyses fitted the standard 67 harmonics and used a signal to noise ratio of 10. To predict high tides, the method employed involved calculating tidal harmonics annually and then computing their vector average. The tidal predictions deliberately excluded the gravitational solstice tides, namely  $S_a$  and  $S_{sa}$ , as they were instead accounted for in the seasonal sea-level cycle. The rationale behind this exclusion is that solstice tides, although typically insignificant, are not solely influenced by solar gravity. They receive a boost from other factors tied to the sun's seasonal cycles, such as solar heating of the oceans and atmospheric circulation changes (Boon 2013). Consequently, it is appropriate to incorporate these effects into the sea level anomaly (SLA) component.

Figure 5-1, Figure 5-2, Figure 5-3, Figure 5-4 and Figure 5-5 provide graphical representations of the tide exceedance curves for Whitianga, Kawhia, Tararu, Raglan and Manu Bay relative to a mean sea level (MSL) set to zero. The corresponding data used to construct these plots is summarized in Table 5-1. To convert from MSL=0 to the local vertical datum (LVD), a datum offset should be added. This offset can be found in Table 4-2. MHWS elevations are presented using several definitions for the calculation of MHWS.

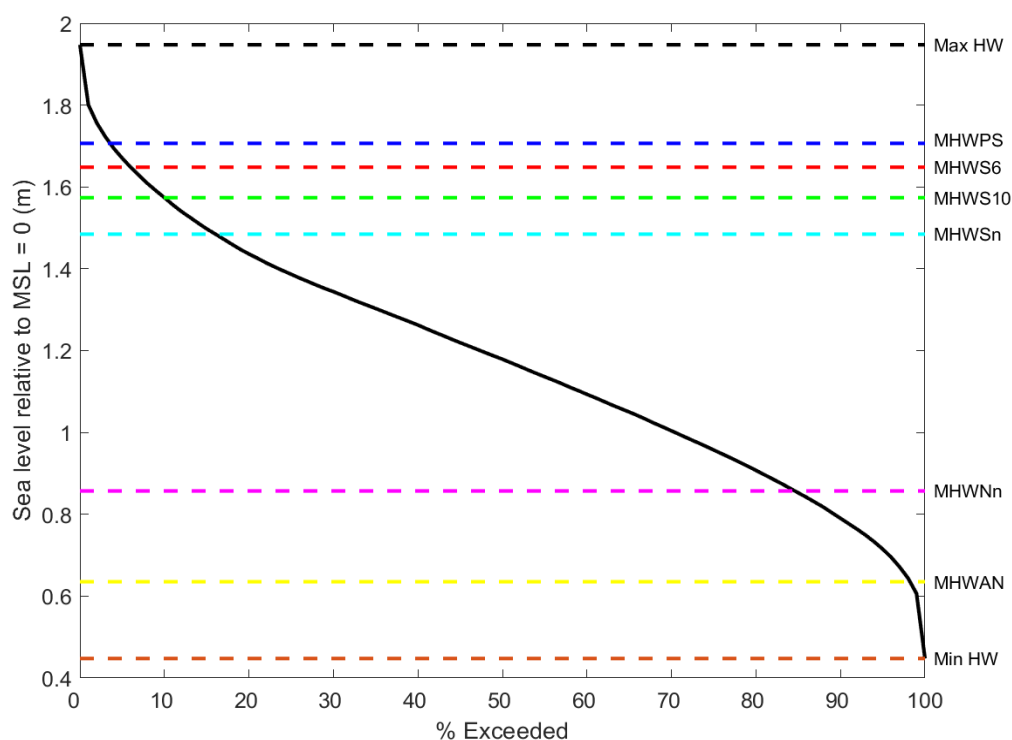
In New Zealand, the intersection of the mean high-water springs (MHWS) elevation with the land delineates the landward jurisdictional boundary of the coastal marine area. However, MHWS can be defined in different ways. For instance, one nautical definition equates  $MHWS_n$  to the sum of  $M_2$  (principal lunar semi-diurnal) and  $S_2$  (principal solar semi-diurnal) components (Pugh 1987). Alternatively, NIWA's red-alert tide calendar notifies users when high-tide peaks equal or surpass the combined amplitudes of the three largest tidal harmonics. This combination is known as mean high-water perigean springs (MHWPS) and includes  $M_2$ ,  $S_2$ , and  $N_2$  tidal constituents (larger lunar elliptic semi-diurnal) (Walters et al. 2001). Although New Zealand's tidal regime is predominantly semi-diurnal, with minor diurnal constituents, there exists a contrast between the west and east coasts.  $M_2$  and  $S_2$  dominate the tides on the west coast, resulting in fortnightly spring and neap tides of nearly equal amplitudes. Conversely, the east coast experiences a tidal regime dominated by the 27.5-day cycle of perigean and apogean tides, with a single prominent spring tide per month due to the diminished amplitude of the  $S_2$  solar tide (Walters et al. 2001). Given the variability in tide regimes, the definitions of MHWS (or red-alert elevations) can become inconsistent when tidal characteristics vary significantly along the New Zealand coast (Stephens et al. 2014).

Bell (2010) demonstrated an approach to address this inconsistency by utilizing high-tide exceedance curves based on the cumulative distribution function (CDF) of long-term tide predictions. This method enables a consistent definition of MHWS based on a common exceedance threshold that is independent of the tide regime. For example, MHWS–10 can be defined as the elevation equalled or exceeded by only the largest 10% of all high tides. Similarly, MHWS–6 corresponds to the elevation equalled or exceeded by the largest 6% of all high tides. The use of tidal exceedances allows for a more standardized and comparable characterization of MHWS across different tidal environments (Bell 2010).

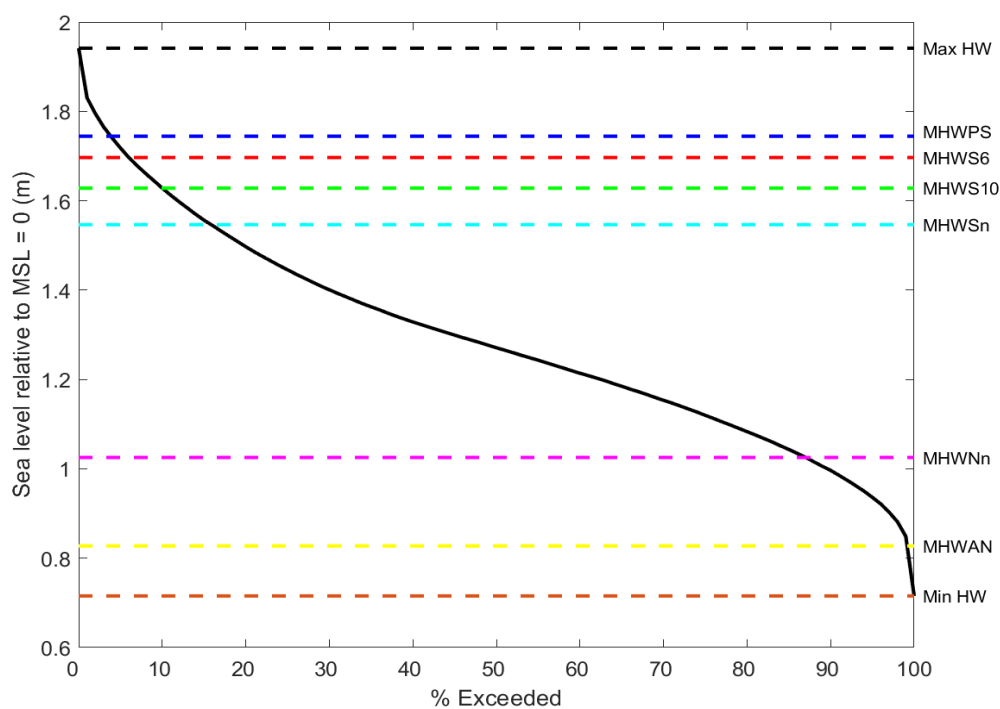
Mean high water spring cadastral (MHWS\_C) is based on the average of the heights of two successive high waters during a period of about 24-hours in each semi-lunation (approximately every 14 days) cycle when the tide is the greatest (Baker, 1991)



**Figure 5-1: High-tide markers at Whitianga relative to MSL=0.** MAX/MIN HW = maximum and minimum high waters from predicting 100 years of high tides; MHWS–6 = tide height exceeded by 6% of all tides; MHWS–10 = tide height exceeded by 10% of all tides; MHWPS = mean high water perigean springs ( $M_2 + N_2 + S_2$ ), MHWNn = Mean high-water neap, MHWAN = Mean high water apogean neap.

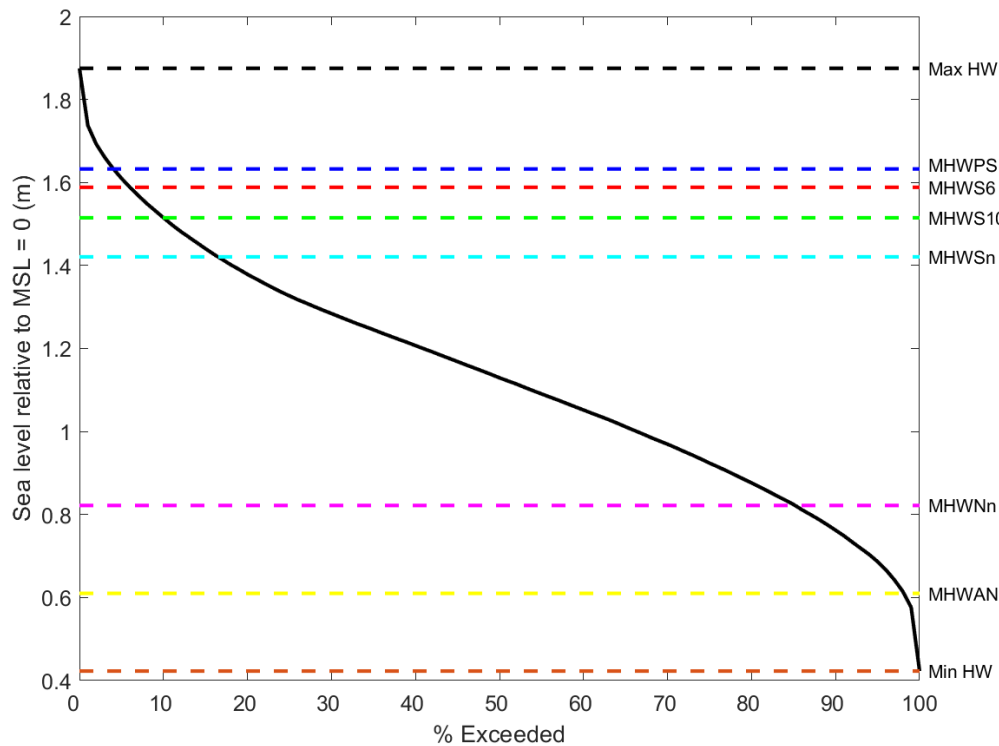


**Figure 5-2: High-tide markers at Kawhia relative to MSL=0.** MAX/MIN HW = maximum and minimum high waters from predicting 100 years of high tides; MHWS-6 = tide height exceeded by 6% of all tides; MHWS-10 = tide height exceeded by 10% of all tides; MHWPS = mean high water perigean springs ( $M_2 + N_2 + S_2$ ), MHWNn = Mean high-water neap, MHWAN = Mean high water apogean neap.

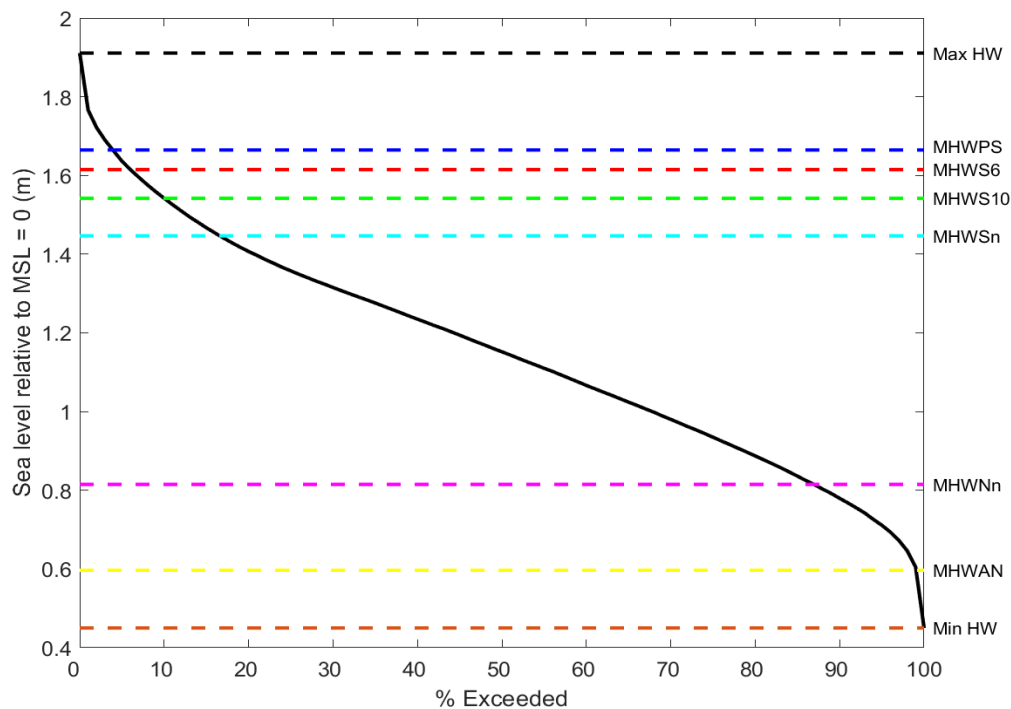


**Figure 5-3: High-tide markers at Tararu relative to MSL=0.** MAX/MIN HW = maximum and minimum high waters from predicting 100 years of high tides; MHWS-6 = tide height exceeded by 6% of all tides; MHWS-10 = tide height exceeded by 10% of all tides; MHWPS = mean high water perigean springs ( $M_2 + N_2 + S_2$ ), MHWNn = Mean high-water neap, MHWAN = Mean high water apogean neap.





**Figure 5-4: High-tide markers at Raglan relative to MSL=0.** MAX/MIN HW = maximum and minimum high waters from predicting 100 years of high tides; MHWS-6 = tide height exceeded by 6% of all tides; MHWS-10 = tide height exceeded by 10% of all tides; MHWPS = mean high water perigean springs ( $M_2 + N_2 + S_2$ ), MHWNn = Mean high-water neap, MHWAN = Mean high water apogean neap.



**Figure 5-5: High-tide markers at Manu Bay relative to MSL=0.** MAX/MIN HW = maximum and minimum high waters from predicting 100 years of high tides; MHWS-6 = tide height exceeded by 6% of all tides; MHWS-10 = tide height exceeded by 10% of all tides; MHWPS = mean high water perigean springs ( $M_2 + N_2 + S_2$ ), MHWNn = Mean high-water neap, MHWAN = Mean high water apogean neap.

**Table 5-1: Analysis of high waters at Whitianga, Kawhia and Tararu relative to MSL = 0.** MHWS\_C = mean high water spring cadastral, MHWS-6 = mean high water spring height exceeded by 6% of all tides, MHWS-10 = mean high water spring height exceeded by 10% of all tides, MHWPS = mean high water perigean spring ( $M_2 + S_2 + N_2$ ). The MHWS elevations presented here are given relative to a zero MSL. To calculate the elevations relative to MVD-53, add the present-day MSL datum offsets in Table 4-2.

MHWS marker	Whitianga	Kawhia	Tararu	Raglan	Manu Bay
Lowest					
Astronomical Tide (m) (LAT)	0.36	0.49	0.69	0.45	0.45
MHWPS (m)	0.89	1.70	1.74	1.63	1.66
MHWS_C (m)	0.84	1.62	1.61	1.53	1.53
MHWS-6 (m)	0.88	1.67	1.69	1.57	1.58
MHWS-10 (m)	0.85	1.59	1.63	1.50	1.51
Highest					
Astronomical Tide (m) (HAT)	1.03	1.97	1.93	1.86	1.88

## 5.1 Mean high-water springs in the Waikato region

Similar to the earlier work undertaken by Stephens, S. A. et al. (2015) we find that tidal amplitudes inside Whitianga Harbour are lower than those outside of the Harbour. Stephens, S. A. et al. (2015) describes how the tidal signal at Whitianga is dampened due to tidal shoaling over the ebb-tidal delta, which reduces the amplitude of the tidal wave inside the harbour. This tidal damping of the main tidal constituents was also noted by Goring, Derek G. (1999) and how the presence of overtides were generated by seabed friction through the shallow entrance to the harbour. Consequently, the MHWS-10 value of 0.96 m, as derived from the EEZ-tidal model, should apply to the open coast of Mercury Bay (including Cooks Beach, Maramaratotara Bay, Ohuka Bay and Buffalo Beach away from the Entrance). However, GIS map analyses derived from LiDAR should include the lower MHWS-10 value of 0.85 m for evaluating the inundation potential within the environs of Whitianga Harbour and Entrance.

NIWA used the EEZ tide model to generate tidal predictions for high tides over a 100-year period and analysed the exceedance distribution curve to evaluate the 10% exceedance value known as MHWS-10 and MHWS-6. The baseline for this analysis was a MSL = 0 (i.e., the tide rides on the back of a still water level set to zero). A MSL offset from the relevant local vertical datum is then required to situate MHWS values locally with respect to the required datum (see below).

MHWS-10 values for the Waikato west coast from the EEZ tide model compare well with the values from the Kawhia and Port Taranaki gauges, so no adjustments were needed for the Waikato west coast.

Comparisons of the EEZ tidal model results with gauge data on the east coasts showed:

- MHWS-10 in the Firth of Thames was slightly underestimated by the EEZ tide model by up to 4 cm at the southern end at Thames (probably due to the tide wave shoaling with no mean tide set-up included in ocean tide model). The value at Thames was adjusted upwards based on MHWS-10 derived from the Tararu gauge, and then proportionately interpolated throughout the Firth up to Port Jackson and Waiheke

Island where the tide model values agree with spring-tide ranges from other data sources (e.g., Secondary Port data from the LINZ Nautical Almanac).

- On the east Coromandel coast, most gauge data records (e.g., Port Charles, Whangamata, Tairua) indicated the model-derived MHWS-10 or alternative Mean HW Perigean Spring (MHWPS) values were in close alignment.

The final set of MHWS-10 estimates from the EEZ tidal model, adjusted where needed as described above, are shown for the Waikato regional coastlines in Table A-1.

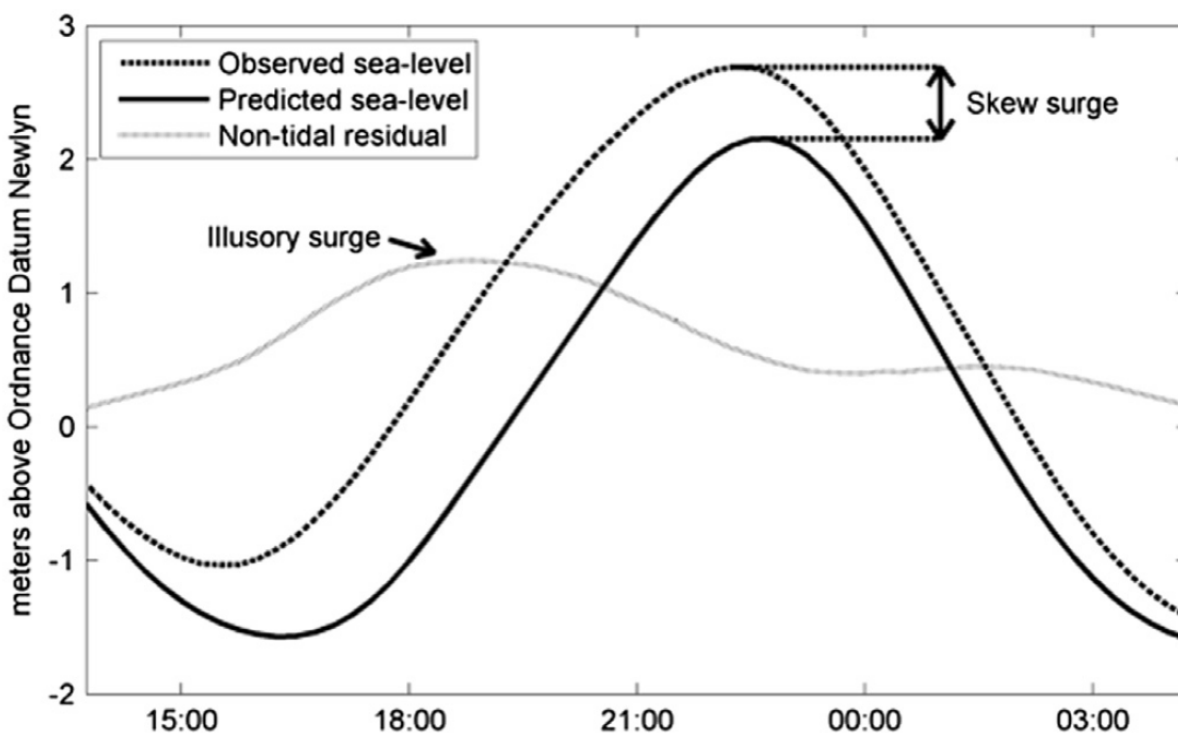
Note: On open-coast beaches, a purely-tidally derived MHWS will underestimate the height of the upper part of the natural beach due to wave set-up and run-up from breaking waves, which help to form the beach.

## 6 Skew Surge

The earlier work by Stephens, S. A. et al. (2015) reported on storm-surge. We chose to use skew surge instead of storm surge for these analyses.

Skew surge is a more relevant metric of surge in tidally dominant locations like NZ (Merrifield et al. 2013), because the extreme storm tide and resulting flooding exposure (excluding wave overtopping) usually occurs for a few hours around the high tide. Also, we employed the skew-surge joint-probability method as best practice to undertake the extreme sea-level analyses (Batstone et al., 2013).

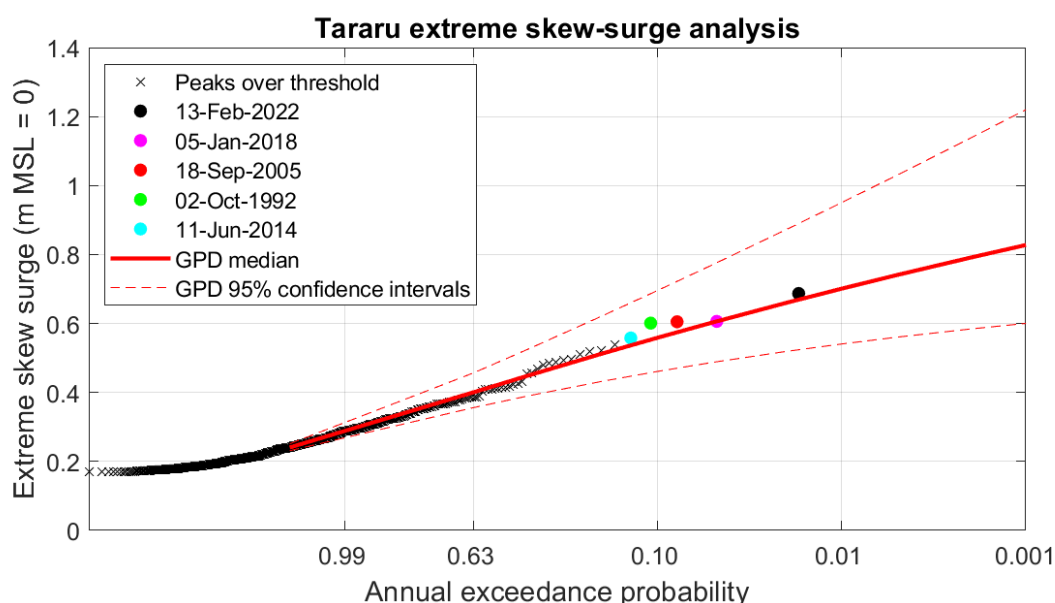
Whereas storm surge is calculated by subtracting the predicted tide at the same sampling interval as the sea-level record, skew surge was calculated as the absolute difference between the maximum recorded storm tide (Figure 6-1) during each tidal cycle and the predicted maximum astronomical tidal level for that cycle, irrespective of differences in timing between these (Batstone et al., 2013; Williams et al., 2016). Skew surge may occur at a different time to the tide peak, hence the term skew surge—skewed in time. There is one skew-surge measurement per high tide.



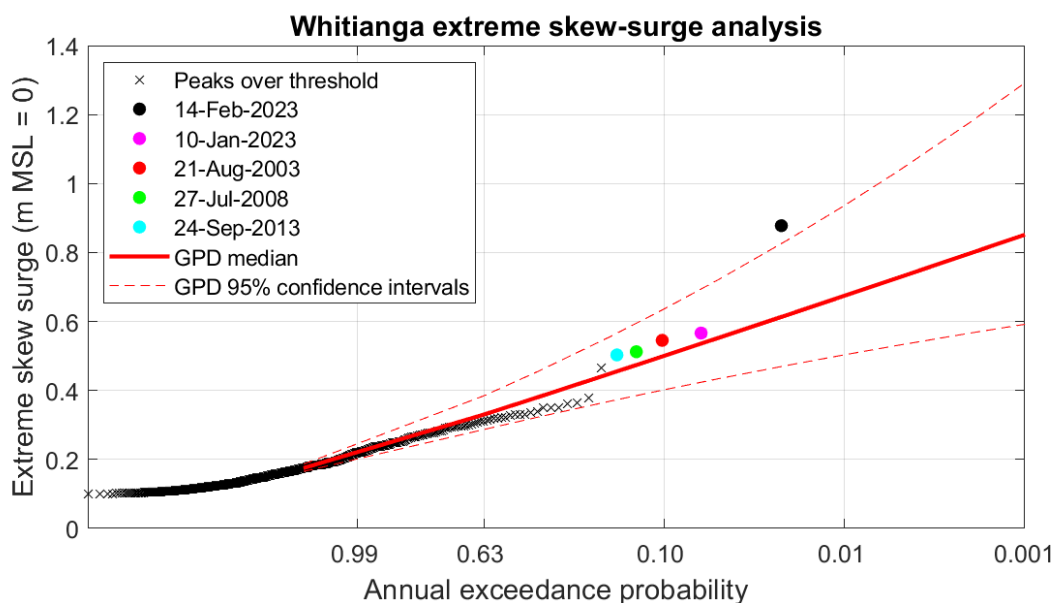
**Figure 6-1: Skew-surge illustration.** Source: (Batstone et al. 2013). Sea level observed by the tide gauge at Sheerness, UK, during the passage of a storm surge on 11–12 January 2006. The non-tidal residual is the result of subtracting the predicted tide level from the observed sea level in this shallow region. The increase in water depth due to the storm surge leads to an increase in the tidal wave speed, resulting in high water occurring, in this case, 30 minutes early. The ‘skew-surge’ is the difference between observed and predicted sea-levels at high water, irrespective of any timing difference. It provides a more reliable measure of surge than the non-tidal residual. The latter includes ‘illusory surges’ that are an artefact of the calculation process of the components and do not represent actual surge magnitudes.

Extreme skew surge distributions were fitted to each skew surge record using a generalised Pareto distribution (GPD) fitted to skew surge maxima selected using peaks-over-threshold (POT) method. The POT were separated by a minimum of at least 3 days to ensure independence (i.e., sampling only one maxima for any storm). The skew-surge height threshold for POT selection was chosen as the smallest value for which the shape and scale factors of the GPD fit simultaneously remained within 95<sup>th</sup> percent confidence intervals (Coles, 2001). The GPD was fitted using the 'gpfitt.m' function within Matlab software. The function using a maximum likelihood method to fit the GPD and returns 95% confidence intervals for parameter estimates. This is a standard methodology for extreme value fitting—the method by which POT data are selected has the biggest influence on results (Coles, 2001).

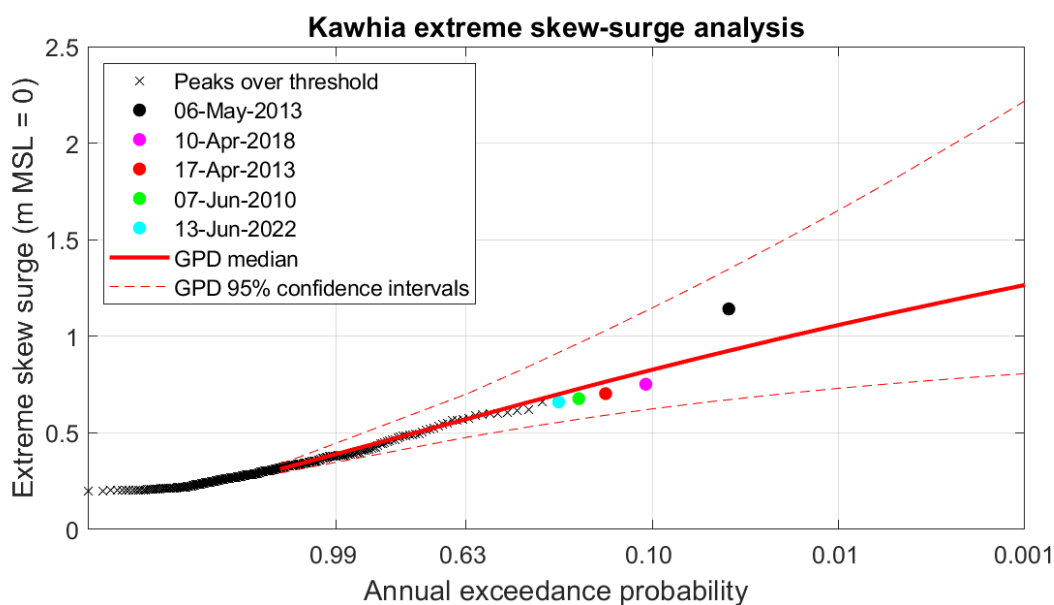
We note that there is statistical uncertainty in the extreme skew surge models at all five sites (Figure 6-2, Figure 6-3, Figure 6-4, Figure 6-5 and Figure 6-6), but the Raglan and Manu Bay extreme storm surge distributions have higher uncertainty due to their short records, particularly Manu Bay which also exhibits a bounded (downward curving) nature. Nevertheless, all of the measured skew surges fall inside the confidence intervals of the fitted extreme skew-surge distribution. Some of this uncertainty is statistical due to the model fitting—the longer the record the more this reduces. Some of it is due to the weather systems that drive the surges having different meteorology, and so the models are an imperfect fit to the inhomogeneous surge population. There are different populations of storms and surges, certain types of storms drive the largest surges. For a very long record, the surges could be separated into populations and extreme-value modelling could be done for unique storm types. But for records the length of these, all surges must be used to reduce statistical uncertainty as much as possible. Table 6-1 provides the frequency–magnitude distribution of extreme skew-surges.



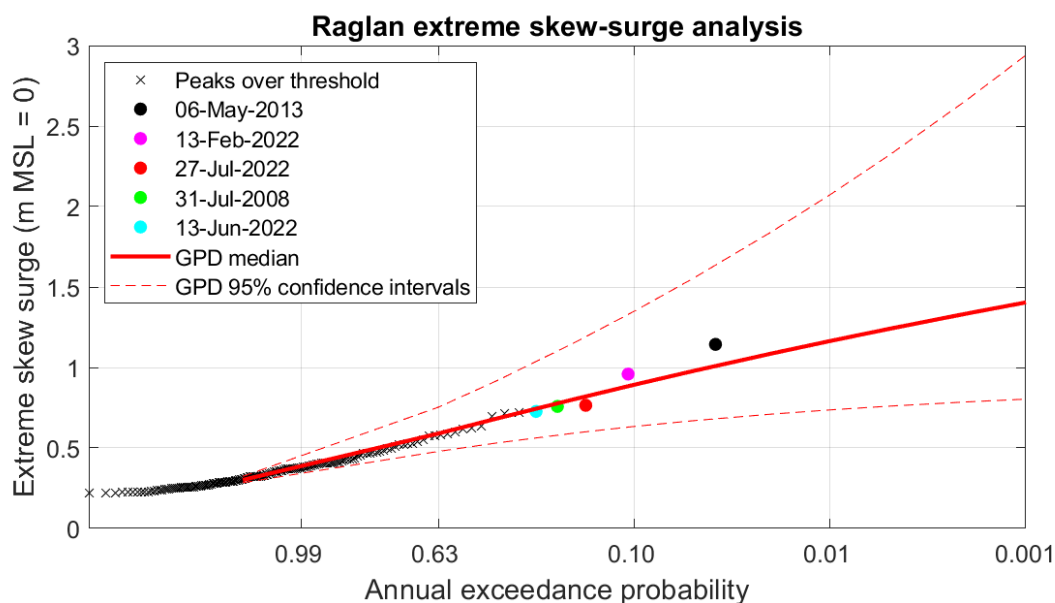
**Figure 6-2: Tararu extreme value analysis of skew surges using a GPD fitted to skew surges over a high threshold.** GPD = generalised Pareto distribution fitted to skew surge peaks. Red dashed lines represent 95% confidence intervals.



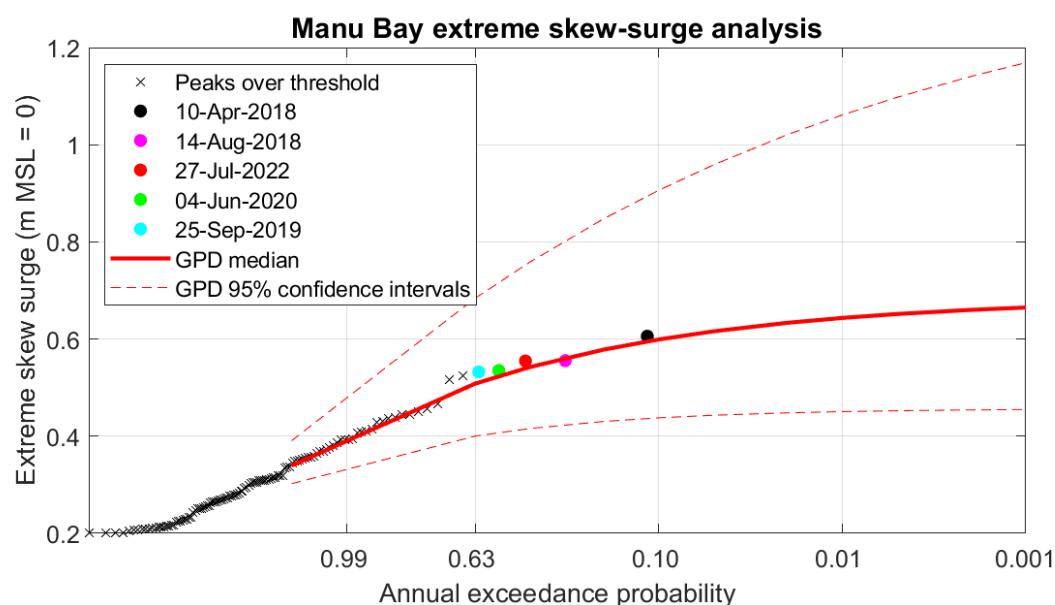
**Figure 6-3: Whitianga extreme value analysis of skew surges using a GPD fitted to skew surges over a high threshold.** GPD = generalised Pareto distribution fitted to skew surge peaks. Red dashed lines represent 95% confidence intervals.



**Figure 6-4: Kawhia extreme value analysis of skew surges using a GPD fitted to skew surges over a high threshold.** GPD = generalised Pareto distribution fitted to skew surge peaks. Red dashed lines represent 95% confidence intervals.



**Figure 6-5: Raglan extreme value analysis of skew surges using a GPD fitted to skew surges over a high threshold.** GPD = generalised Pareto distribution fitted to skew surge peaks. Red dashed lines represent 95% confidence intervals.



**Figure 6-6: Manu Bay extreme value analysis of skew surges using a GPD fitted to skew surges over a high threshold.** GPD = generalised Pareto distribution fitted to skew surge peaks. Red dashed lines represent 95% confidence intervals.

**Table 6-1: Frequency–magnitude distribution of extreme skew-surges.** Skew surge heights (m) were modelled using GPD fitted to peaks-over-threshold data.

AEP	ARI	Whitianga	Tararu	Kawhia	Raglan	Manu Bay
		GPD	GPD	GPD	GPD	GPD
0.63	1	0.33	0.4	0.57	0.59	0.46
0.39	2	0.38	0.45	0.65	0.68	0.49
0.18	5	0.45	0.52	0.75	0.81	0.53
0.10	10	0.5	0.57	0.83	0.9	0.55
0.05	20	0.55	0.62	0.90	0.98	0.57
0.02	50	0.61	0.68	1.00	1.09	0.59
0.01	100	0.67	0.73	1.07	1.18	0.6

## 6.1 Descriptive analysis of the largest skew surge events

The largest skew surge events on record for each sea level gauge are described in this Section. The largest five independent skew surges were chosen for Whitianga, Tararu and Kawhia records and the largest three for the shorter Raglan and Manu Bay records.

In many cases, the dates of the largest skew-surge events differ from the dates of the largest storm-surge events identified in the 2015 study. There are two reasons for this:

1. Skew-surge and storm surge are different metrics. In 2015 the storm surge was calculated using a wavelet filtering method, which was in common use in New Zealand at the time for the separation of various sea-level components (Goring, D. G. et al. 2011). We no longer use wavelet filtering because the sum of the components doesn't exactly add to the original totals, due to signal leakage in the filter. This is another good reason to use skew surge as an unambiguous measure.
2. Surge is derived from the non-tidal residual, which includes MSL. The non-tidal residual must be detrended before calculating surge, otherwise surges would appear to be increasing in height through time, but this is an artifact of sea-level rise. The record durations to 2024 are longer than to 2015 so the long-term linear fits and the detrending is different. For example, at Whitianga location, the linear detrend was 0.49 mm/year to 2015, whereas was 6.2 mm/year to January 2024. The MSL trends have steepened since 2015, so the detrending slightly elevates more surge events from earlier in the record, relative to those which are slight depressed late in the record. These differences are of only ~12 mm, but, along with the change to use of the skew-surge metric as opposed to the storm surge metric used in the 2015 report, they are enough to change the ordering of the largest surge events identified.
3. One limitation of skew-surge analysis is that it aligns with high tides and may not be useful for planning applications where low-tide surge events are important, such as in flood gate design. Addressing these low-tide surge events would require further analysis, which is beyond the scope of the current work

Multiple wind data sources were needed for the descriptive analysis, and where possible, we have prioritised using WRC weather data. This does not affect the overall description of skew surge responses to meteorological conditions. Using local meteorological data is preferable for analysing



significant skew surge events. However, when combined with weather maps, we believe the descriptive analyses remain valid. Spatial plots of mean sea-level pressure and winds were sourced from NIWA's EcoConnect Forecast Archive for dates after 2007, while maps for dates prior to 2007 were created using the fifth-generation ECMWF reanalysis (ERA5). Atmospheric pressure fields do not vary significantly over the spatial scales considered, meaning inverse barometer calculations are unlikely to be strongly impacted.

The inverse barometer (IB) was analysed at each sea level gauge. In the deep ocean, far from land, changing atmospheric pressure results in the IB effect:

- a 1 hPa fall in pressure results in approximately a 10 mm rise in sea level, and
- a 1 hPa rise in pressure results in approximately a 10 mm fall in sea level.

The IB effect at each site was determined by processing mean sea level pressure (MSLP) data using Equation 6-1:

**Equation 6-1: Inverse barometer equation.**

$$(m - ssMSLP) * 10 \text{ mm}$$

where  $m$  is the long term mean MSLP; and  $ssMSLP$  is the instantaneous MSLP. For consistency with the 2015 work  $ssMSLP$  was calculated by wavelet filtering (Goring, D. G. et al. 2011) MSLP to obtain only the periods of motion between 24 hours and 1 month.. Wavelet filtering was not undertaken on surge data due to use of the skew surge metric.

For each event described, synoptic weather maps were provided (where possible) to show the individual storms and give context to the skew surge events. Finally, monthly boxplots of the largest skew surge events each year were constructed to highlight seasonality in skew-surge hazard.

### 6.1.1 Tararu

The largest five skew surge events at Tararu are summarised in Table 6-2. Three out of the five largest events occurred during winter. However, the two largest skew surge events occurred in the summer months. MSLP data for Tararu was supplied for the duration of the sea level gauge record, from MetService AWS located in Paeroa and NIWA EWS located in the Firth of Thames. Stephens (2018) provided a thorough analysis of the extreme storm-tide distribution at Tararu by adding the 1938 storm into the analysis. Stephens (2018) estimated that the 1938 storm produced a 0.86 m skew-surge at Tararu, which is larger than anything else on record since.

Stephens (2018) identified four of the same 5 highest skew-surge events on record (Table 6-2), the 13 Feb 2022 being more recent than Stephens (2018) analysis. We obtained a different ordering of the highest skew surge events than Stephens (2018). This occurs because the difference in skew-surge height of the 3–5 ranked events is only a couple of centimetres, yet the updated linear MSL trend is considerably higher (0.69 m/century) than used in 2018 (0.52 m/century). On removing the larger trend, this elevates the ranking of older events relative to more recent events. This difference in ranking is inconsequential.

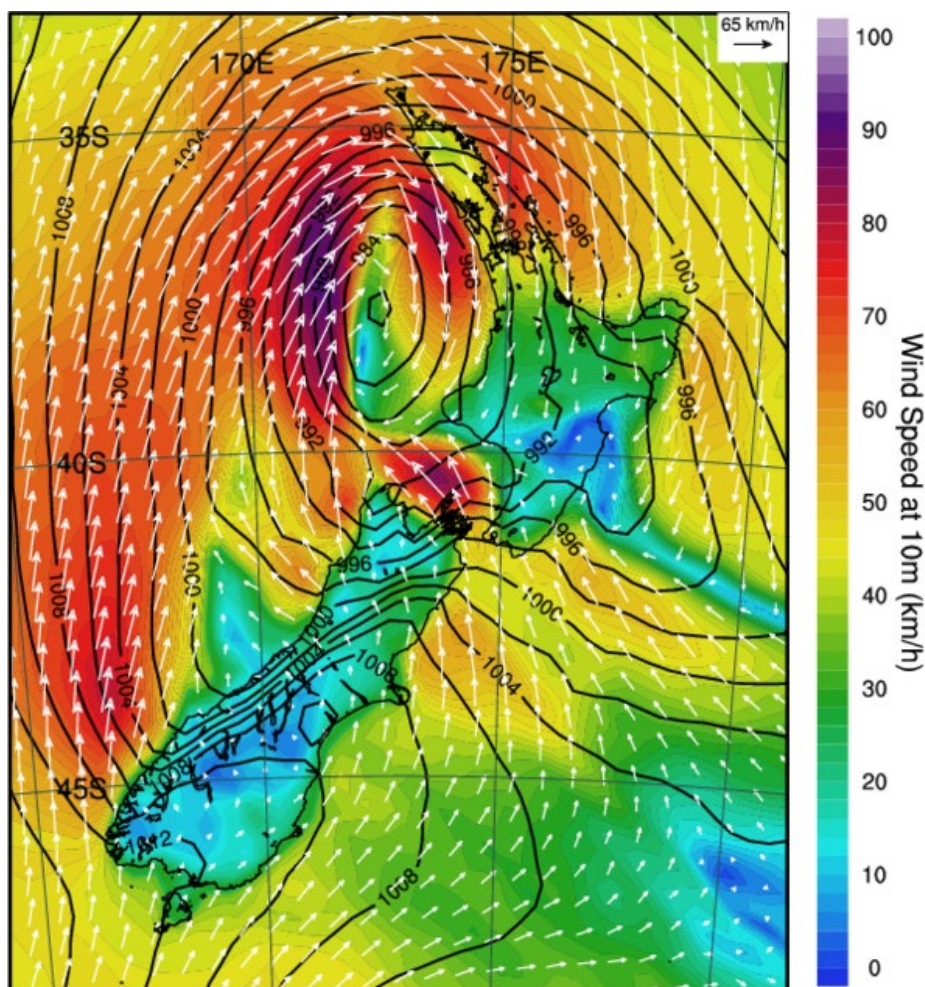
**Table 6-2: The top five skew surges on record at Tararu.**

Date	Skew surge (m)	Lowest barometric pressure (hPa)	IB component at peak skew surge (m)	Non-IB component (m)	IB contribution to skew surge (%)	Non-IB contribution to skew surge (%)
13-Feb-2022	0.67	991.5	0.25	0.42	38%	62%
05-Jan-2018	0.66	988.3	0.24	0.42	37%	63%
02-Oct-1992	0.60	984.5	0.24	0.36	40%	61%
18-Sep-2005	0.59	986.3	0.23	0.36	39%	61%
11-Jun-2014	0.56	999.8	0.16	0.39	29%	71%

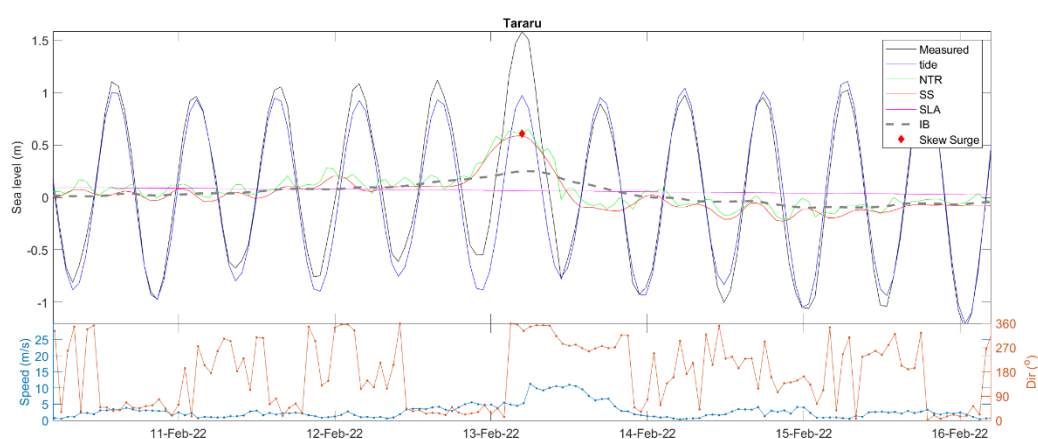
### 13 February 2022 skew surge

The largest skew surge at Tararu occurred on 13 February 2022, this skew surge measuring 0.686 m and was generated by a broad active trough, which moved into the Tasman Sea (Figure 6-7). This meteorological system was accompanied by intense north-westerly winds and made its way from the northwest to the southeast, over a two-day period making land fall in Taranaki.

At Tararu the barometric pressure dropped to 991 hPa, leading to an inverse-barometer sea level increase of 0.25 m. The dominant factor contributing to the skew surge was the wind setup, accounting for 0.42 m (as outlined in Table 6-2). The skew surge was a result of persistent high winds blowing from the northwest (toward the southeast), with the peak wind speed recorded at the Firth of Thames EWS reached 11.3 m/s, approximately 1-hours after high tide (Figure 6-8). The weather situation at 8 am on 13 February 2022, is depicted in Figure 6-7.



**Figure 6-7:** Mean sea-level pressure map at 5 am, 13-Feb-2022 around the time of the largest measured skew surge at Tararu.



**Figure 6-8:** Measured sea-level and its components during 13 February 2022 surge Tararu. NTR = non-tidal residual, SS = Storm Surge, SLA = sea-level anomaly and IB = inverse barometer.

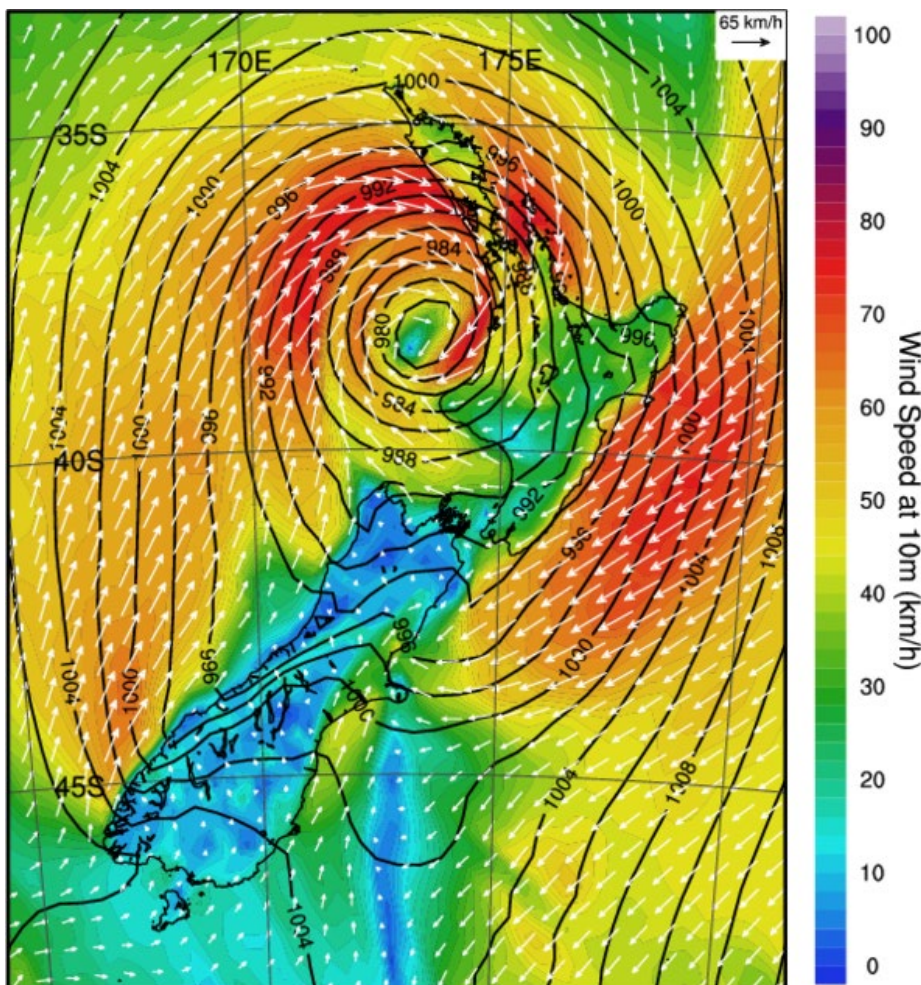


### 05 January 2018 skew surge

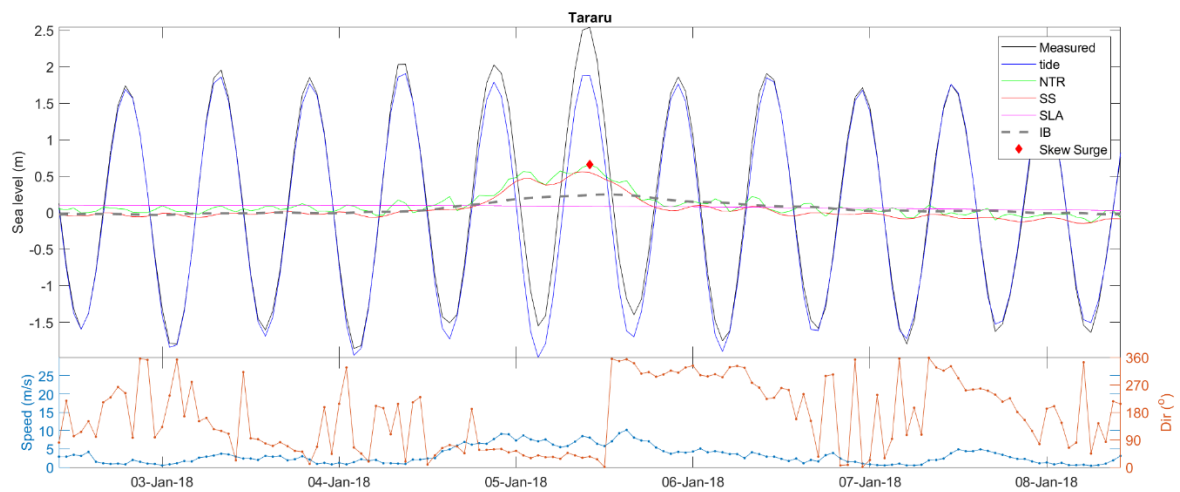
The skew surge on 5 January 2018 was generated by a very similar weather event to that of the 13 February 2022 skew surge. A slow-moving low-pressure system that traversed the upper North Island, making its way from the northwest to the southeast over a period of 2–3 days. This weather system led to a skew surge of 0.66 m at Tararu, accompanied by a drop in the mean sea level barometric pressure to 988.3 hPa. The decrease in mean sea level barometric pressure contributed to an inverse-barometer sea level rise of 0.24 m (Figure 6-9).

The primary driving force behind this skew surge was the wind setup, contributing 0.42 m to the overall surge (as indicated in Table 6-2). The surge's generation could be attributed to sustained high winds offshore, with the maximum wind speed recorded at Paeroa reaching 11.8 m/s, approximately 1-hour before high tide.

As the low-pressure system traversed the upper North Island the winds wrapping around the northern region of the island. These wind stresses exerted a considerable force on the water, leading to the accumulation of water against the Firth of Thames on the eastern side of the North Island. This process, in turn, caused the wind setup component of the measured skew surge (see Figure 6-9). To illustrate the weather situation at 10 am on 5 January 2018, please refer to Figure 6-10.



**Figure 6-9: Mean sea-level pressure map at 10 am, 05-Jan-2018 around the time of the largest measured skew surge at Tararu.** NTR = non-tidal residual, SS = Storm Surge, SLA = sea-level anomaly and IB = inverse barometer.



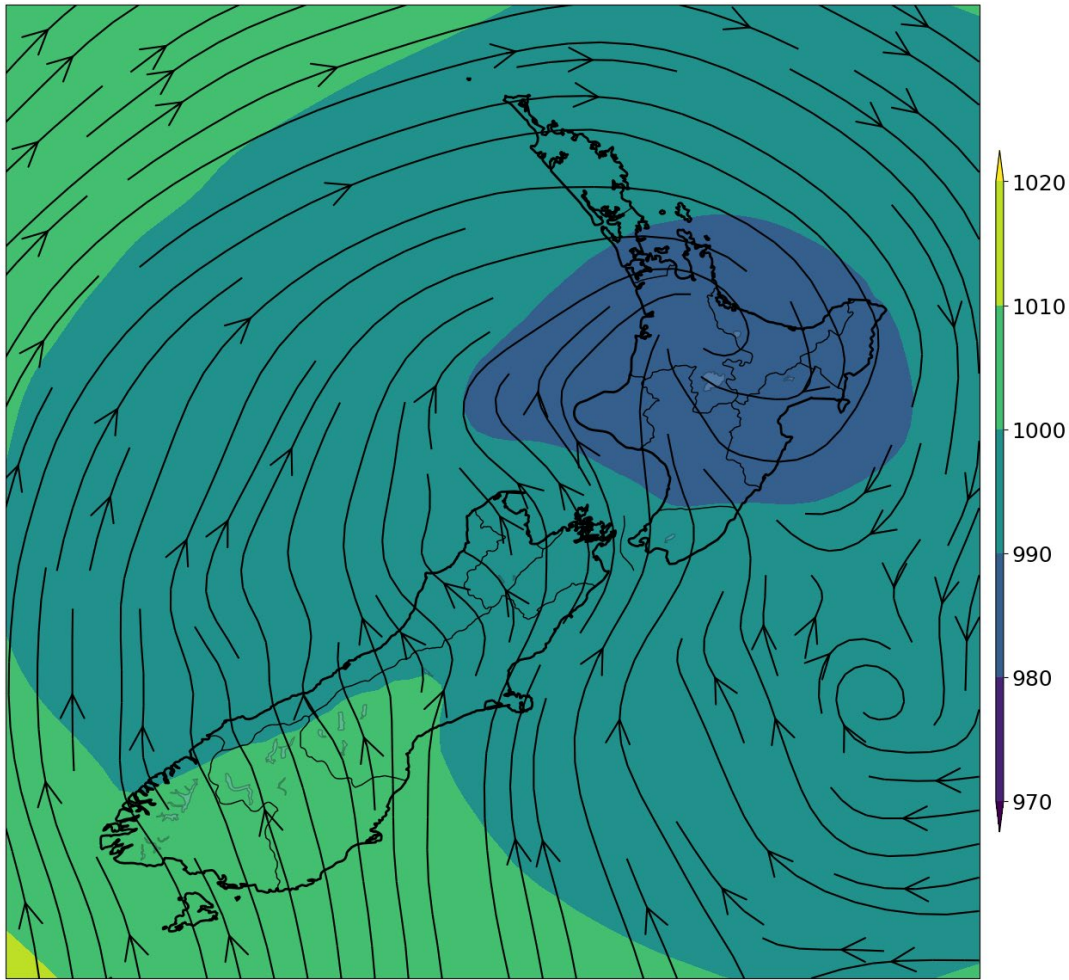
**Figure 6-10: Measured sea-level and its components during 05 January 2018 surge Tararu.** NTR = non-tidal residual, SS = Storm Surge, SLA = sea-level anomaly and IB = inverse barometer.

## 2 October 1992 skew surge

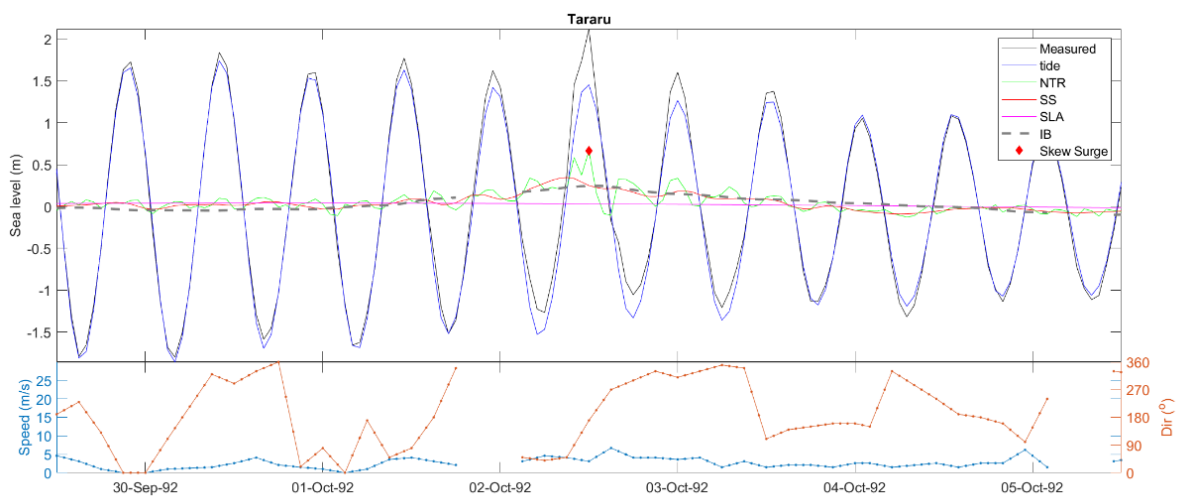
Like the event on 11 June 2014, the skew surge that occurred on 2 October 1992 was also caused by a slow-moving low-pressure system that tracked across the upper North Island, moving from the northwest to the southeast over a span of 2-3 days. This weather phenomenon led to a skew surge of 0.66 m at Tararu, accompanied by a drop in the mean sea level barometric pressure to 984 hPa. The decrease in mean sea level barometric pressure contributed to an inverse-barometer sea level rise of 0.25 m.

The primary driver of the skew surge was the wind setup, responsible for 0.42 m of the total skew surge (as outlined in Table 6-2). This wind setup was generated by sustained high winds offshore, with the maximum wind speed recorded at Paeroa reaching 4.3 m/s, approximately 1 hour before high tide.

As the low-pressure system moved over the upper North Island, the winds wrapped around the northern part of the island. These wind stresses exerted a force on the water, causing water to pile up against the Firth of Thames on the eastern side of the North Island. This process resulted in the wind setup component of the measured skew surge (refer to Figure 6-12). The weather situation at 12 pm on 2 October 1992 is depicted in Figure 6-11.



**Figure 6-11: Mean sea-level pressure map at 12 pm, 02-Oct-1992 around the time of the largest measured skew surge at Tararu.**



**Figure 6-12: Measured sea-level and its components during 02 October 1992 skew surge Tararu. NTR = non-tidal residual, SS = Storm Surge, SLA = sea-level anomaly and IB = inverse barometer.**

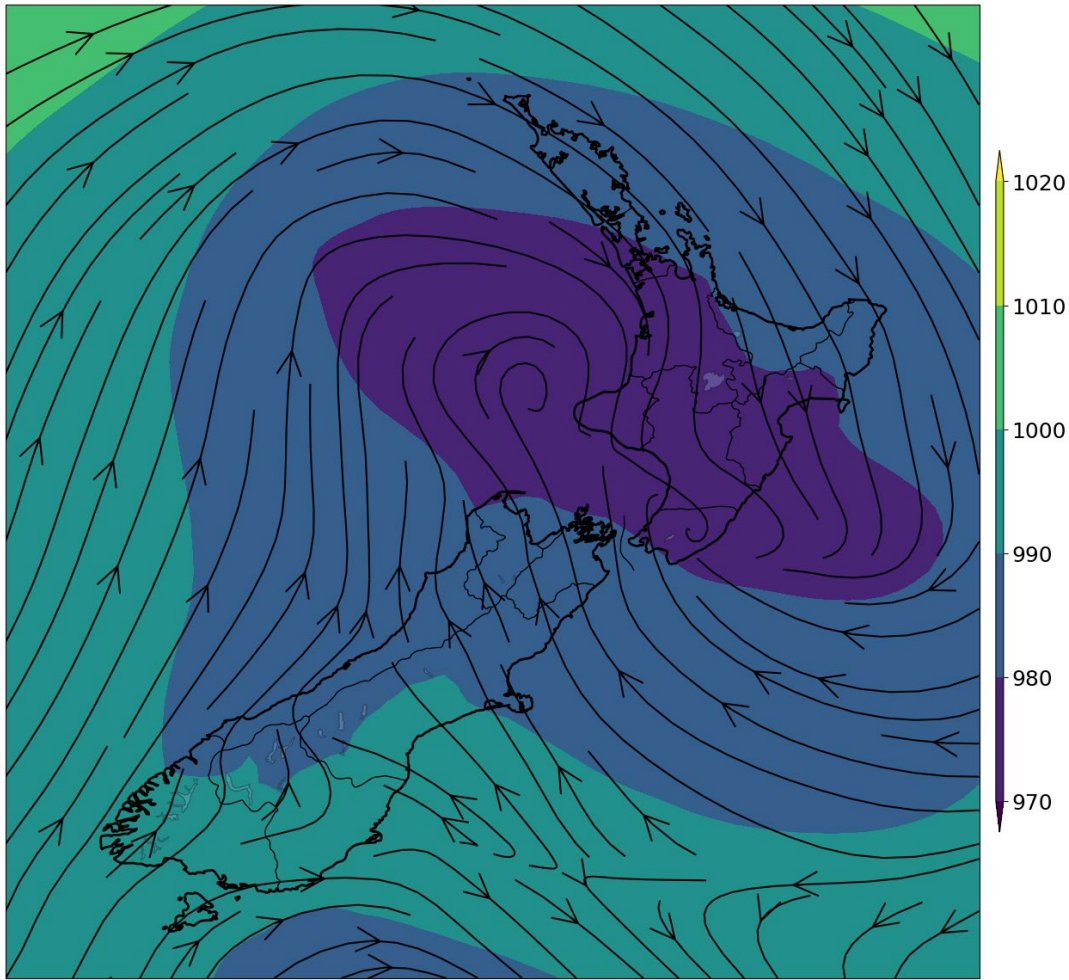
### 18 September 2005 skew surge

The skew surge event on 18 September 2005 bore resemblances to the occurrence on 2 October 1992. It was triggered by a slow-moving low-pressure system that traversed the upper North Island, making its way from the northwest to the southeast over a period of 2-3 days. As a result of this weather system, Tararu experienced a skew surge measuring 0.59 m, accompanied by a drop in the mean sea level barometric pressure, which plummeted to 986 hPa. This drop in barometric pressure caused an inverse-barometer sea level rise, reaching 0.23 m (Figure 6-14).

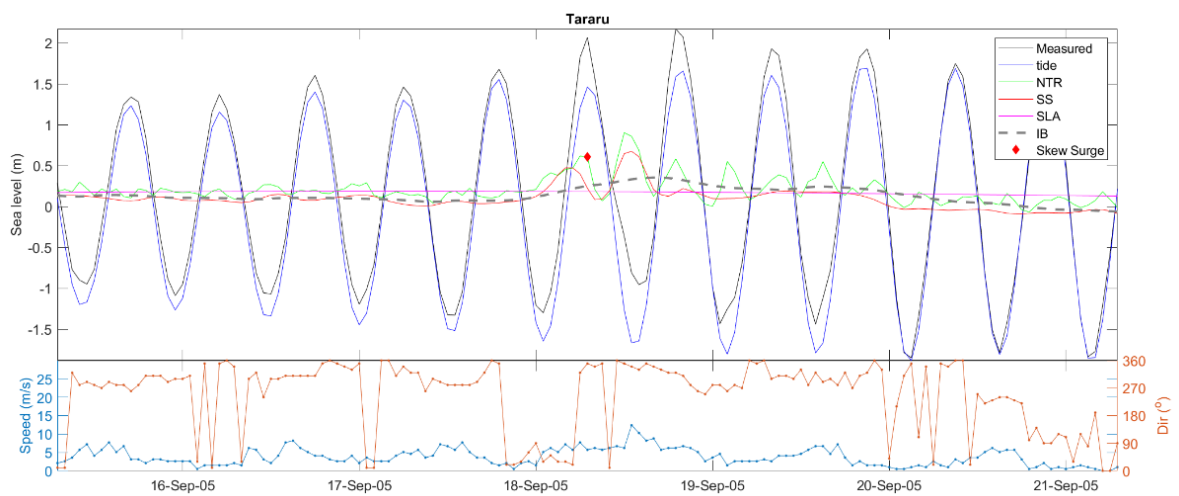
The primary driving force behind this skew surge was the wind setup, contributing 0.35 m to the overall surge (as indicated in Table 6-2). The surge's generation could be attributed to sustained high winds offshore, with the maximum wind speed recorded at Paeroa reaching 7.7 m/s, approximately 5 hours before high tide.

As the low-pressure system traversed the upper North Island the winds wrapping around the northern region of the island. These wind stresses exerted a considerable force on the water, leading to the accumulation of water against the Firth of Thames on the eastern side of the North Island. This process, in turn, caused the wind setup component of the measured skew surge (see Figure 6-14). To illustrate the weather situation at 7 am on 18 September 2005, please refer to Figure 6-13.





**Figure 6-13: Mean sea-level pressure map at 7 am, 18-Sep-2005 around the time of the largest measured skew surge at Tararu.**



**Figure 6-14: Measured sea-level and its components during 18 September 2005 skew surge Tararu. NTR = non-tidal residual, SS = Storm Surge, SLA = sea-level anomaly and IB = inverse barometer.**

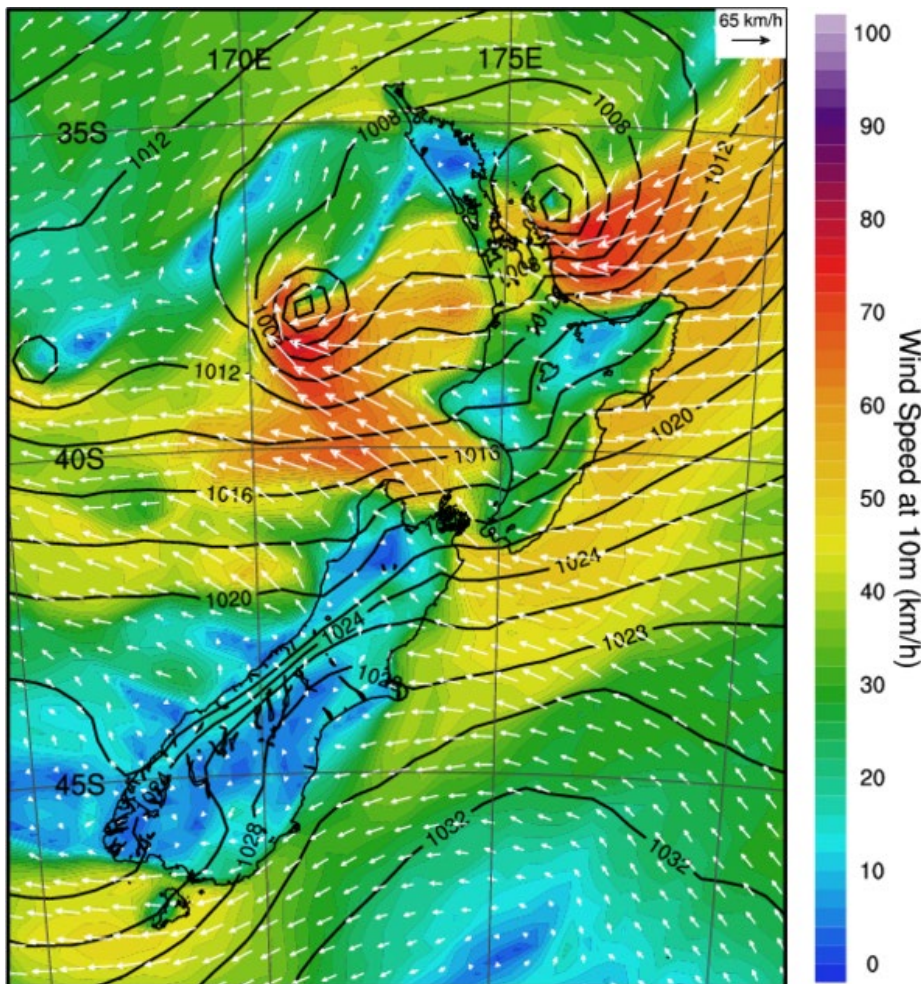


### 11 June 2014 skew surge

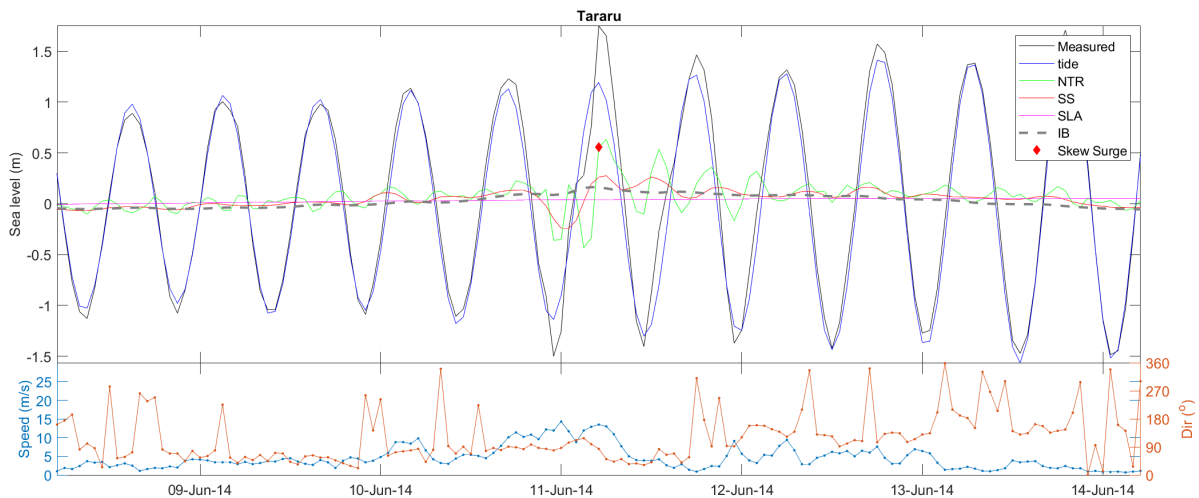
On 11 June 2014, a slow-moving low-pressure system made its way across the upper North Island, traveling from the northwest to the southeast over a period of 2 days. This weather event resulted in a skew surge of 0.56 m at Tararu and a drop in barometric pressure to 1003 hPa. Additionally, an inverse-barometer sea level rise of 0.16 meters was observed.

The primary contributor to the skew surge was the wind setup, accounting for 0.39 m (as detailed in Table 6-2). The skew surge was generated by sustained high winds offshore, with the maximum wind speed recorded at Paeroa reaching 14.3 m/s, approximately 2 hours before high tide.

As the low-pressure system passed over the upper North Island, the winds wrapped around the top of the island. These wind stresses exerted a pushing force on the water, leading to an accumulation of water against the Firth of Thames on the eastern side of the North Island. This resulted in the wind setup component of the measured skew surge (Figure 6-16). The weather situation at 6 am on 11 June 2014 is depicted in Figure 6-15.



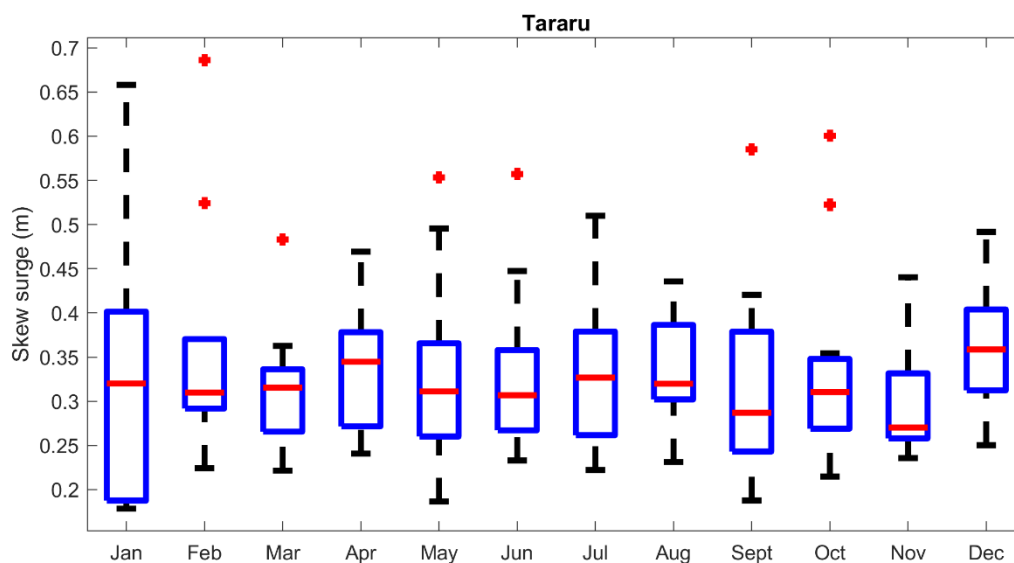
**Figure 6-15: Mean sea-level pressure map at 6 am, 11-Jun-2014 around the time of the largest measured skew surge at Tararu.**



**Figure 6-16: Measured sea-level and its components during 11 June 2014 skew surge Tararu.** NTR = non-tidal residual, SS = Storm Surge, SLA = sea-level anomaly and IB = inverse barometer.

### Seasonality of skew surges

At Tararu, a monthly boxplot was constructed for the 5 largest skew surge events each year to highlight any seasonality in skew surge (Figure 6-17). With a sea-level record close to 25 years, skew surge seasonality should be more robustly defined than at Kawhia or Whitianga. Skew surges larger than 0.5 m tend to occur from late winter to late spring. A frequency count of the top 5 skew surges each month reveals that months June to October have the most skew surges (15-27), with July having the most (27), followed by August (22) and October (19). From November to March, the frequency of largest skew surges events drops off, with large skew surges varying from 11-5 each month. Large skew surges at Tararu are driven more by winter weather systems, which drive wind southward into the enclosed Firth of Thames.



**Figure 6-17: Monthly boxplot of the 5 largest skew surge events per year at Tararu.** Median (red line), top and bottom of boxes represent 3rd and 1st quartiles respectively. Maximum and minimum (excluding outliers) (black lines), outliers (red dots) correspond to values greater than  $Q3 + 1.5(Q3-Q1)$  or less than  $Q1 - 1.5(Q3-Q1)$ .

## Summary of skew surge analysis for Tararu

The largest skew surges at Tararu are driven by wind stress, with only a relatively small IB component. All five skew surges occur during complex low-pressure systems or troughs that result in strong offshore wind speeds from the northwest, sustained over many hours. These weather systems are larger in scale and slower moving. Extreme skew surge analyses indicate that 1% AEP skew surges have a maximum likelihood of about 0.71 m – as discussed in Section 6.

### 6.1.2 Whitianga

As is the case for Tararu, 3 out of 5 of the largest skew surge events occur during winter (Table 6-3). However, the two largest skew surge events in the current record are associated with summer Tropical Cyclones (Gabrielle and Hale). The 12 March 2011 event, was the result of a Tsunami, the 2011 Tohoku tsunami generated a +0.44 m skew surge (relative to MSL = 0) at Whitianga.

MSLP data for Whitianga was supplied for the duration of the sea level gauge record, from MetService and NIWA. Before February 2007, MSLP was obtained from a MetService weather station at Whitianga aero which is 2.8 km away from the Tararu gauge, after 2007 MSLP comes from a sensor located at the gauge. As with MSLP, winds initially come from Whitianga aero, however after 2005 the wind record ceases, with the next closest available wind record coming from Slipper Island AWS which is located 32 km east of the gauge site.

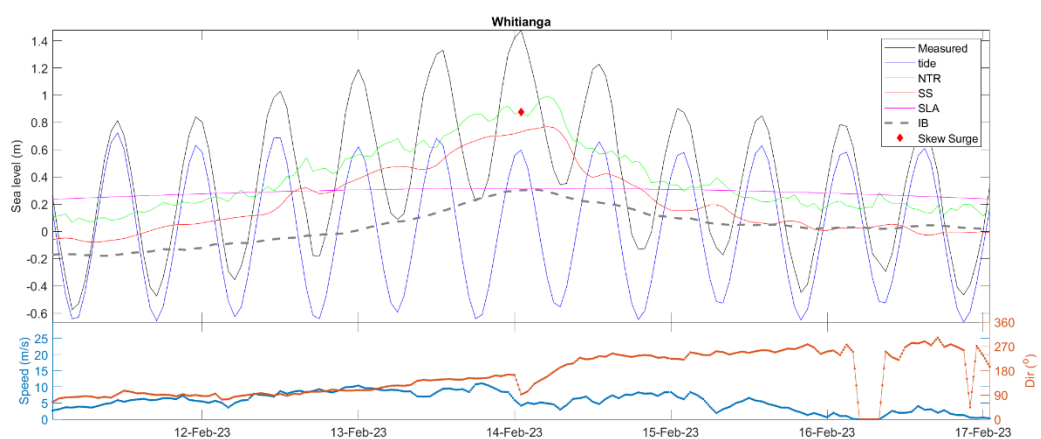
**Table 6-3: The top five skew surges on record at Whitianga.** Measurements denoted by an asterisk (\*) signify that these values are deduced from meteorological weather maps.

Date	Skew surge (m)	Lowest barometric pressure (hPa)	IB component at peak skew surge (m)	Non-IB component (m)	IB contribution to skew surge (%)	Non-IB contribution to skew surge (%)
14-Feb-2023	0.88	968	0.30	0.58	34%	65%
10-Jan-2023	0.61	985	0.26	0.32	43%	52%
24-Sep-2013	0.54	991	0.19	0.32	37%	63%
27-Jul-2008	0.50	968*	0.41*	0.1	80%	20%
11-Jun-2014	0.45	999.8	0.19	0.26	42%	58%
<b>12-Mar-2011</b>	<b>0.44</b>	<b>1026</b>	<b>-0.1</b>	<b>Tsunami</b>		

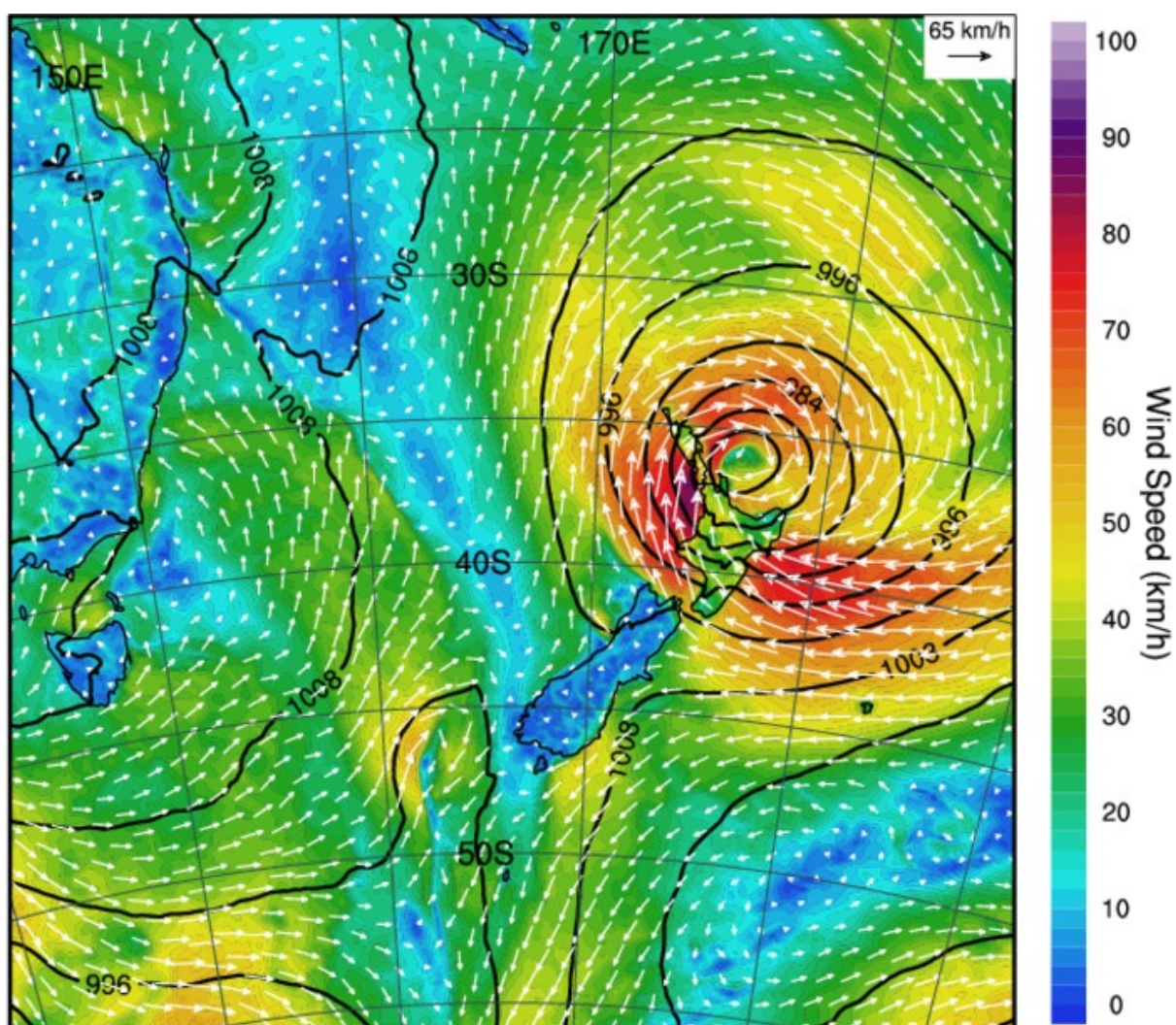
### 14 February 2023 skew surge

On 14 February 2023, a low-pressure system associated with Tropical Cyclone Gabrielle tracked along the east coast of the upper North Island over a span of seven days. This weather event caused a skew surge which measured 0.88 m at Whitianga Wharf. The weather conditions at 1 am on 14<sup>th</sup>, is depicted in Figure 6-19. Strong wind stresses exerted a on the water, leading to its accumulation in Mercury Bay. Consequently, the wind setup component became a significant factor in the measured skew surge (Figure 6-18).





**Figure 6-18: Measured sea-level and its components during 14 February 2023 skew surge Whitianga.**  
 NTR = non-tidal residual, SS = Storm Surge, SLA = sea-level anomaly and IB = inverse barometer.



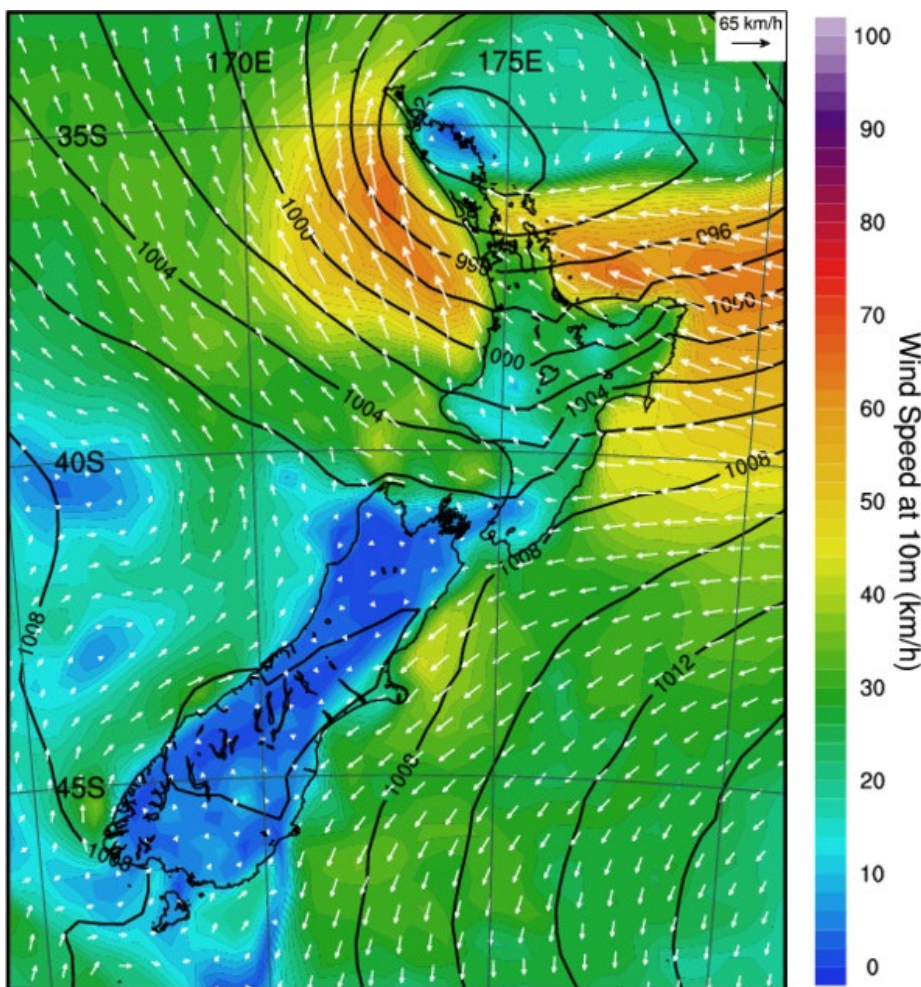
**Figure 6-19: Mean sea-level pressure map at 1 am, 14-Feb-2023 around the time of the largest measured skew surge at Whitianga.**

### 10 January 2023 skew surge

On 10 January 2023, a slow-moving low-pressure system associated with Tropical Cyclone Hale, which originated from the Pacific and proceeded to track along the east coast of the upper North Island, spanning a duration of 2 days. This weather phenomenon caused a skew surge of 0.57 m at Whitianga, accompanied by a drop in barometric pressure to 985.7 hPa and the resulting inverse-barometer sea level rise of 0.26 m was observed.

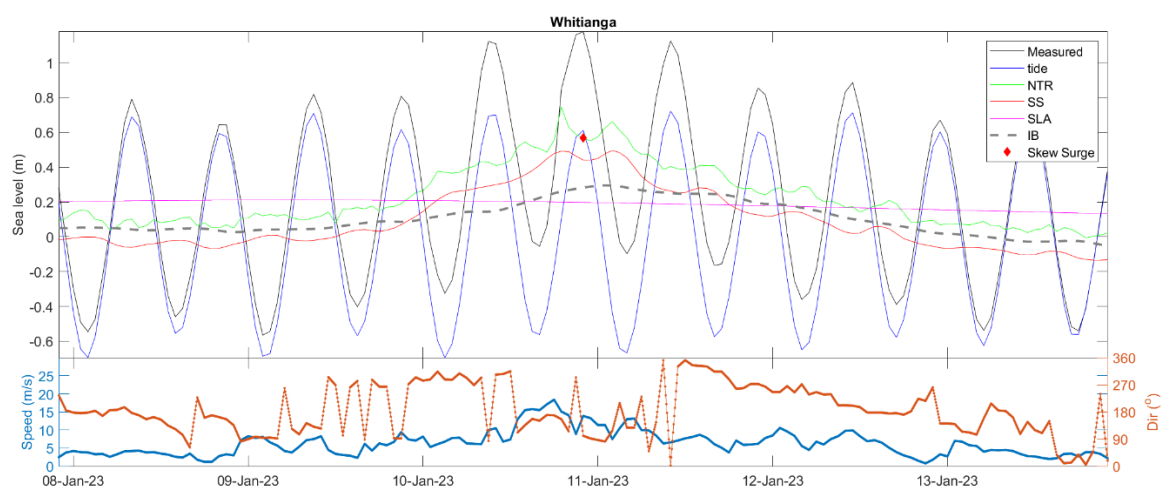
Like Tararu, the dominant factor contributing to the skew surge was the wind setup, accounting for 0.31 m (as outlined in Table 6-3). The skew surge was a result of persistent high winds offshore, with the peak wind speed recorded at Slipper Island reaching 18.4 m/s, approximately 2 hours before high tide.

As the trough of the system traversed along the East coast, cyclonic high winds blew in from the east-southeast direction. These strong wind stresses exerted a pushing force on the water, leading to water accumulation in Mercury Bay. Consequently, the wind setup component became a significant factor in the measured skew surge (Figure 6-20). Figure 6-21 shows the local weather situation on 10 January 2024.



**Figure 6-20: Mean sea-level pressure map at 11 pm, 10-Jan-2023 around the time of the largest measured skew surge at Whitianga.**

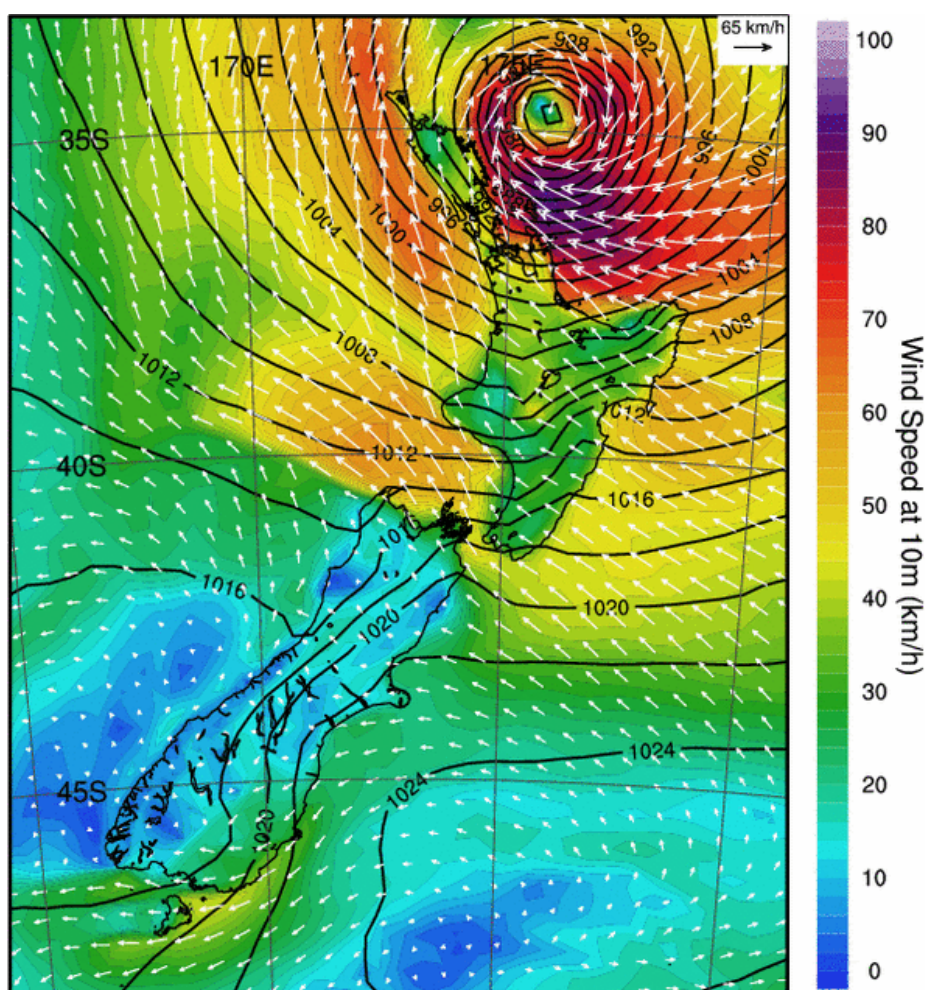




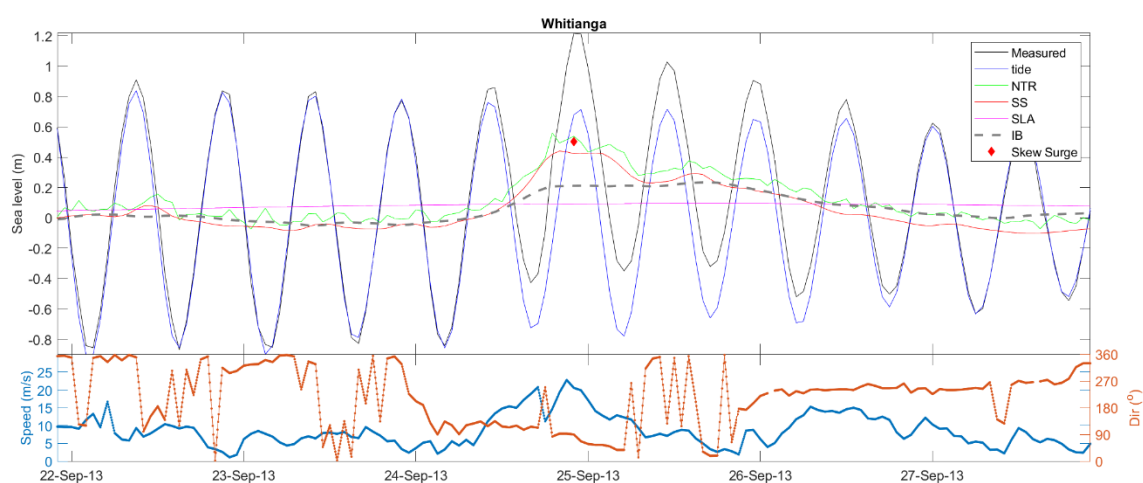
**Figure 6-21: Measured sea-level and its components during 10 January 2023 skew surge Whitianga.** NTR = non-tidal residual, SS = Storm Surge, SLA = sea-level anomaly and IB = inverse barometer.

### 24 September 2013 skew surge

On 24 September 2013, a low-pressure system travelled down from the Pacific. This system made its way from the northeast to the southwest, almost heading into the Firth of Thames over a two-day period. It caused a 0.55 m skew surge at Whitianga and dropped the barometric pressure to 991 hPa. A 0.17 m inverse-barometer sea level rise was also observed Figure 6-23. The wind setup, particularly from sustained high winds offshore, contributed 0.37 m to the skew surge, with a maximum wind speed of 22.8 m/s at Slipper Island recorded 2 hours before high tide. The cyclonic high winds from the east-southeast direction pushed water, leading to its accumulation in Mercury Bay, contributing to the skew surge. The weather situation at 9 pm on 24 September 2013 is depicted in Figure 6-22.



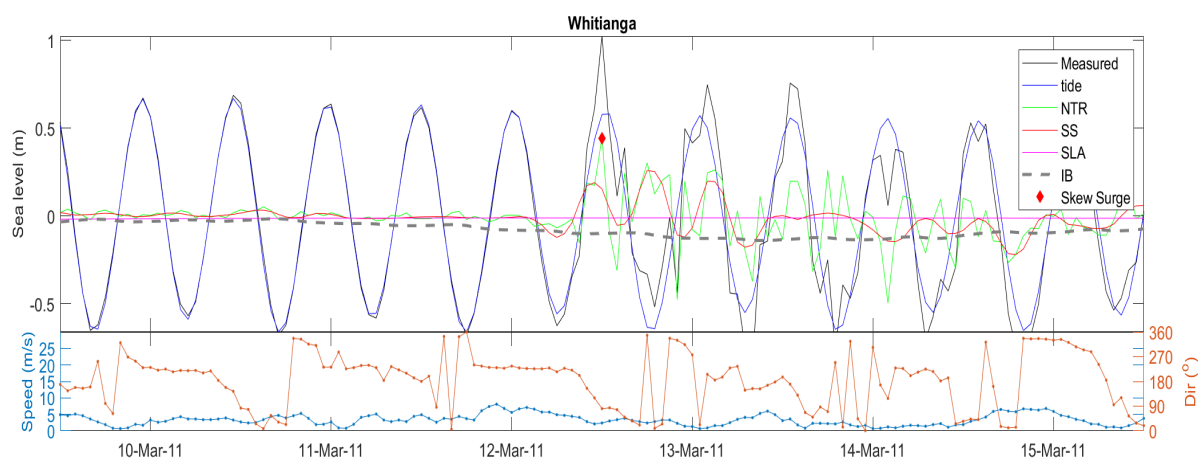
**Figure 6-22: Mean sea-level pressure map at 9 pm, 24-Sep-2013 around the time of the largest measured skew surge at Whitianga.**



**Figure 6-23: Measured sea-level and its components during 24 September 2013 skew surge Whitianga.** NTR = non-tidal residual, SS = Storm Surge, SLA = sea-level anomaly and IB = inverse barometer.

## 12 March 2011 Tsunami

The Tohoku (Japan) tsunami (discussed in Section 0) was recorded on 12 March 2011 at the Whitianga gauge. This shows as a skew surge in Figure 6-24 but it is a tsunami and was not associated with a weather event.



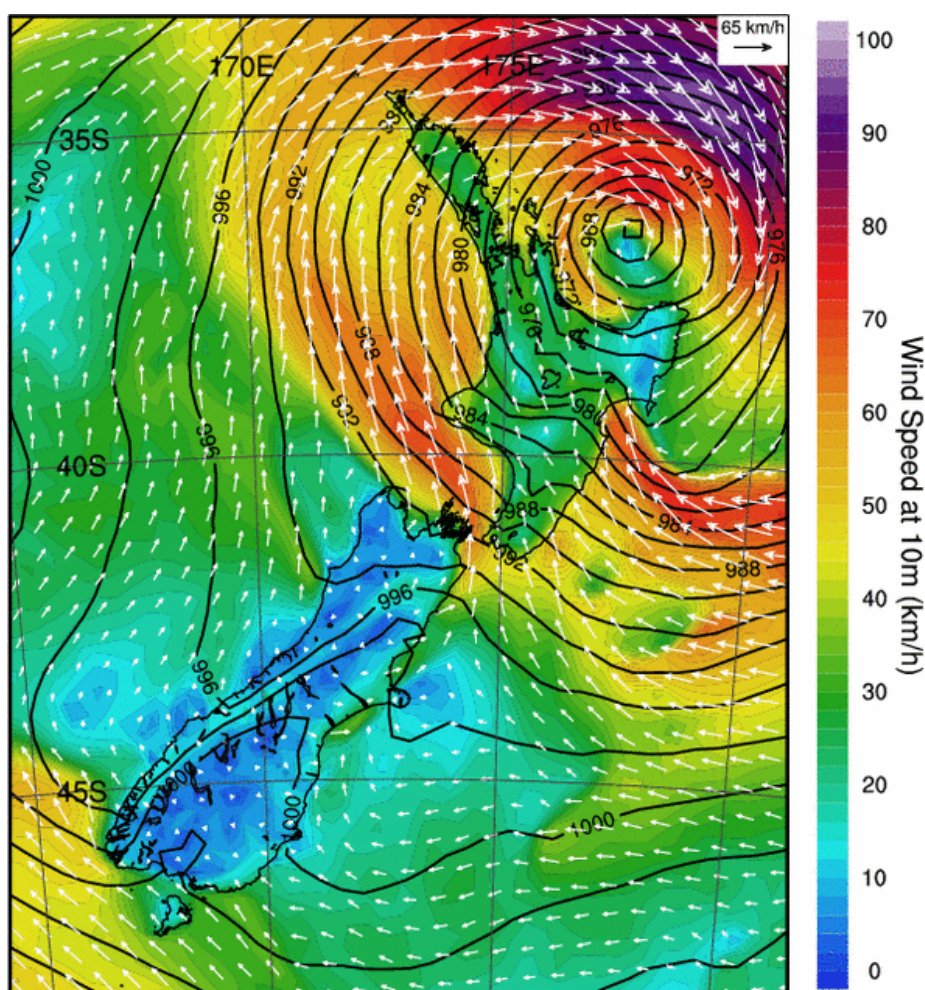
**Figure 6-24: Tsunami signal in measured at Whitianga on 12 March 2011.** NTR = non-tidal residual, SS = Storm Surge, SLA = sea-level anomaly and IB = inverse barometer.

## 27 July 2008 skew surge

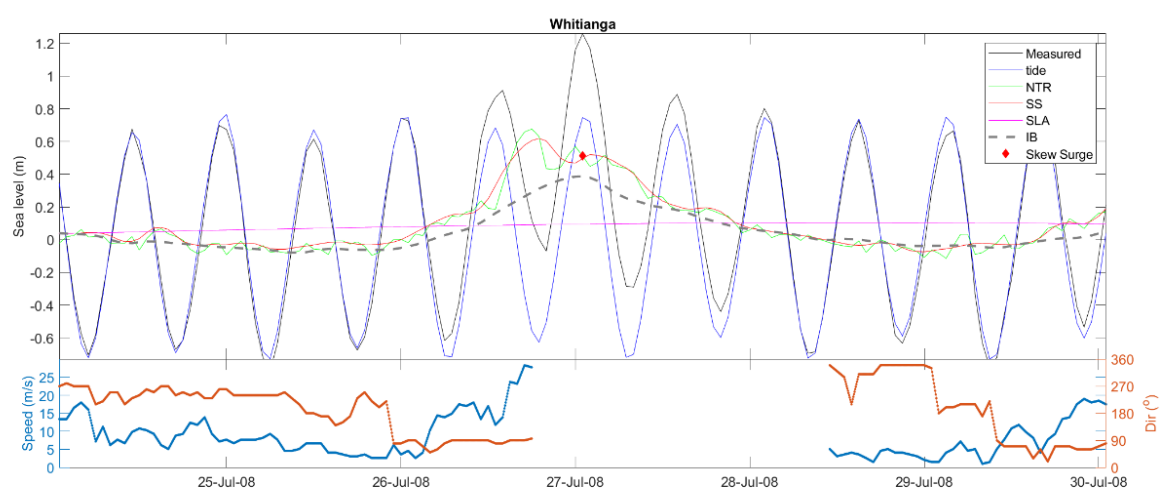
On 27 July 2008, similar to the event on 10 January 2023, storm a slow-moving low-pressure system originated from the Pacific and tracked along the east coast of the upper North Island, spanning a duration of 2 days. This weather event caused a skew surge of 0.42 m at Whitianga. Unfortunately, there is no pressure or wind record available at either Whitianga or Slipper Island (Figure 6-26). However, the pressure map in Figure 6-25 suggests the MSLP off the east coast dropped as low as 968 hPa at its centre and approximately 972 hPa near Whitianga. Which would imply a IB sea level rise offshore of  $\sim 0.446$  m and  $\sim 0.405$ .

The weather situation at 2 am on 27 July 2008 is visually represented in Figure 6-25.





**Figure 6-25: Mean sea-level pressure map at 2 am, 27-Jul-2008 around the time of the largest measured skew surge at Whitianga.**

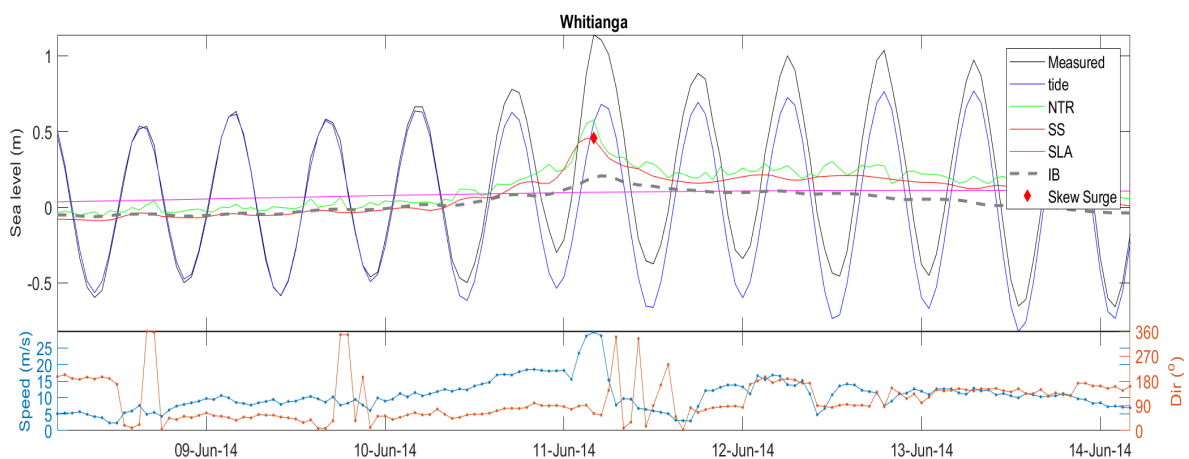


**Figure 6-26: Measured sea-level and its components during 27 July 2008 skew surge Whitianga.** NTR = non-tidal residual, SS = Storm Surge, SLA = sea-level anomaly and IB = inverse barometer.

### 11 June 2014 skew surge

On 11 June 2014 a slow-moving low-pressure system originated from the Pacific and proceeded to track along the east coast of the upper North Island, spanning a duration of 2 days. This weather system is the same system that caused the 5<sup>th</sup> largest skew surge event at Tararu. At Whitianga this weather system generated a smaller skew surge of 0.44 m compared with 0.55 m at Tararu. There was no difference in air pressure between the two sites, the difference in geography of both sites, with the wind set-up being larger at Tararu 0.39 m compared to 0.26 m at Whitianga.

The weather situation at 6 am on 11 June 2014 is visually represented in Figure 6-15.



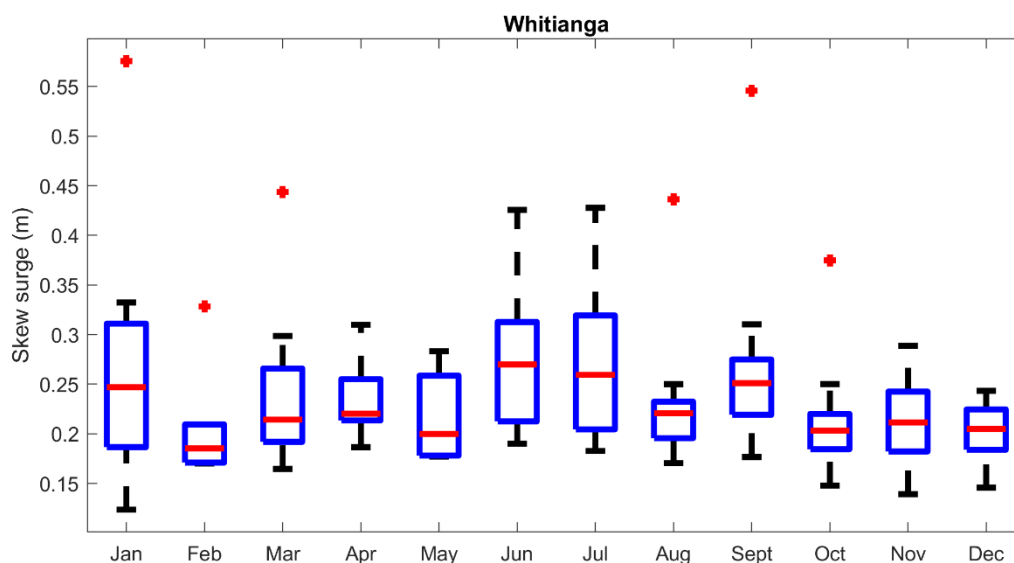
**Figure 6-27: Measured sea-level and its components during 11 June 2014 skew surge Whitianga.** NTR = non-tidal residual, SS = Storm Surge, SLA = sea-level anomaly and IB = inverse barometer.

### Seasonality of skew surges at Whitianga

Monthly boxplots were constructed for the 5 largest skew surge events each year to highlight any seasonality in skew surge from the Whitianga skew surge data (Figure 6-28).

The Whitianga sea-level record now spans nearly 24 years, allowing for a reasonably robust analysis of seasonal skew surges. Skew surges, which exceed 0.4 meters in height, tend to occur predominantly during the winter months and mid-summer (Figure 6-28). An examination of the top 5 skew surges each month reveals that July experiences the highest number of skew surges (32), followed by September with the second-highest count (15).

As we move from October to December, the frequency of the largest skew surge events declines, with only 2 to 4 such occurrences observed each month. It becomes evident that the occurrence of large skew surges in Whitianga is more prevalent during winter, primarily due to the influence of winter weather systems that drive strong winds into Mercury Bay.



**Figure 6-28: Monthly boxplot of the 5 largest skew surge events per year at Whitianga.** Median (red line), top and bottom of boxes represent 3rd and 1st quartiles respectively. Maximum and minimum (excluding outliers) (black lines), outliers (red dots) correspond to values greater than  $Q3 + 1.5(Q3 - Q1)$  or less than  $Q1 - 1.5(Q3 - Q1)$ .

### Summary of skew surge analysis for Whitianga

Wind stress makes a larger contribution than IB to the largest skew surges at Whitianga. Except for the Tsunami on 12 March 2011, all the skew surges occur during complex low-pressure systems or troughs that result in strong onshore wind speeds from the easterly direction, sustained over many hours. These weather systems are larger in scale and slower moving. The extreme skew surge analysis indicates that 1% AEP skew surges have a maximum likelihood of about 0.643 m – as discussed in Section 6.

#### 6.1.3 Kawhia

Unlike, Tararu and Whitianga only one of the five largest skew surge events at Kawhia occurred during winter. However, three events occur in the Autumn. Before February 2010, MSLP was obtained from a weather station at Taharoa which is 45 km away from the Kawhia gauge, after 2010 MSLP data is recorded at the gauge. The largest five skew surge events at Kawhia are summarised in Table 6-4. Skew surges at Kawhia appear to be significantly larger than at Whitianga and Tararu, despite only a 15-year long record. The skew surge event that occurred on 6 May 2013 was larger than 1 m.

**Table 6-4: The top five skew surges on record at Kawhia.**

Date	Skew surge (m)	Lowest barometric pressure (hPa)	IB component at peak skew surge (m)	Non-IB component (m)	IB contribution to skew surge (%)	Non-IB contribution to skew surge (%)
06-May-2013	1.16	985	0.26	0.90	22%	78%
10-Apr-2018	0.75	987	0.25	0.5	33%	67%
20-Jun-2013	0.67	984	0.28	0.39	42%	58%
17-Apr-2013	0.67	998	0.15	0.52	22%	77%
07-Jun-2010	0.67	987	0.22	0.45	33%	67%

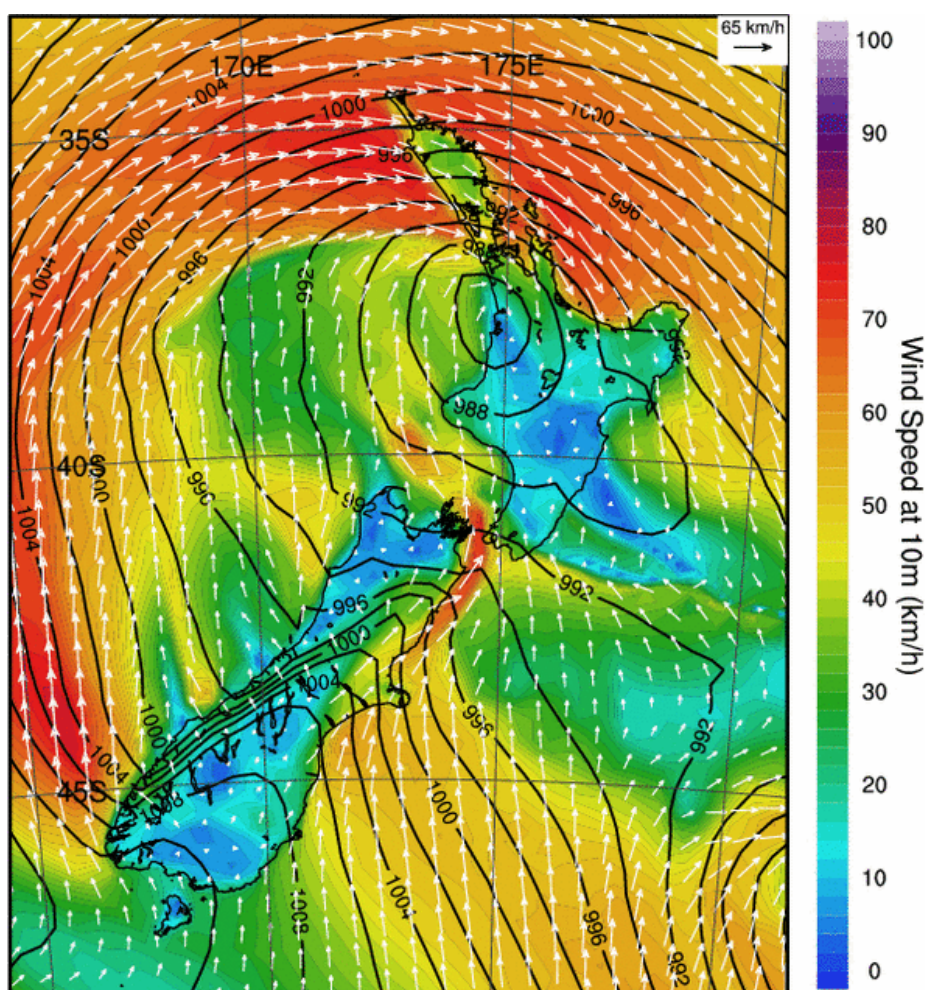
### 6 May 2013 skew surge

From 4 May to 6 May 2013, a storm persisted for approximately three days. During the overnight hours of the 4<sup>th</sup>, the trough moved and merged with the existing low, forming a much deeper low-pressure system centred to the west of the North Island, New Zealand on the 5<sup>th</sup>. This system brought heavy rainfall, thunderstorms, and gale force NW winds to northern and western areas.

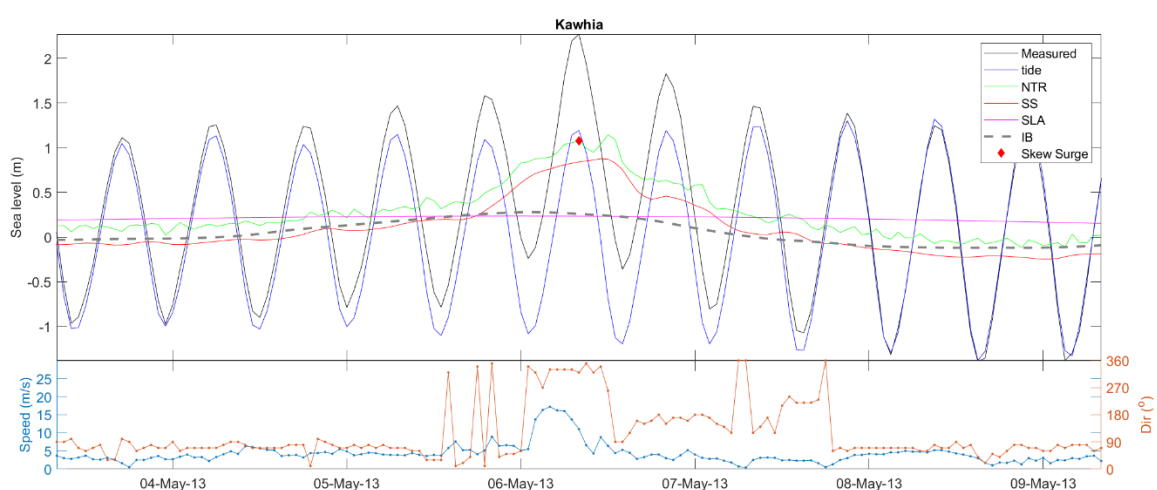
By May 6<sup>th</sup>, the low-pressure system moved onto the North Island. The weather situation at 6 am on 11 June 2014, is visually represented in Figure 6-29.

The primary factor contributing to the skew surge, amounting to 0.9 m (as specified in Table 6-4), was the wind setup. The skew surge resulted from persistent high offshore winds, with peak wind speed recorded at Taharoa AWS reaching 17.2 m/s, approximately 4 hours before high tide. The local weather measurements on 24 May 2014 are shown in Figure 6-30.





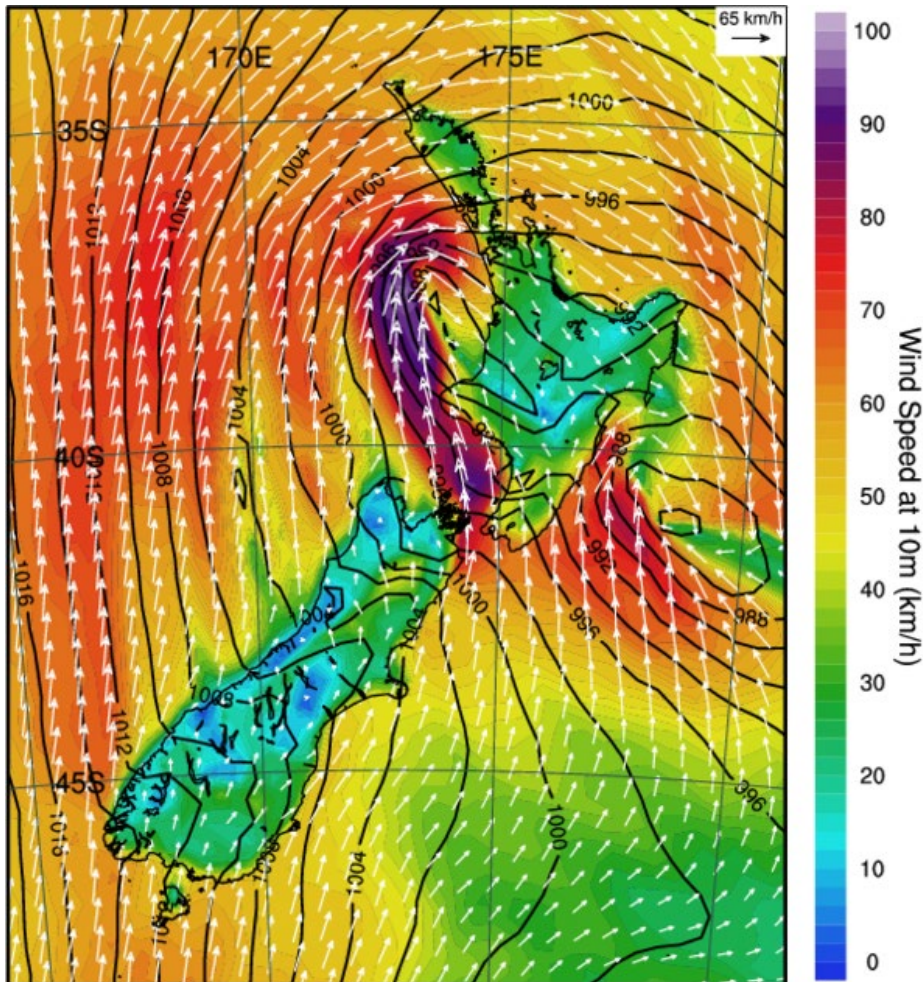
**Figure 6-29: Mean sea-level pressure map at 8 am, 6-May-2013 around the time of the largest measured skew surge at Kawhia..**



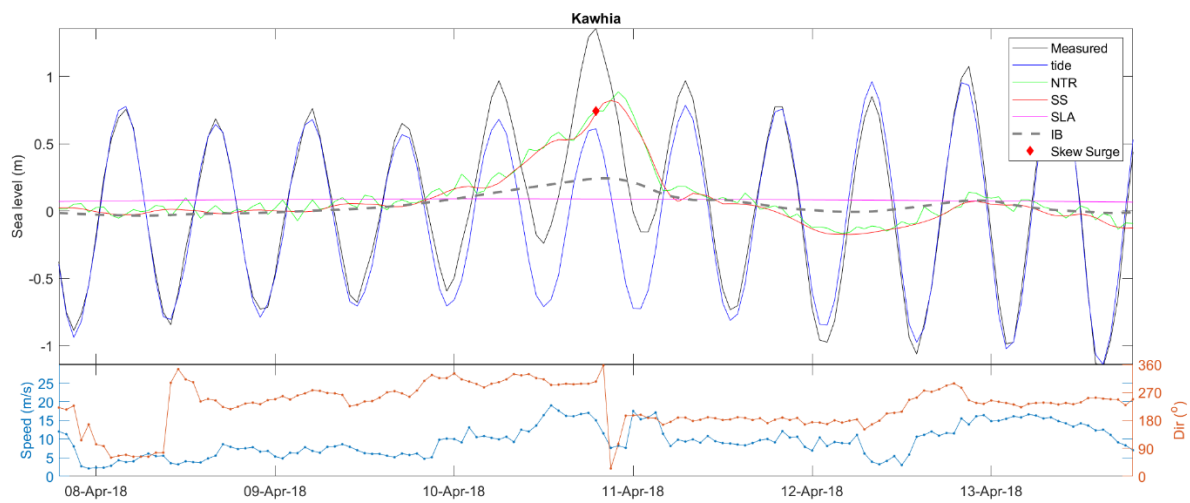
**Figure 6-30: Measured sea-level and its components during 24 May 2013 skew surge Kawhia.** NTR = non-tidal residual, SS = Storm Surge, SLA = sea-level anomaly and IB = inverse barometer.

### 10 April 2018 skew surge

During this weather event on 10 April 2018, a storm originated in the Southern Ocean and followed a trajectory along the West coast of the South Island before making landfall near Kawhia on the West coast of the North Island (Figure 6-31). The mean sea level barometric pressure dropped significantly, reaching 987 hPa. The skew surge recorded during this storm amounted to 0.75 meters. At its peak, the wind speed reached 19 m/s, occurring approximately 3 hours prior to high tide (Figure 6-32). The wind set-up component of the skew surge accounted for 0.5 meters of the total skew surge observed during this event.



**Figure 6-31: Mean sea-level pressure map at 7 pm, 10-Apr-2018 around the time of the largest measured skew surge at Kawhia.**

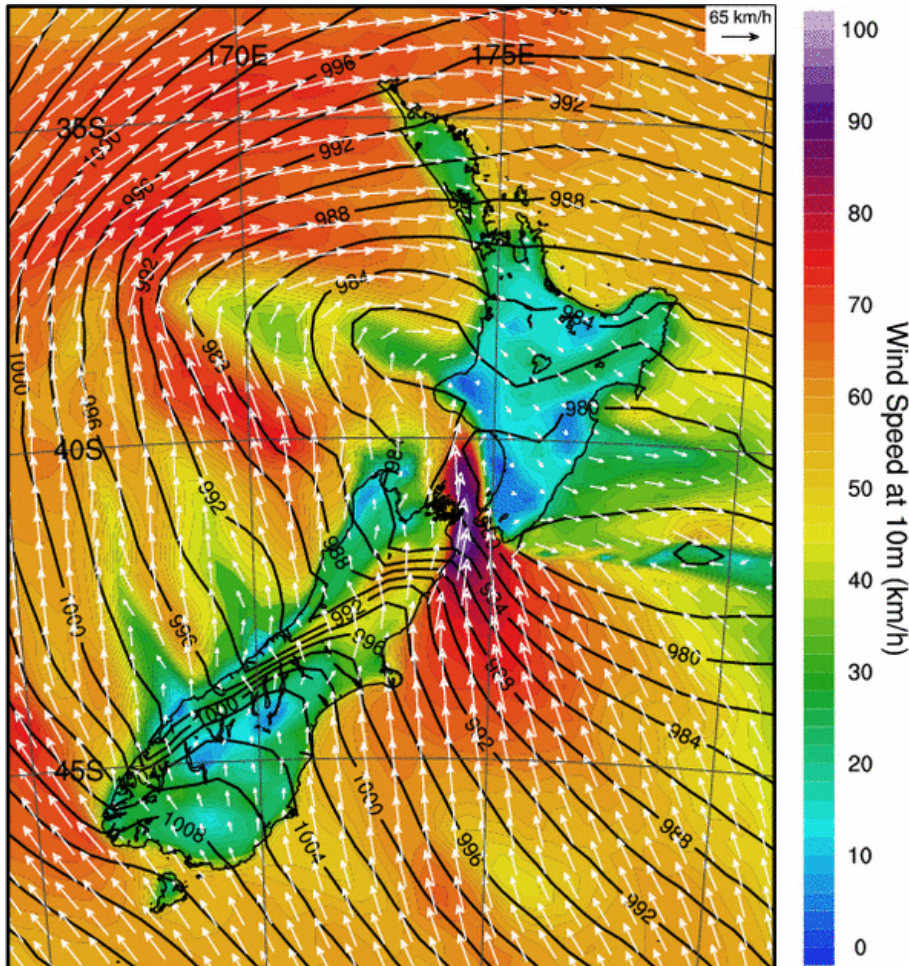


**Figure 6-32: Measured sea-level and its components during 10 April 2018 skew surge Kawhia.** NTR = non-tidal residual, SS = Storm Surge, SLA = sea-level anomaly and IB = inverse barometer.

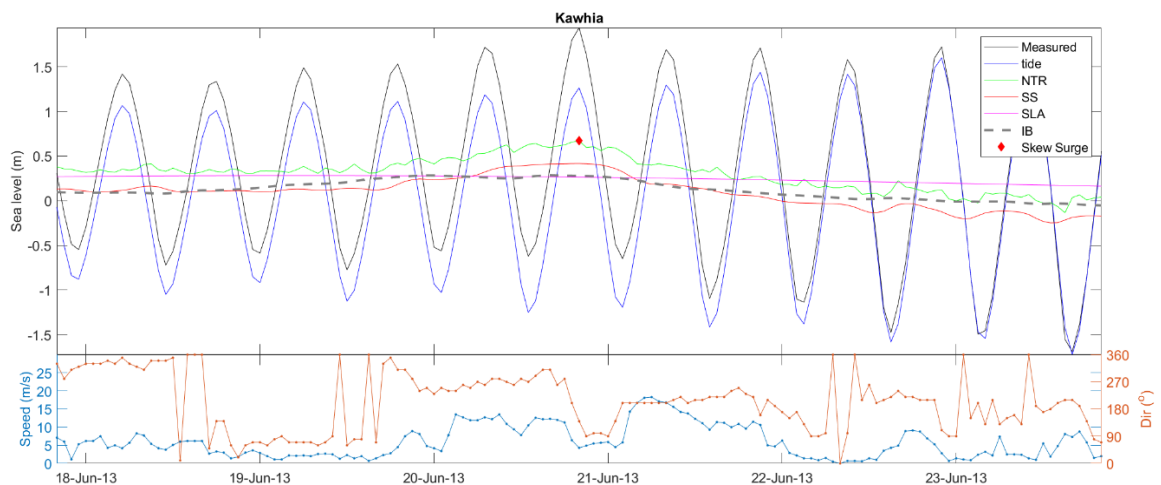


## 20 June 2013 Skew Surge

The weather map and sea level components associated with the 20 June 2013 skew surge event are shown in Figure 6-33 and Figure 6-34.



**Figure 6-33: Mean sea-level pressure map at 8 pm, 20-Jun-2013 around the time of the largest measured skew surge at Kawhia.**

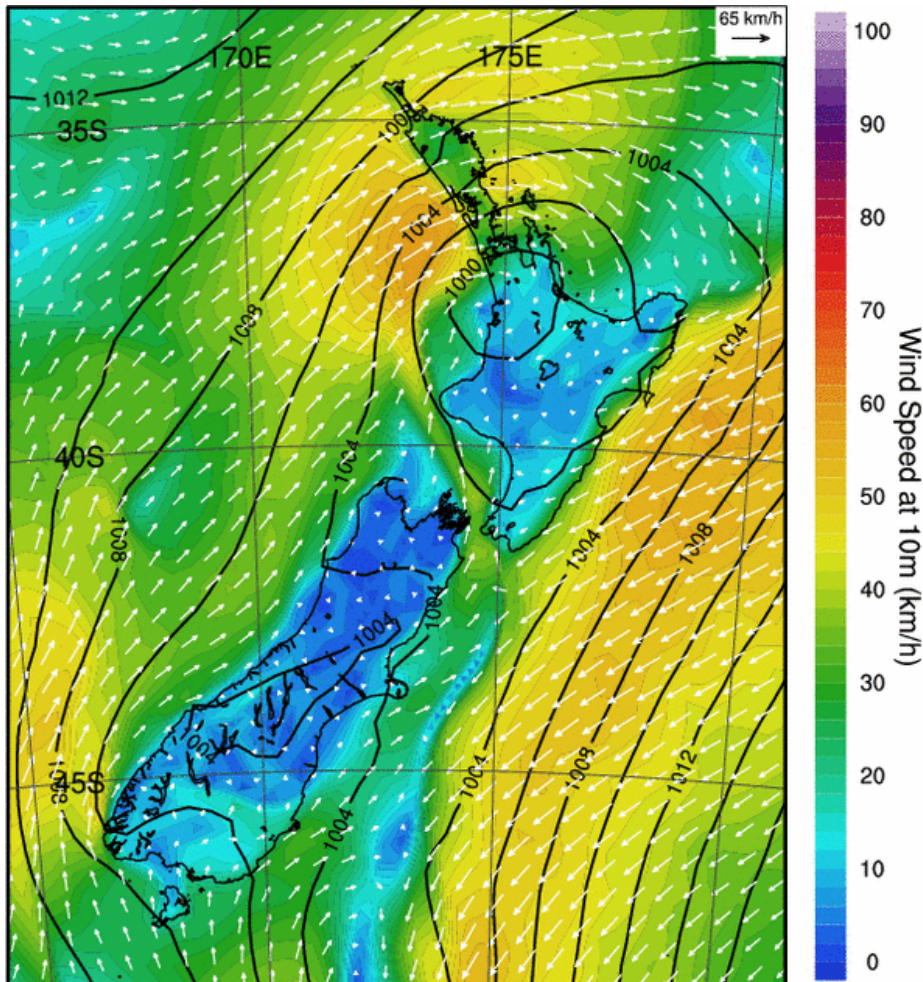


**Figure 6-34: Measured sea-level and its components during 20 June 2013 skew surge Kawhia.** NTR = non-tidal residual, SS = Storm Surge, SLA = sea-level anomaly and IB = inverse barometer.

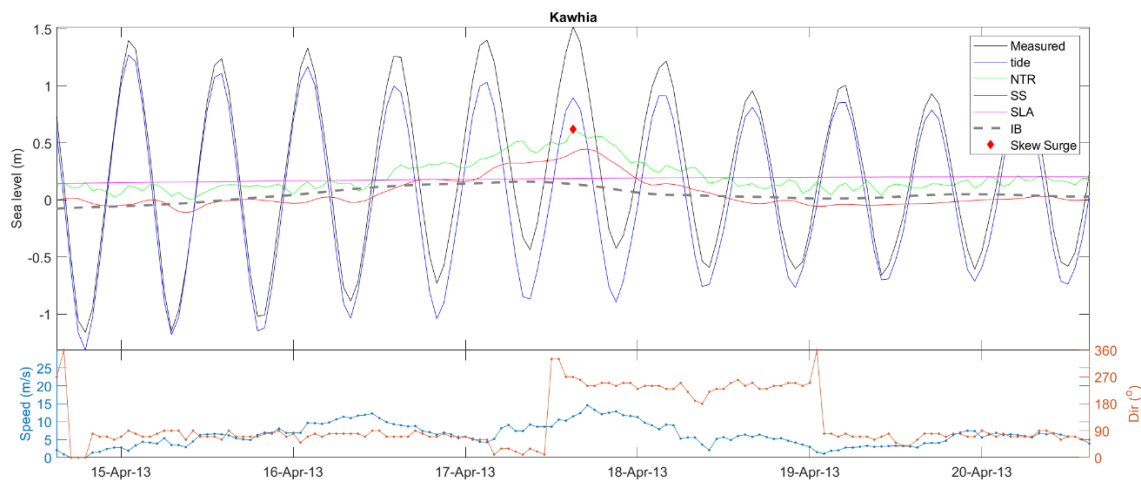


### 17 April 2013 skew surge

On 17 April 2013, a low-pressure system travelled across the Tasman Sea from Australia. This system made its way from the northwest to the southeast, over a two-day period making land fall in Taranaki. This event caused a 0.62 m skew surge at Kawhia and dropped the barometric pressure to 998 hPa. A 0.14 m inverse-barometer sea level rise was also observed (Figure 6-36). The wind setup, particularly from sustained high winds offshore, contributed 0.48 m to the skew surge, with a maximum wind speed of 11.5 m/s at Taharoa recorded 1-hour before high tide. The weather situation at 3 pm on 17 April 2013, is depicted in Figure 6-35.



**Figure 6-35:** Mean sea-level pressure map at 3 pm, 17-Apr-2013 around the time of the largest measured skew surge at Kawhia.

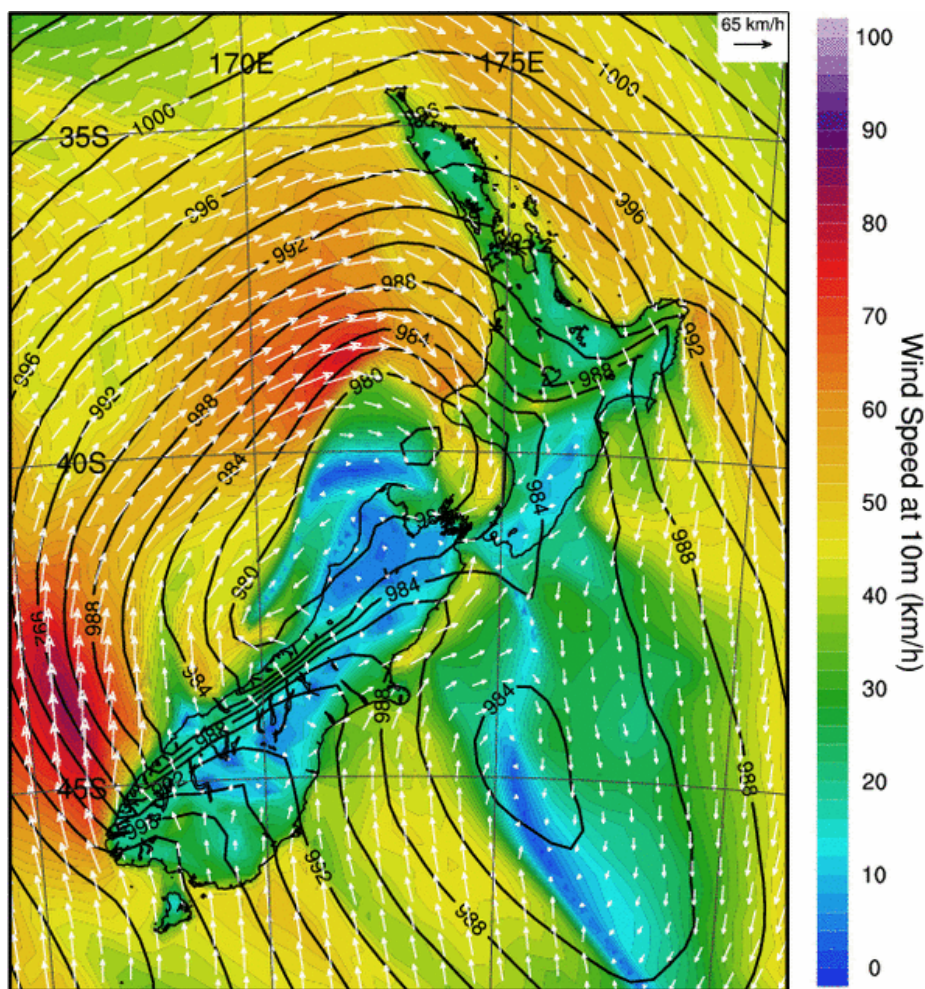


**Figure 6-36: Measured sea-level and it's components during 17 April 2013 skew surge Kawhia.** NTR = non-tidal residual, SS = Storm Surge, SLA = sea-level anomaly and IB = inverse barometer.

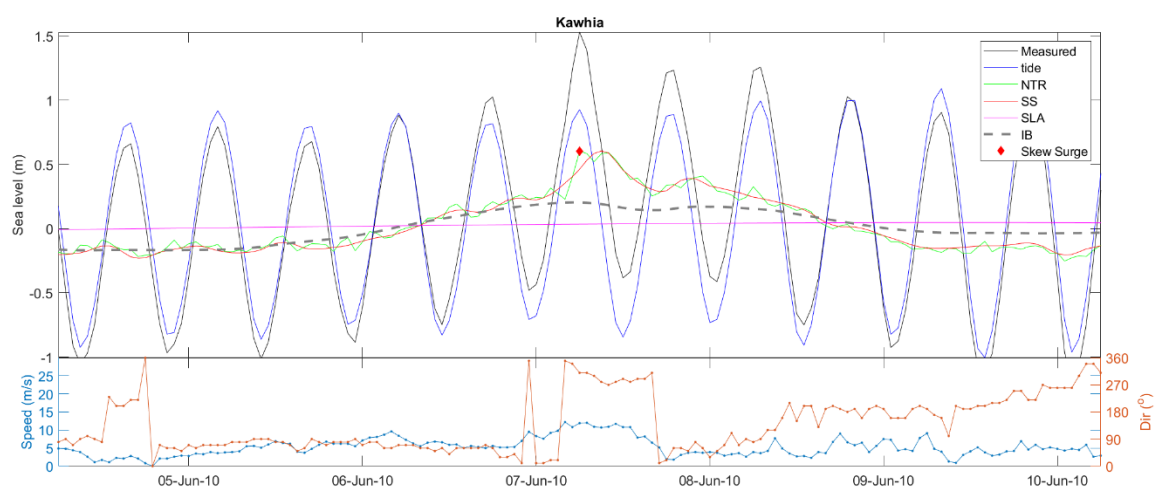
### June 2010 skew surge

Similar to the skew surge even on the 17 April 2013, the 7 June 2010 event was caused by a slow-moving low-pressure system which travelled across the Tasman Sea from Australia. This system made its way from the northwest to the southeast. This weather phenomenon caused a skew surge of 0.6 m at Kawhia, accompanied by a drop in barometric pressure to 987hPa and an inverse-barometer sea level rise of 0.2 m. The dominant factor contributing to the skew surge was the wind setup, accounting for 0.4 meters (as outlined in Table 6-4). The skew surge was a result of persistent high winds offshore, with the peak wind speed recorded at Slipper Island reaching 12.2 m/s, approximately 2-hours before high tide.

The weather situation at 6 am on 7 June 2010, is shown in Figure 6-37 and Figure 6-38.



**Figure 6-37: Mean sea-level pressure map at 6 am, 7-Jun-2010 around the time of the largest measured skew surge at Kawhia.**

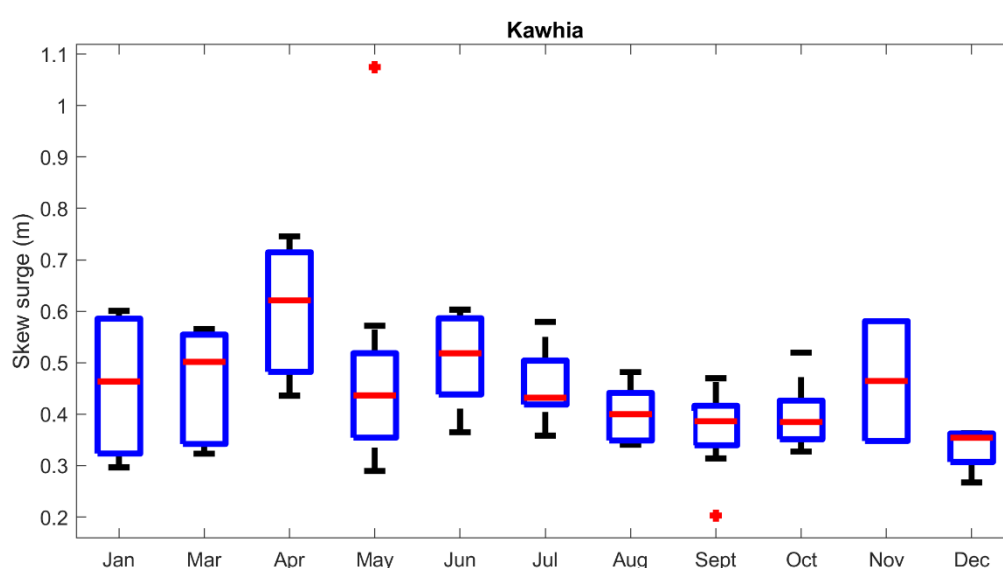


**Figure 6-38: Measured sea-level and its components during 7 June 2010 skew surge Kawhia. NTR = non-tidal residual, SS = Storm Surge, SLA = sea-level anomaly and IB = inverse barometer.**

### Seasonality of skew surges at Kawhia

The Kawhia sea-level record now spans nearly 15 years, the record is still too short for a robust analysis of seasonal skew surges. However, we present the results in Figure 6-39, but stress caution be used in the interpretation of these results. Monthly boxplots were constructed for the 5 largest skew surge events each year to highlight any seasonality in skew surge from the Kawhia skew surge data (Figure 6-39).

Skew surges, which exceed 0.5 meters in height, tend to occur predominantly during the late summer and fall months. An examination of the top 5 storm surges each month reveals that July experiences the highest number of skew surges (13), followed by May and September with the second-highest counts (10).



**Figure 6-39: Monthly boxplot of the 5 largest skew surge events per year at Kawhia.** Median (red line), top and bottom of boxes represent 3rd and 1st quartiles respectively. Maximum and minimum (excluding outliers) (black lines), outliers (red dots) correspond to values greater than  $Q3 + 1.5(Q3-Q1)$  or less than  $Q1 - 1.5(Q3-Q1)$ .

### Summary of skew surge analysis for Kawhia

At Kawhia the largest skew surges are driven by persistent high northerly wind speeds generated by low-pressure system which originate in the Tasman Sea or Southern Ocean. A skew surge of over 1 m was recorded at Kawhia this is the largest event measured and any of the five Waikato Regional Council sea-level gauges, the extreme skew surge analysis indicates that this event was a 1% AEP (Table 6-1).

#### 6.1.4 Raglan

The largest three skew surge events at Raglan are summarised in Table 6-5. MSLP data for Raglan was provided at the sea level gauge after June 2010. Before June 2010, MSLP is provided from the Port Taharoa AWS which is 45 km away from the Raglan gauge. A comparison of the overlapping portion of the Raglan gauge MSLP record shows that MSLP measured at Port Taharoa is a good fit to the Raglan data and no offsets were required.

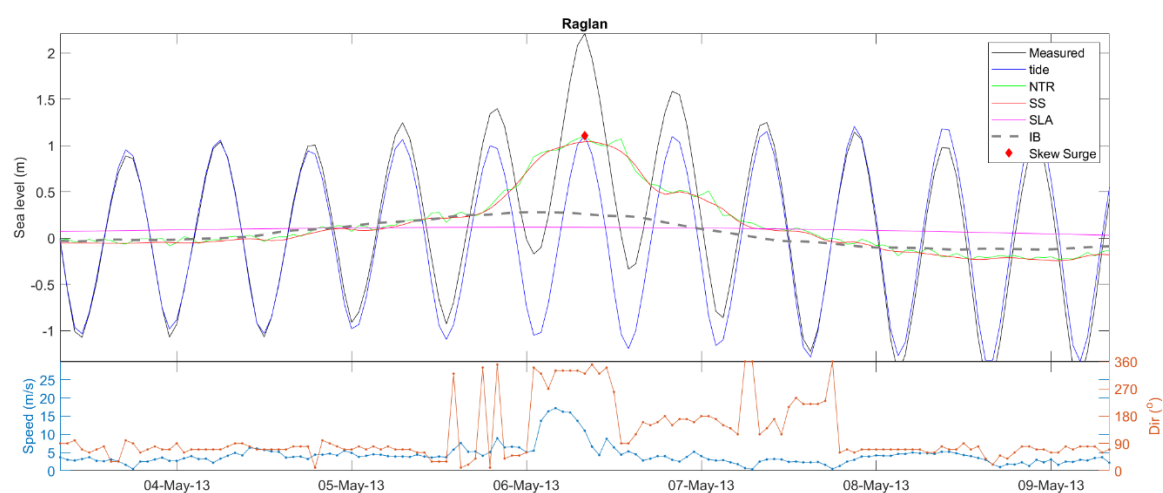


**Table 6-5: The top three skew surges on record at Raglan.**

Date	Skew surge (m)	Lowest barometric pressure (hPa)	IB component at peak skew surge (m)	Non-IB component (m)	IB contribution to skew surge (%)	Non-IB contribution to skew surge (%)
06-May-2013	1.16	985	0.26	0.90	22%	78%
13-Feb-2022	1.01	988	0.28	0.73	28%	72%
31-Jul-2008	0.75	990	0.09	0.66	12%	88%

### 6 May 2013 skew surge

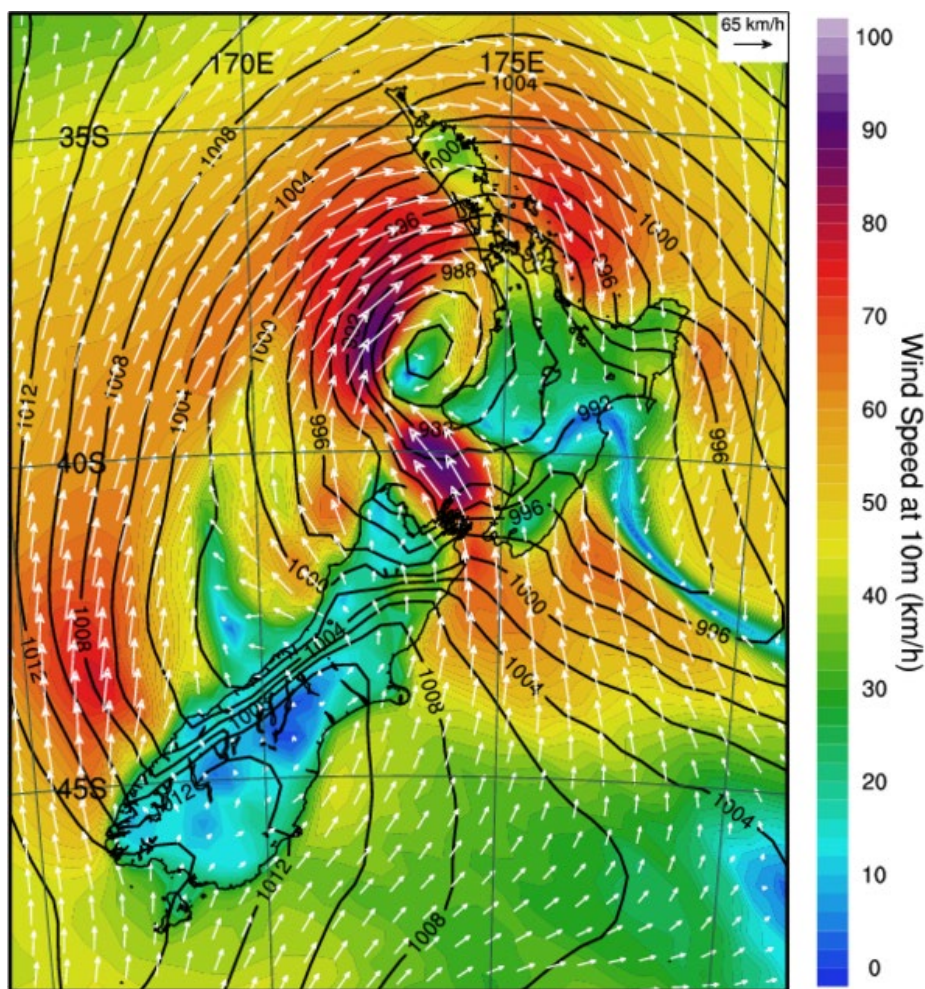
This storm event was also recorded at Kawhia (Section 6.1.3 and Figure 6-29). At Raglan a skew surge of 1.16 m was measured (1.10 m at Kawhia). There was no difference in air pressure between the two sites, the difference in bathymetry of both sites is the probable cause for the slightly different skew surge sizes (Figure 6-40).



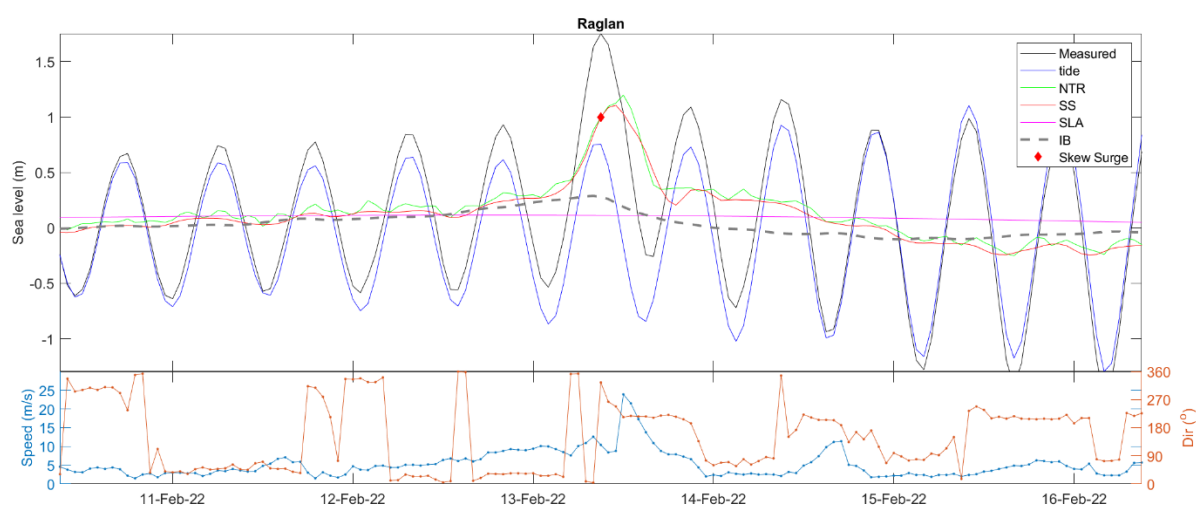
**Figure 6-40: Measured sea-level and its components during 6 May 2013 skew surge Raglan.** NTR = non-tidal residual, SS = Storm Surge, SLA = sea-level anomaly and IB = inverse barometer.

### 13 February 2022 skew surge

On 13 February 2022 a skew surge measuring 1.01 m at Raglan was generated by a broad active trough, which moved into the Tasman Sea (Figure 6-42). This meteorological system was accompanied by intense north-westerly winds and made its way from the northwest to the southeast, over a two-day period making land fall in Taranaki. At Raglan the barometric pressure dropped to 988 hPa, leading to an inverse-barometer sea level increase of 0.28 m. The dominant factor contributing to the skew surge was the wind setup, accounting for 0.733 m (as outlined in Table 6-5). The skew surge was a result of persistent high winds offshore, with the peak wind speed recorded at Taharoa reaching 12.6 m/s, approximately 1 hours before high tide. The weather situation at 1 pm on 13 February 2022, is depicted in Figure 6-41.



**Figure 6-41: Mean sea-level pressure map at 1 pm, 13-Feb-2022 around the time of the largest measured skew surge at Raglan.**



**Figure 6-42: Measured sea-level and its components during 13-Feb-2022 skew surge Raglan.** NTR = non-tidal residual, SS = Storm Surge, SLA = sea-level anomaly and IB = inverse barometer.

### 31 July 2008 skew surge

On 31 July 2008, a skew surge of 0.75 m occurred due to a slow-moving low-pressure system moving across the Tasman Sea from Australia. The system made its way from the northwest to the southeast over a two-day period, making landfall near Taranaki. The barometric pressure was 990 hPa, and an inverse-barometer sea level rise of 0.09 m (Figure 6-44). The primary factor responsible for the skew surge was wind setup, accounting for 0.662 m (as outlined in Table 6-5). The skew surge was a result of persistent high winds offshore, with the peak wind speed recorded at Taharoa reaching 17.5 m/s, approximately 4 hours before high tide. The weather situation at 1 pm on 31 July 2008, is depicted in Figure 6-43.

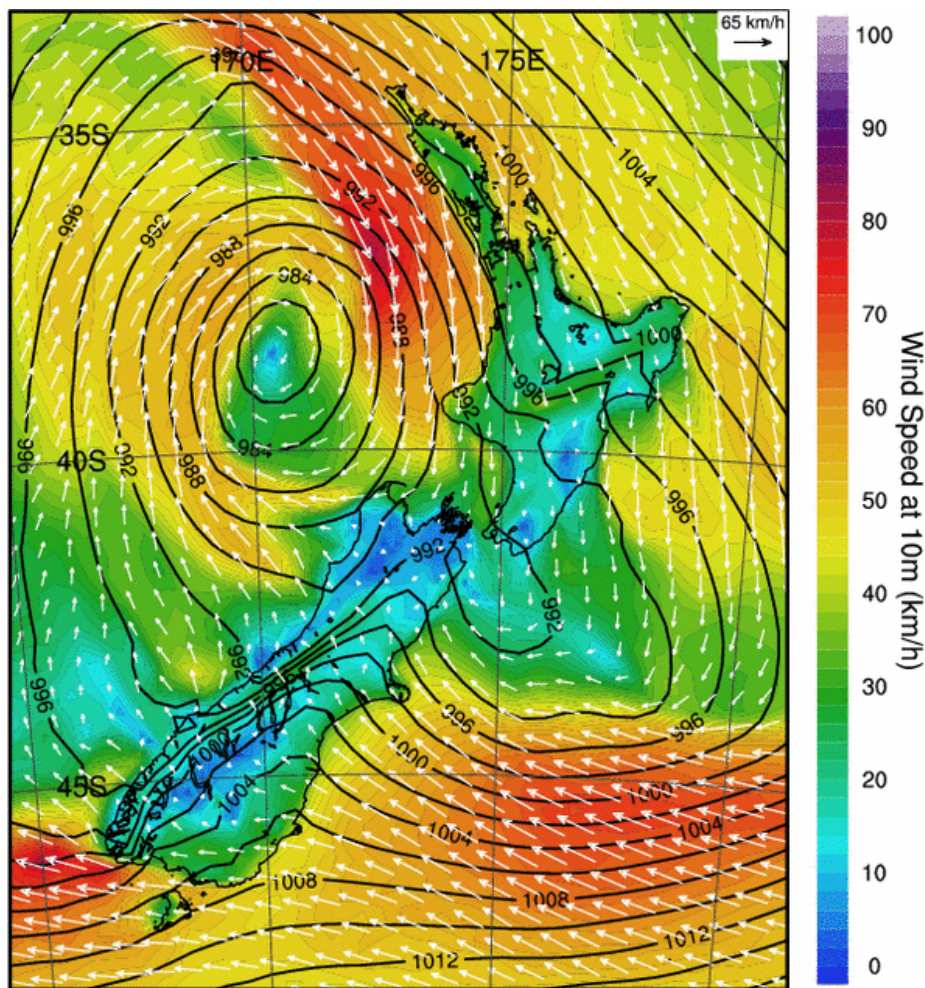
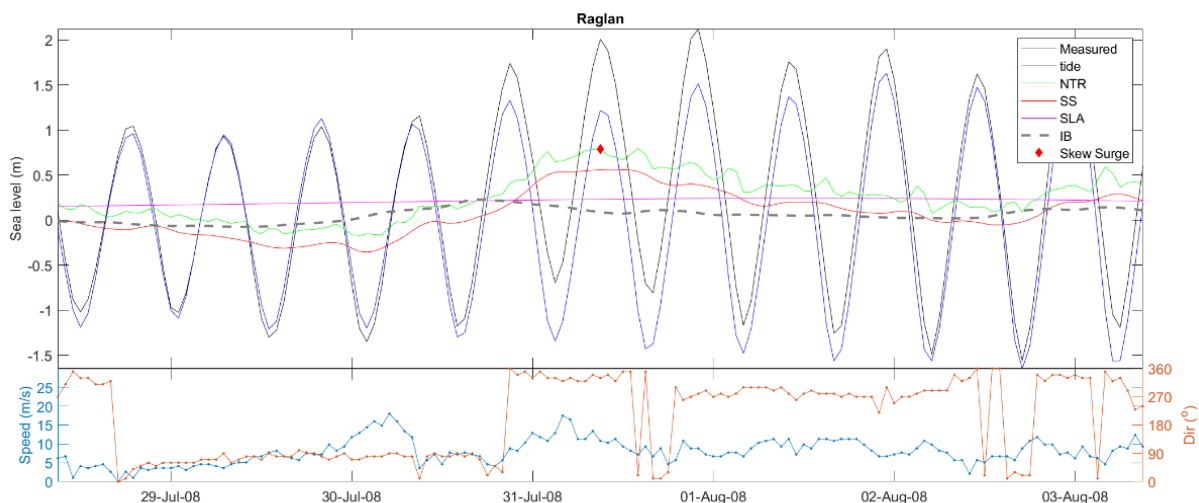


Figure 6-43: Mean sea-level pressure map at 1 pm, 31-Jul-2008 around the time of the largest measured skew surge at Raglan.





**Figure 6-44: Measured sea-level and its components during 31 July 2013 skew surge Raglan.** NTR = non-tidal residual, SS = Storm Surge, SLA = sea-level anomaly and IB = inverse barometer.

### Seasonality of skew surges

The sea-level record at Raglan is too short to meaningfully examine the seasonality of skew surge.

### Summary of skew surge analysis for Raglan

The largest skew surges at Raglan are driven by wind stress, with only a relatively small IB component. The large skew surges occur during complex low-pressure systems or troughs that result in strong wind speeds from the northwest, which are sustained over many hours. With three surges greater than 0.7 m and 1 event large than 1 m in just 14 years of record, it appears that Raglan is subject to large wind-driven skew surges that could conceivably reach well over 1 m in magnitude.

#### 6.1.5 Manu Bay

The largest three skew-surge events at Manu Bay are summarised in Table 6-6. The three largest skew -surge events in Manu Bay were all recorded in 2018. At the time of writing report NIWA's feed to the MSLP recorded at Manu Bay gauge site was not working correctly and all the pressure values were only to two significant figures. Because of this issue we used MSLP measured at the Raglan gauge site for this analysis. Table 6-6 shows the three largest skew-surges recorded at Manu Bay over the 5-year analysis period.

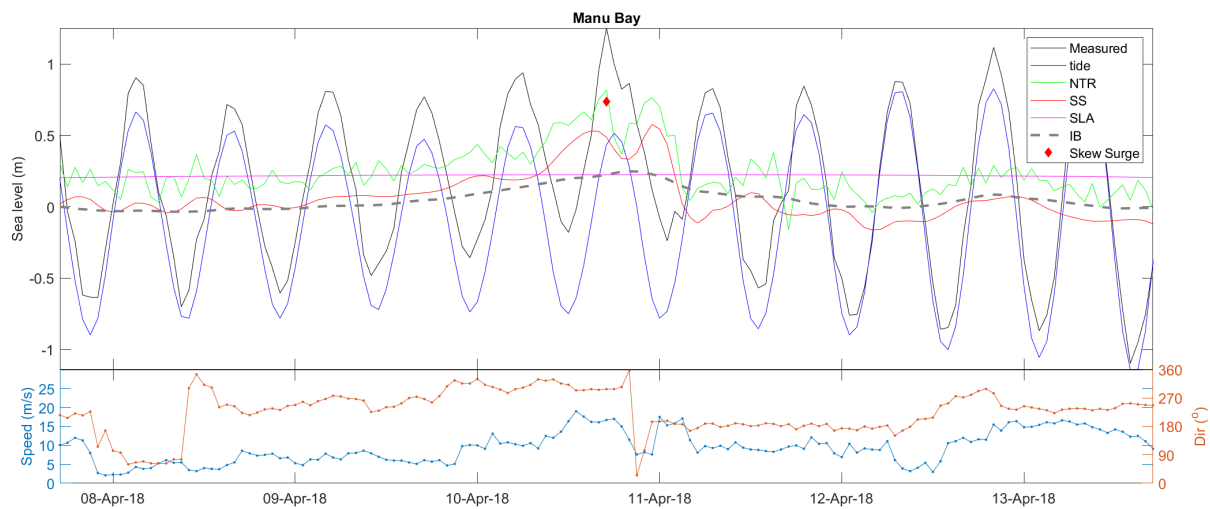
**Table 6-6: The top three skew surges on record at Manu Bay.**

Date	Skew surge (m)	Lowest barometric pressure (hPa)	IB component at peak skew surge (m)	Non-IB component (m)	IB contribution to skew surge (%)	Non-IB contribution to skew surge (%)
10-Apr-2018	0.74	988.7	0.23	0.51	31%	70%
14-Aug-2018	0.67	994.4	0.15	0.52	22%	78%
17-Jul-2021	0.59	999.4	0.04	0.55	7%	93%



### 10 April 2018 skew surge

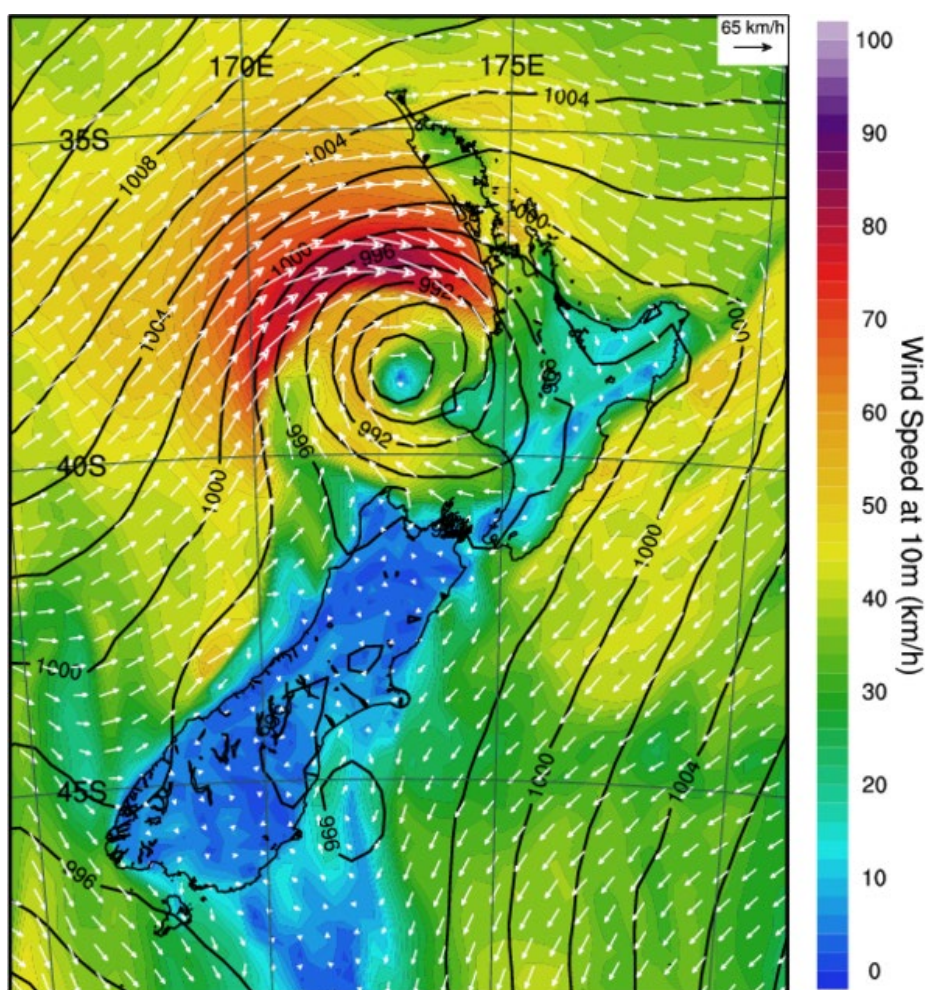
As described earlier for the 10 April event at Kawhia (Section 6.1.3), this weather system also caused a skew surge of 0.74 m at Manu Bay. Comparing the skew surges, Manu Bay experienced a slightly smaller skew surge when compared to Kawhia's 0.75 m. Analysing the contributing factors, it was noted that Kawhia exhibited a larger inverse barometer component at 0.25 m, while Manu Bay had a slightly smaller value at 0.23 m. However, the wind setup played a more significant role at Manu Bay, with a value of 0.51 m, compared to Kawhia's 0.5 m. In conclusion, the primary driver behind the skew surge was identified as the wind setup, responsible for a considerable 0.51 m contribution, as specified in Table 6-6. Figure 6-45 provides a breakdown of the event components.



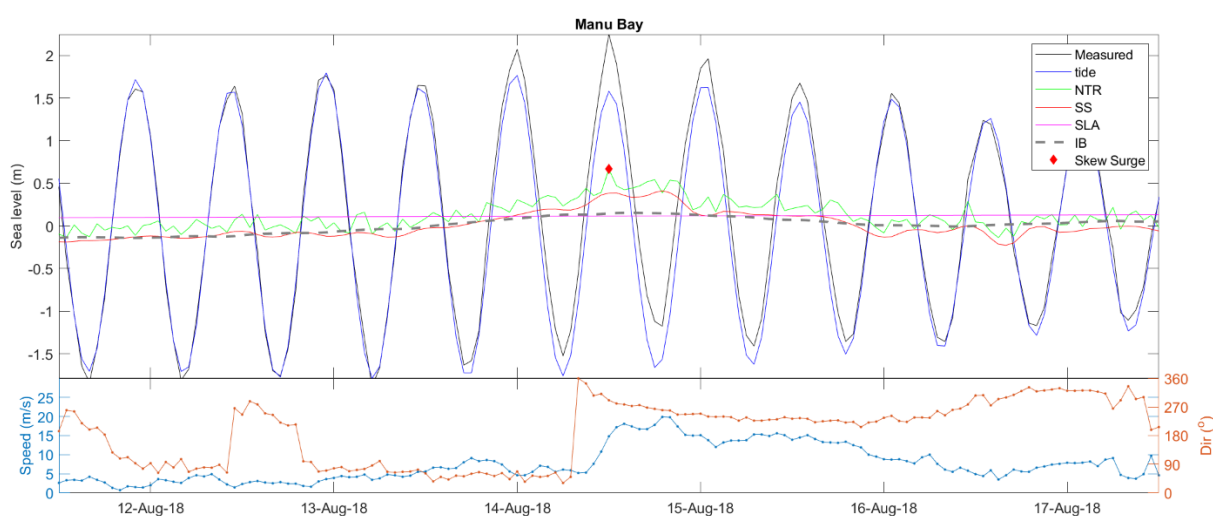
**Figure 6-45: Measured sea-level and its components during 10 April 2018 skew surge Manu Bay.** NTR = non-tidal residual, SS = Storm Surge, SLA = sea-level anomaly and IB = inverse barometer.

### 14 August 2018 skew surge

The 14 August 2018 a skew surge event at Manu Bay measuring 0.67 m was recorded. This event was generated by a strong sustained north-westerly winds, which blew up through the Tasman Sea, the peak wind speed recorded at Port Taharoa was 17.8 m/s (Figure 6-47). Late on 13 August a low-pressure system formed, and the barometric pressure dropped to 994 hPa resulting in an inverse-barometer sea level rise of 0.14 m. The dominant factor contributing to the skew surge was the wind setup, accounting for 0.52 m (as outlined in Table 6-6). The weather situation at 1 pm on 14 August 2018, is depicted in Figure 6-46.



**Figure 6-46: Mean sea-level pressure map at 1 pm, 14-Aug-2018 around the time of the largest measured skew surge at Manu Bay.**



**Figure 6-47: Measured sea-level and its components during 14 August 2018 skew surge Manu Bay.** NTR = non-tidal residual, SS = Storm Surge, SLA = sea-level anomaly and IB = inverse barometer.

### 17 July 2021 skew surge

On 17 July 2021 a low-pressure system in the Tasman Sea began to move towards New Zealand. By the 17<sup>th</sup>, the low system had dissipated somewhat, and the mean sea level barometric pressure measured at Port Taharoa was 999 hPa. This resulted in a IB of 0.04. The skew surge recorded during this event amounted to 0.55 m. At its peak, the wind speed reached 11 m/s, occurring approximately 3 hours prior to high tide (Figure 6-49). The wind set-up component of the skew surge measuring 0.54 m. The Taharoa weather station measures local conditions—the weather map indicates that this event was driven by strong offshore winds piling water up against the West Coast of the North Island. The weather situation at 4 pm on 17 July 2021 is depicted in Figure 6-48.

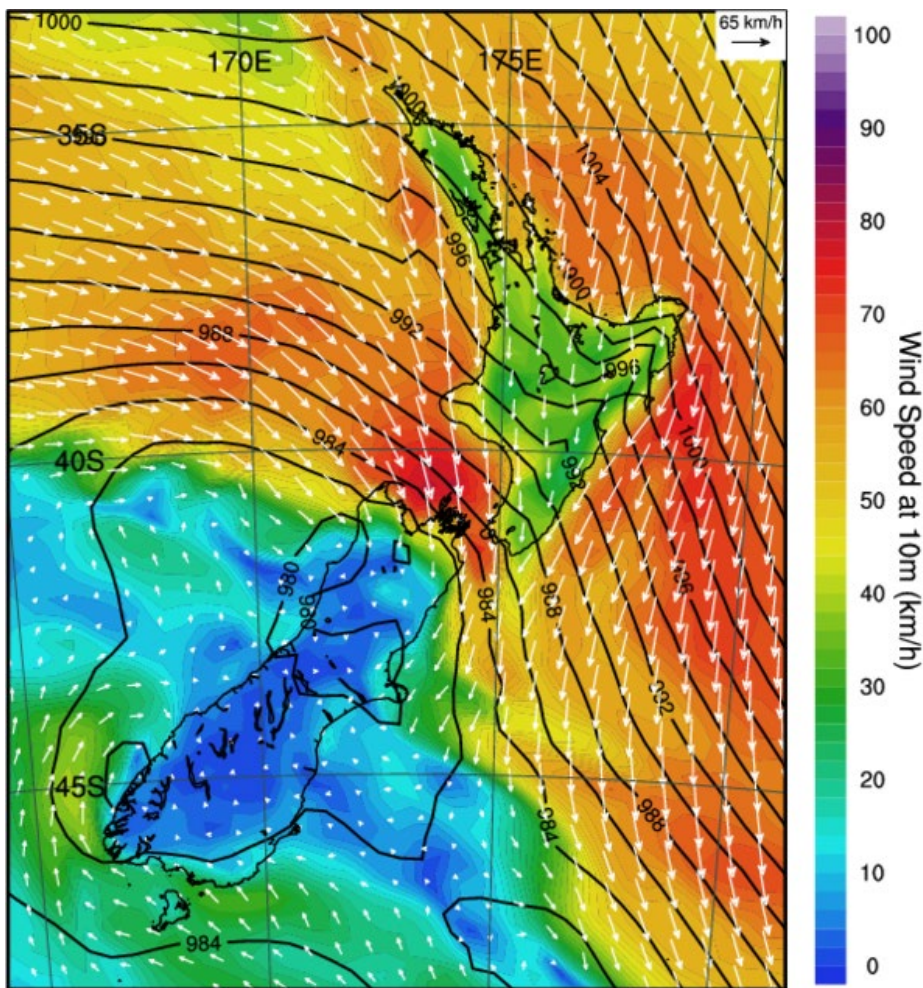
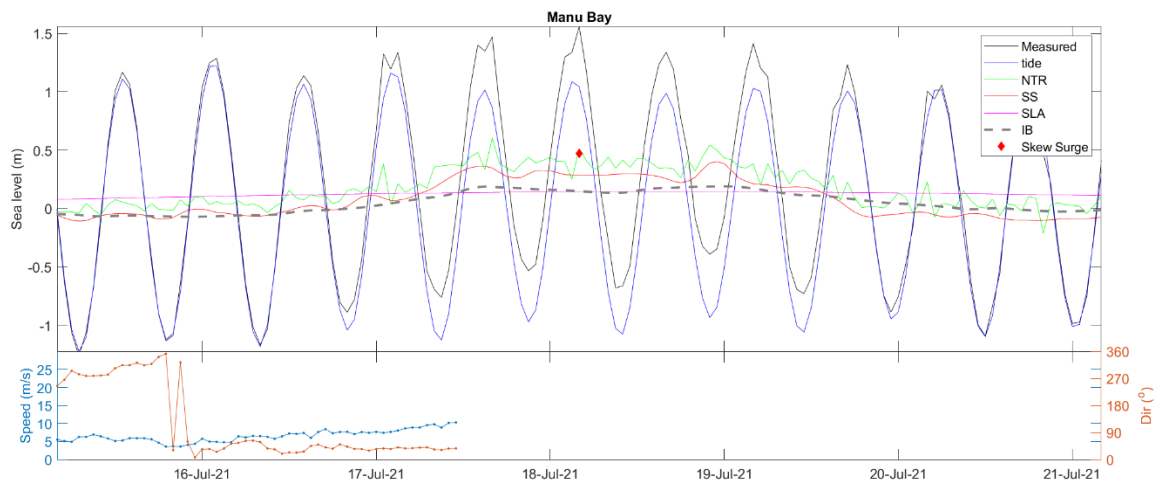


Figure 6-48: Mean sea-level pressure map at 4 pm, 17-Jul-2021 around the time of the third largest skew surge measured at Manu Bay.





**Figure 6-49: Measured sea-level and its components during 17 July 2021 skew surge Manu Bay.** NTR = non-tidal residual, SS = Storm Surge, SLA = sea-level anomaly and IB = inverse barometer.

### Seasonality of storm surges

The sea-level record at Manu Bay is too short to meaningfully examine the seasonality of storm surge.

### Summary of skew surge analysis for Manu Bay

Like Raglan, the largest skew surges at Manu Bay are driven by wind stress, with a minor contribution from the IB component. The largest skew surges occur during complex low-pressure systems or troughs that result in strong offshore wind speeds which blow from the north-westerly and westerly direction, which are sustained over many hours. With three surges greater than 0.5 m all recorded, it appears that Manu Bay could be subject to large wind-driven skew surges similar to Raglan and Kawhia.

#### 6.1.6 Summary of skew-surge records

The weather-map analysis shows different storm climates between the east (Whitianga and Tararu) and west (Kawhia, Raglan and Manu Bay) coasts of New Zealand - as found by Stephens et al. (2020).

At all sites the non-IB (wind setup) component of the skew surge was larger than the IB (drop in MSLP) component. The 2015 analysis found IB to be a larger component of storm surge at Whitianga. That is due to the difference in the analysis of IB between 2015 and 2023. We sampled IB at the time of the skew surge peaks which are aligned to high tide. The peak in IB is not aligned to high tide but to the weather system. In the 2015 work we identified the peak in hourly storm surge and the corresponding IB at the time, which is likely to align better with the weather system. This leads to difference in the relative proportion of the IB contribution between the two studies.

Tides and surges interact nonlinearly, meaning the total water level is not simply the sum of the two. Mid-tide conditions often align with the strongest dynamic response in the coastal system, where wind and pressure effects are maximised, resulting in larger storm surges. A clear example of this can be seen in Figure 6-45 at Manu Bay. This pattern occurs because storm surge effects are influenced by the underlying tidal cycle, particularly at coastal gauges. At low tide, water levels may be too low

for the surge to reach its full impact, while at high tide, the shallow coastal profile can limit additional water level rise due to friction and inundation.

Tararu experienced larger skew surges than Whitianga. The largest skew surges at Tararu occurred when wind fronts aligned with the Firth of Thames.

Skew surges at Kawhia, Raglan and Manu Bay were dominated by the wind setup associated with persistently strong north-westerly winds from weather fronts blowing over several days; they drive surges almost double those experienced at Whitianga with maximum measured storm surges above 1 m in height.

The analysis indicates that locally measured wind speeds and directions may not always be reliable indicators of wind set-up at Tararu. Instead, weather maps provide greater explanatory power. Atmospheric pressure fields remain relatively consistent over the spatial scales considered, meaning inverse barometer effects would not be significantly impacted. Several factors contribute to this:

- **Local Topography Influence:** The local terrain and topography can significantly affect wind patterns. Mountains, buildings, and other geographical features can alter wind direction and speed, making it difficult to predict surge solely based on nearby wind measurements.
- **Offshore Surge Generation:** Storm surges are often generated by wind and pressure acting over considerable fetches, where the storm's energy and wind speeds are typically higher offshore and may be of different directionality compared to local gauge measurements. These surges can then propagate towards the coastline. Relying solely on local wind measurements may not capture the full extent of the surge potential, especially if it originates farther from the measurement point.

## 7 Storm tide extreme-value analysis

When a coastal storm coincides with a high tide, the storm surge can elevate the water levels, resulting in a storm tide. The storm tide is the total water level observed during the storm, which includes both the storm surge the astronomical tide and the mean sea level anomaly. The effects of a storm tide can be quite severe, especially if it occurs in an area with low-lying coastal regions or inadequate coastal defences. The combination of high-water levels, strong winds, and wave action can result in coastal flooding, erosion, and damage to coastal infrastructure.

The useable data records from Manu Bay and Raglan are short for extreme value analysis. The use of a joint-probability method overcomes this limitation to a degree, but we recommend caution in the use of the skew surge and storm tide extreme value analysis results. Joint-probability methods can yield reliable extreme sea level projections to a return period of approximately 10 times the record length. The gauge records at Manu Bay and Raglan are still short even for the use of joint-probability methods.

### 7.1 Skew-surge joint-probability analysis

**Storm-tide** is defined as the sea-level peak reached during a storm event, from a combination of **MSLA + tide + storm surge**. It is the storm-tide that is primarily measured by sea-level gauges such as the Whitianga, Kawhia and Tararu gauges analysed here. The skew-surge joint-probability method was used to predict the extreme storm-tide distribution for a range of Annual Exceedance Probabilities (AEP's). Stephens (2018) compared the SSJPM and Monte-Carlo joint-probability method used by Stephens et al. (2015), at Tararu, and found the methods to return similar median fits, but the SSJPM used here has more realistic (wider) confidence intervals due to the bootstrapping method used.

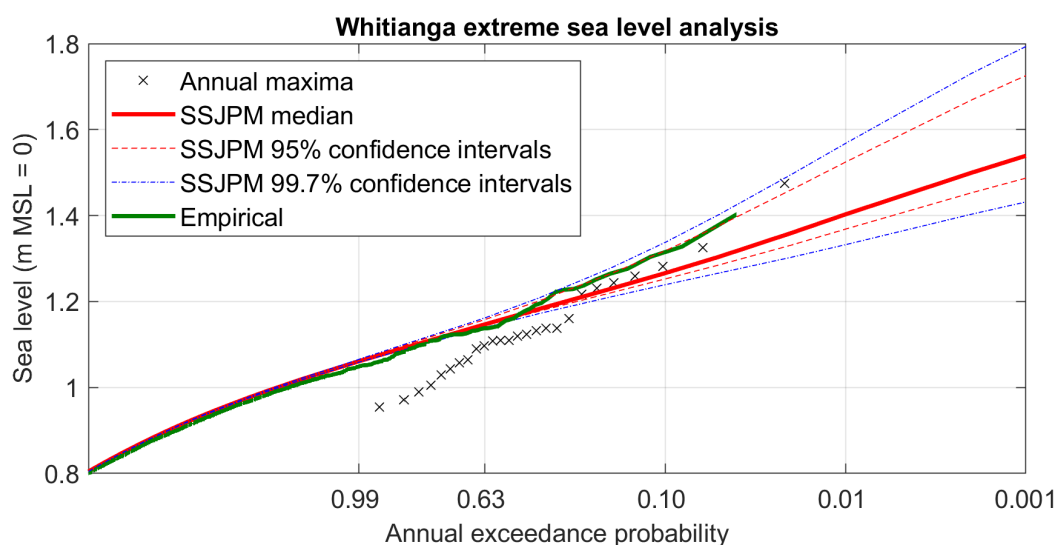
Joint-probability methods provide a more robust low-frequency magnitude estimates for short-duration records because they overcome the main theoretical limitations of extreme value theory application to sea levels—splitting the sea level into its deterministic (predictable) tidal and stochastic (e.g., unpredictable, storm-driven) non-tidal components, and analysing the two components separately before recombining (e.g., (Tawn and Vassie 1989); (Haigh et al. 2010)). Storm-tide return periods can be estimated from relatively short records because all skew surges are considered, not just those that lead to extreme levels. A limitation of the SSJPM and other joint-probability methods is that it assumes tide and skew surge are independent, which has been shown to be true in the UK (Williams et al. 2016). Costa et al. (2023) showed that tide-surge interaction occurs to some degree in most sea-level gauge records in NZ. However, this interaction seems to affect moderately large storm-tides but not the very largest events—comparisons with direct maxima methods for > 50-year-long records give similar results for return periods  $\geq 10$  years and also match observed maxima well, and thus support the validity of the independence assumption for long-return-period events (Stephens et al. 2020).

We subsampled all sea-level data to 1 h intervals after first applying a 15 min running average to minimize the effect of far infragravity and tsunami waves. The data were linearly detrended to a zero-mean relative to local vertical datum for each gauge, to remove the effects of historical SLR from the sea-level distribution and create a quasi-stationary time series required for extreme value analysis (Coles 2001). Therefore, here we define the term “**storm tide**” as the total water level above MSL from the sum of tide plus skew surge.

For each site, the annual maximum storm tide was compared alongside the storm tide heights (Figure 7-1 to Figure 7-5). Extreme storm tide heights are provided in Table 7-1 to Table 7-5. At Tararu, the results are equivalent within 1 cm to the results obtained by Stephens (2018, Table 3-1) after removing the MSL, infragravity wave and location adjustment made by Stephens (2018). At all locations the median distribution from the SSJPM is similar to that from the MCJPM applied in 2015.

**Table 7-1: Extreme storm-tide distribution at Whitianga.** Elevations for the median and 95% confidence bounds are based on a Skew-surge joint-probability analysis of sea level data at Whitianga wharf. The storm-tide elevations presented here are given relative to a zero MSL. To calculate the elevations relative to MVD-53, add the present-day MSL datum offsets in Table 4-2.

AEP (%)	ARI (years)	Median (m)	Lower 95% C.I (m)	Upper 95% C.I (m)
39	2	1.19	1.18	1.21
18	5	1.25	1.22	1.28
10	10	1.29	1.26	1.34
5	20	1.34	1.29	1.40
2	50	1.41	1.34	1.50
1	100	1.47	1.38	1.57
0.5	200	1.50	1.40	1.61

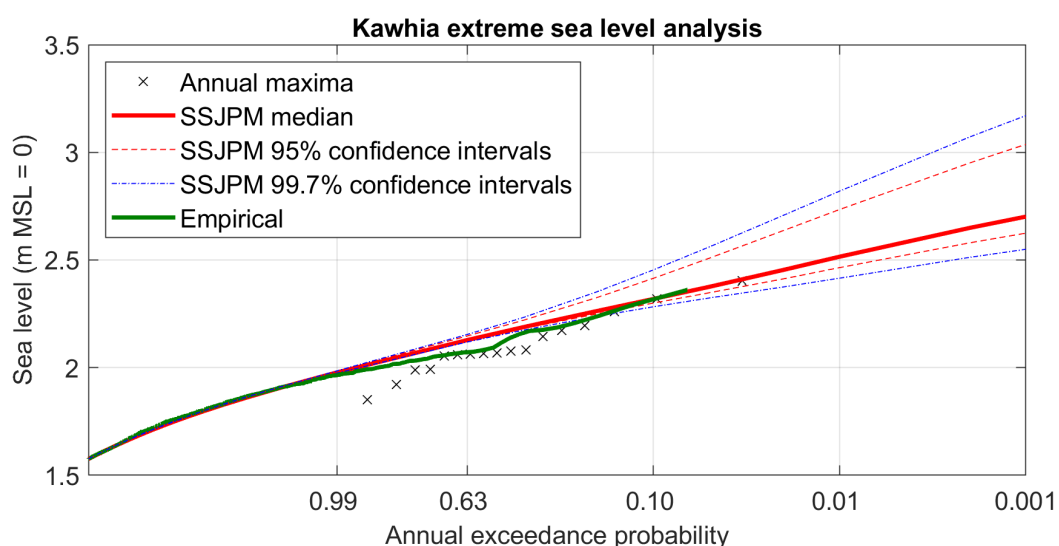


**Figure 7-1: Extreme storm tide prediction levels, and annual maximum sea levels for Whitianga.** Predicted storm tide levels make use of the Skew-surge joint-probability method. Red dashed lines indicate 95% confidence intervals. Blue dashed lines indicate the 99.7% confidence interval. Refer to Table 7-1 for the data in table form.



**Table 7-2: Extreme storm-tide distribution at Kawhia.** Elevations for the median and 95% confidence bounds are based on a Skew-surge joint-probability analysis of sea level data at Kawhia. The storm-tide elevations presented here are given relative to a zero MSL. To calculate the elevations relative to MVD-53, add the present-day MSL datum offsets in Table 4-2.

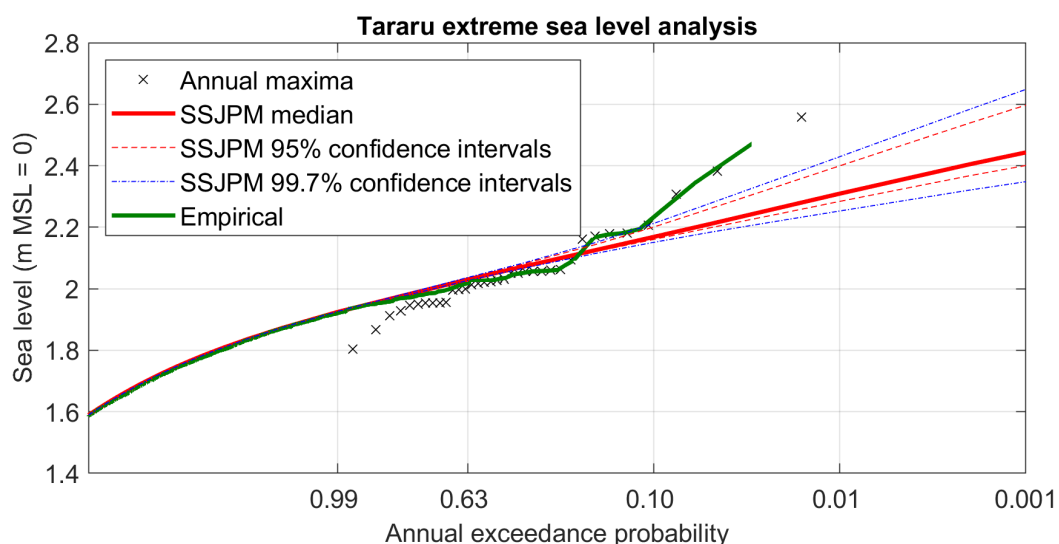
AEP (%)	ARI (years)	Median (m)	Lower 95% C.I (m)	Upper 95% C.I (m)
39	2	2.21	2.18	2.23
18	5	2.30	2.26	2.35
10	10	2.38	2.31	2.45
5	20	2.46	2.36	2.56
2	50	2.57	2.43	2.71
1	100	2.65	2.49	2.82
0.5	200	2.70	2.52	2.88



**Figure 7-2: Extreme storm tide prediction levels, and annual maximum sea levels for Kawhia.** Predicted storm tide levels make use of the Skew-surge joint-probability method. Dashed lines indicate 95% confidence intervals. Refer to Table 7-2 for the data in table form.

**Table 7-3: Extreme storm-tide distribution at Tararu.** Elevations for the median and 95% confidence bounds are based on a Skew-surge joint-probability analysis of sea level data at Tararu. The storm-tide elevations presented here are given relative to a zero MSL. To calculate the elevations relative to MVD-53, add the present-day MSL datum offsets in Table 4-2.

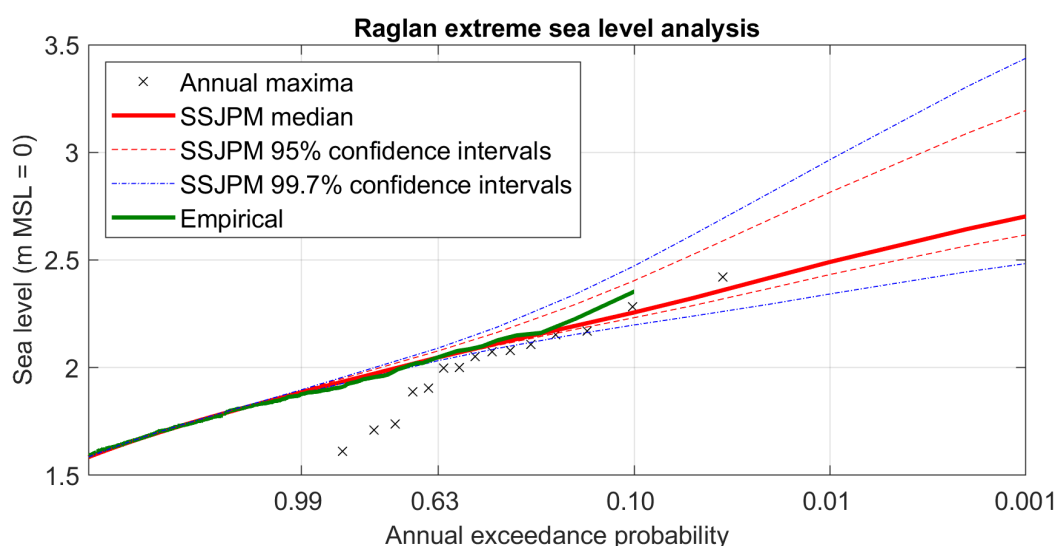
AEP (%)	ARI (years)	Median (m)	Lower 95% C.I (m)	Upper 95% C.I (m)
39	2	2.08	2.07	2.08
18	5	2.14	2.12	2.15
10	10	2.19	2.16	2.21
5	20	2.24	2.20	2.28
2	50	2.31	2.26	2.36
1	100	2.37	2.30	2.43
0.5	200	2.40	2.32	2.47



**Figure 7-3: Extreme storm tide prediction levels, and annual maximum sea levels for Tararu.** Predicted storm tide levels make use of the Skew-surge joint-probability method. Dashed lines indicate 95% confidence intervals. Refer to Table 7-3 for the data in table form.

**Table 7-4: Extreme storm-tide distribution at Raglan.** Elevations for the median and 95% confidence bounds are based on a Skew-surge joint-probability analysis of sea level data at Raglan. The storm-tide elevations presented here are given relative to a zero MSL. To calculate the elevations relative to MVD-53, add the present-day MSL datum offsets in Table 4-2.

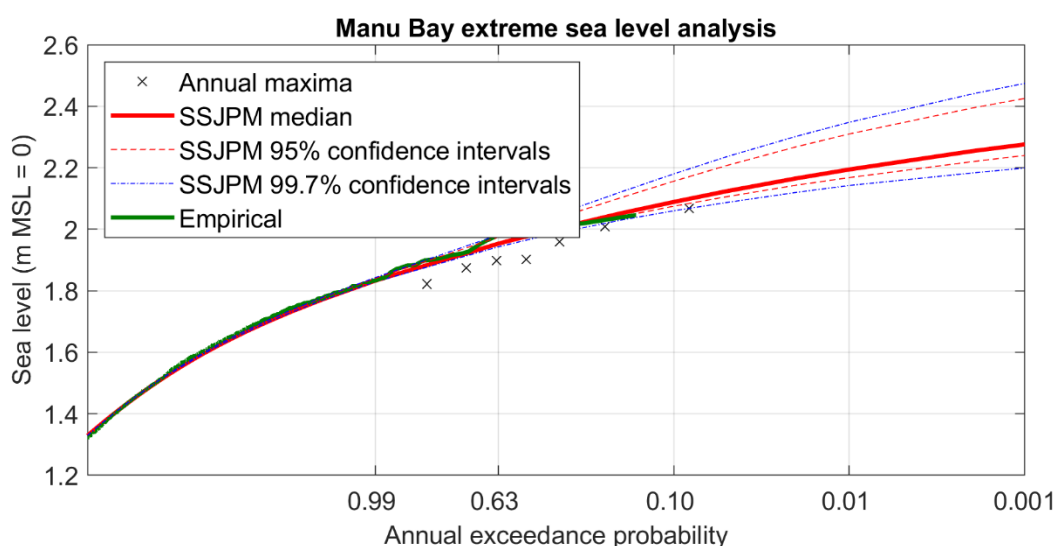
AEP (%)	ARI (years)	Median (m)	Lower 95% C.I (m)	Upper 95% C.I (m)
39	2	2.14	2.11	2.19
18	5	2.25	2.18	2.34
10	10	2.35	2.24	2.47
5	20	2.45	2.30	2.62
2	50	2.59	2.38	2.81
1	100	2.69	2.45	2.97
0.5	200	2.74	2.48	3.05



**Figure 7-4: Extreme storm tide prediction levels, and annual maximum sea levels for Raglan.** Predicted storm tide levels make use of the Skew-surge joint-probability method. Dashed lines indicate 95% confidence intervals. Refer to Table 7-4 for the data in table form.

**Table 7-5: Extreme storm-tide distribution at Manu Bay.** Elevations for the median and 95% confidence bounds are based on a Skew-surge joint-probability analysis of sea level data at Manu Bay. The storm-tide elevations presented here are given relative to a zero MSL. To calculate the elevations relative to MVD-53, add the present-day MSL datum offsets in Table 4-2.

AEP (%)	ARI (years)	Median (m)	Lower 95% C.I (m)	Upper 95% C.I (m)
39	2	2.02	1.99	2.04
18	5	2.08	2.04	2.12
10	10	2.13	2.08	2.18
5	20	2.18	2.11	2.24
2	50	2.23	2.15	2.30
1	100	2.27	2.18	2.35
0.5	200	2.29	2.19	2.37



**Figure 7-5: Extreme storm tide prediction levels, and annual maximum sea levels for Manu Bay.** Predicted storm tide levels make use of the Skew-surge joint-probability method. Dashed lines indicate 95% confidence intervals. Refer to Table 7-5 for the data in table form.

Appendix C presents the storm tide elevations corresponding to the upper 0.5% and lower 39% AEP confidence intervals, converted from MSL to the MVD-53 and NZVD2016 vertical datums.

## 7.2 Breakdown of the largest storm-tide events

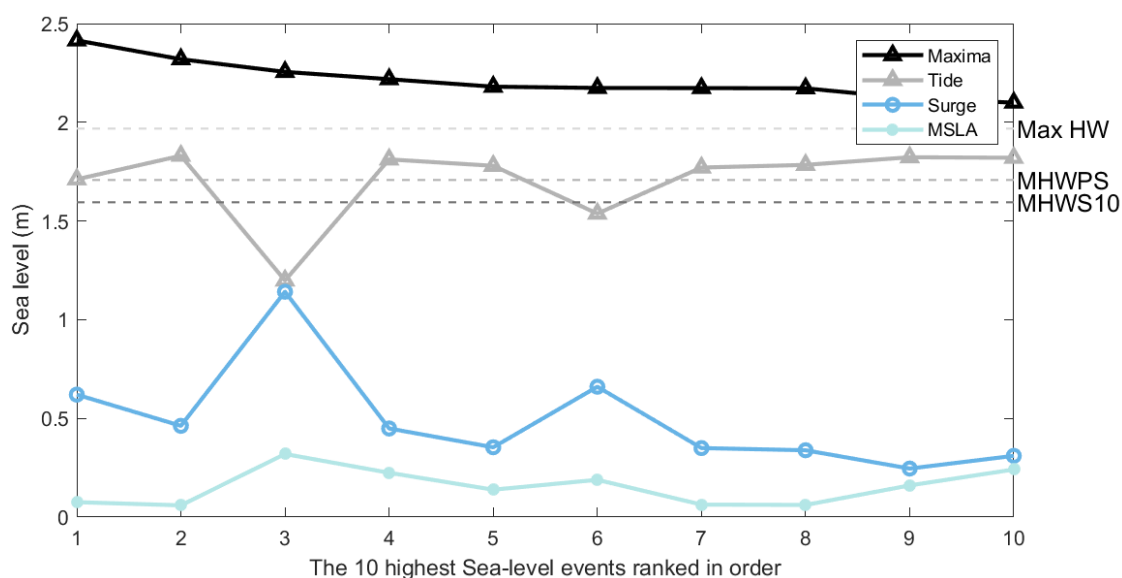
For each sea level gauge, the highest 10 storm tide events and their contributing component elevations (SLA, tide, storm surge, remaining high-frequency oscillations) were determined (Figure 7-6, Figure 7-7, Figure 7-8, Figure 7-9 and Figure 7-10).

To ensure that the selected events were independent of each other, storm-tide peaks separated by at least 3 days were chosen. This 3-day threshold was deemed sufficient to distinguish between storm tide peaks generated by distinct storm events, because weather systems typically pass over New Zealand every 4- 7 days.

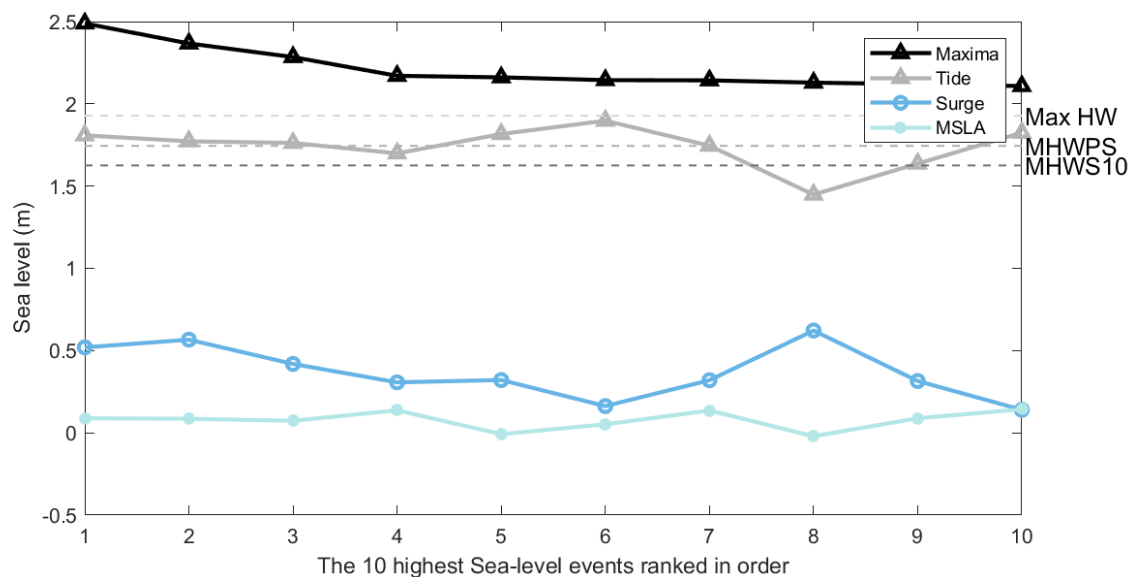
The contributing component elevations were determined by decomposing the quality assured sea level at each gauge as described in Section 6.1.

The data is plotted in Figure 7-6 to Figure 7-10. The following points can be observed:

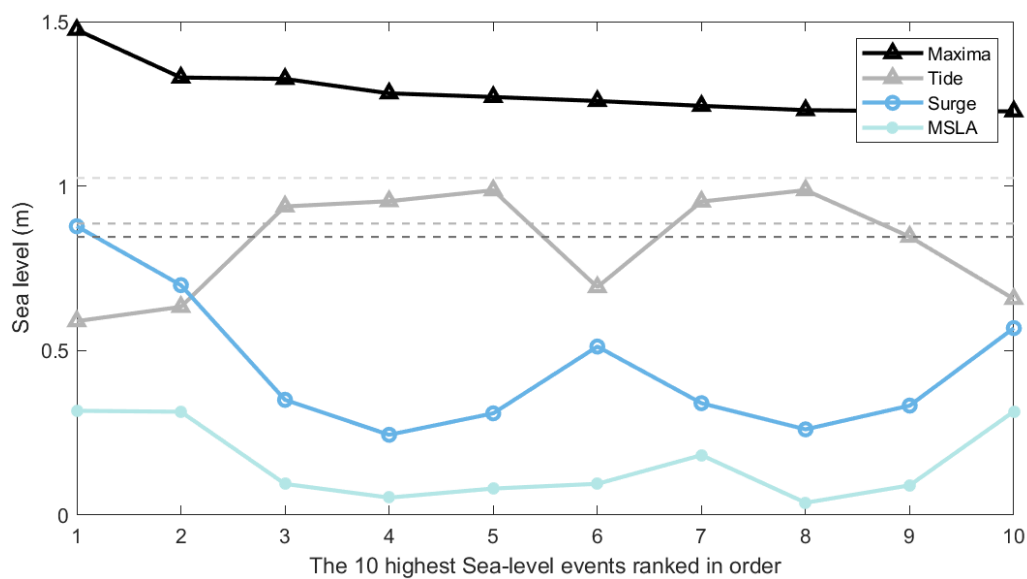
- The tide forms the dominant component of storm-tide at all sites for all cases except for the two most recent storm tides in Whitianga.
- Large storm-tides can consist almost exclusively of tide, compounded by SLA (e.g., Figure 7-8).
- The great majority of storm tides have some positive storm surge component, but often it is relatively small in comparison to the tidal component, particularly at Tararu, Kawhia, Raglan and Manu Bay.



**Figure 7-6: The contributions of tide, skew surge and MSLA to the 10 largest storm tides recorded at the Kawhia sea-level recorder.**

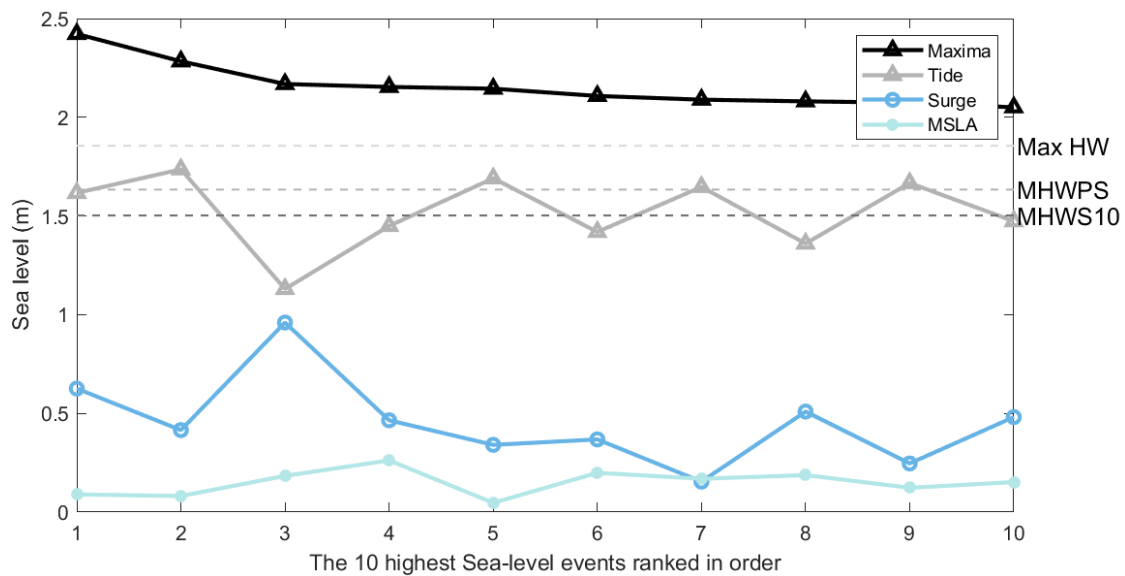


**Figure 7-7:** The contributions of tide, skew surge and MSLA to the 10 largest storm tides recorded at the Tararu sea-level recorder.

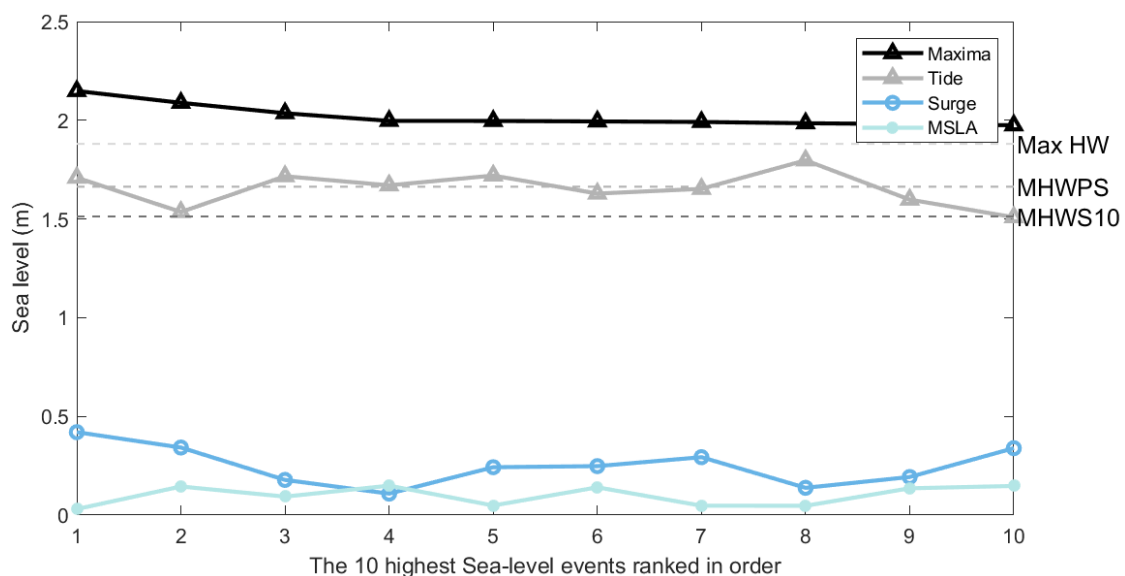


**Figure 7-8:** The contributions of tide, skew surge and MSLA to the 10 largest storm tides recorded at the Whitianga sea-level recorder.





**Figure 7-9:** The contributions of tide, skew surge and MSLA to the 10 largest storm tides recorded at the Raglan sea-level recorder.



**Figure 7-10:** The contributions of tide, skew surge and MSLA to the 10 largest storm tides recorded at the Manu Bay sea-level recorder.

### 7.3 Seasonality of storm tides

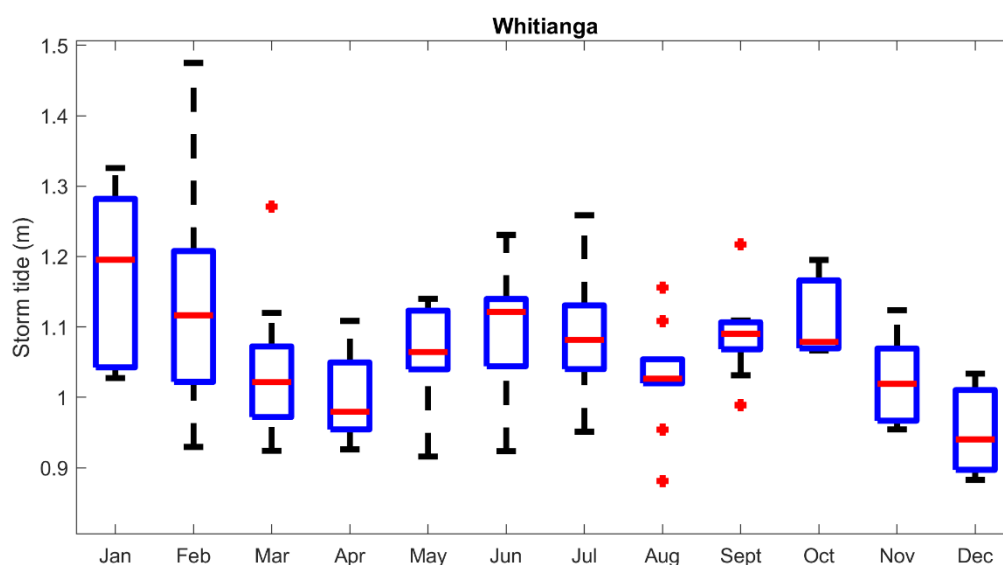
Two types of plot are used in this section:

1. For each site, a monthly boxplot was constructed of the 5 largest storm-tide events per year to highlight any seasonality in storm-tide hazard (created as a subset of the 20 largest storm-tide events). The boxplots show the distribution of height, per month—i.e., do the large storm tides tend to be larger on average than at other times of the year.

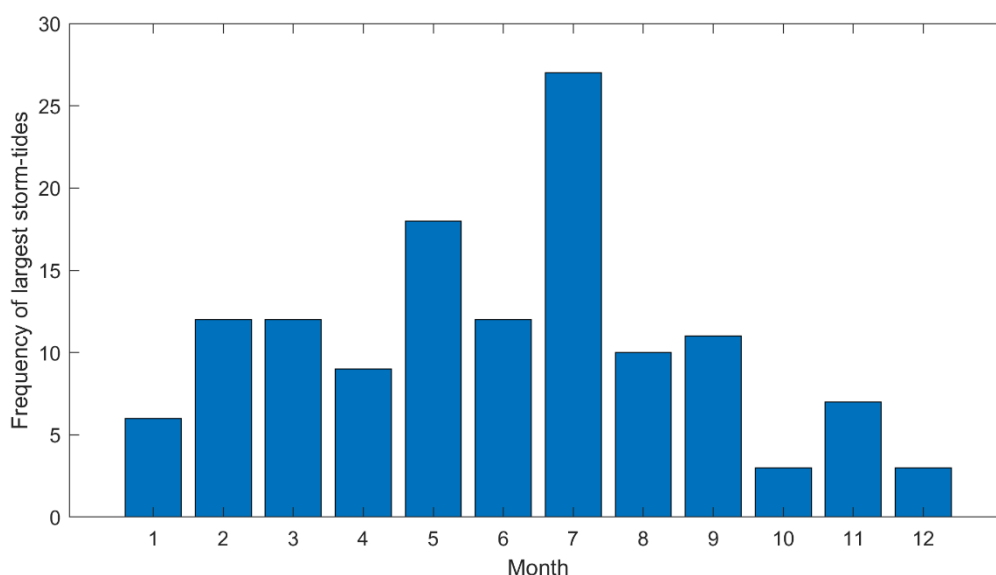
- It is also useful to determine the months where the largest storm-tides most often occur, so a monthly bar chart was created of the month of occurrence largest 5 storm-tides per year (regardless of height).

### 7.3.1 Whitianga

At Whitianga there is no clear seasonal trend in *height* of the largest storm tides (Figure 7-11). There is a seasonal trend in the *frequency* of storm tides, with more storm tides occurring during winter, and fewer occurring in spring and early summer (Figure 7-12).



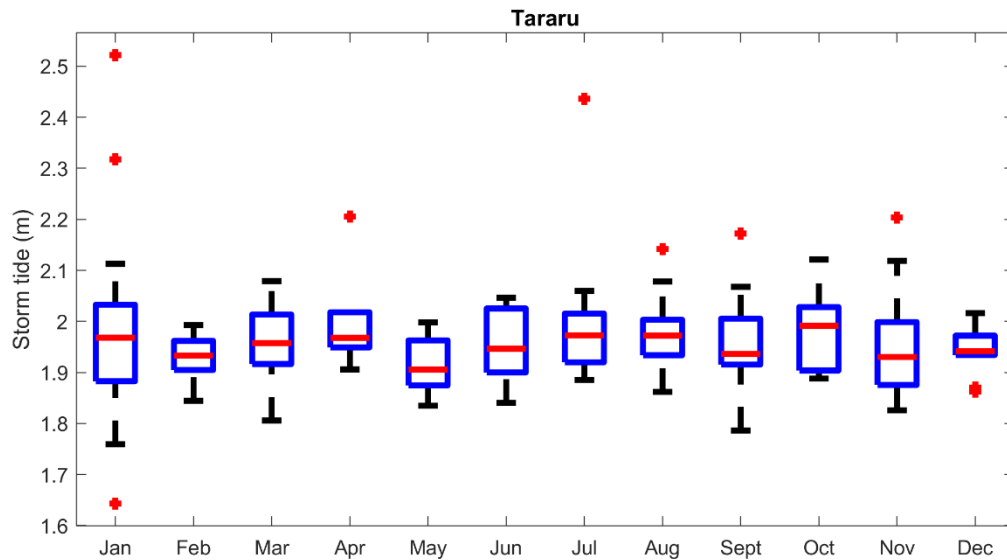
**Figure 7-11: Monthly boxplot of the five largest storm tide events per year at Whitianga.** The mean annual sea-level cycle has been removed. Median (red line), top and bottom of boxes represent 3<sup>rd</sup> and 1<sup>st</sup> quartiles respectively. Maximum and minimum (black lines), outliers (red dots) correspond to values greater than  $Q3 + 1.5(Q3-Q1)$  or less than  $Q1 - 1.5(Q3-Q1)$ .



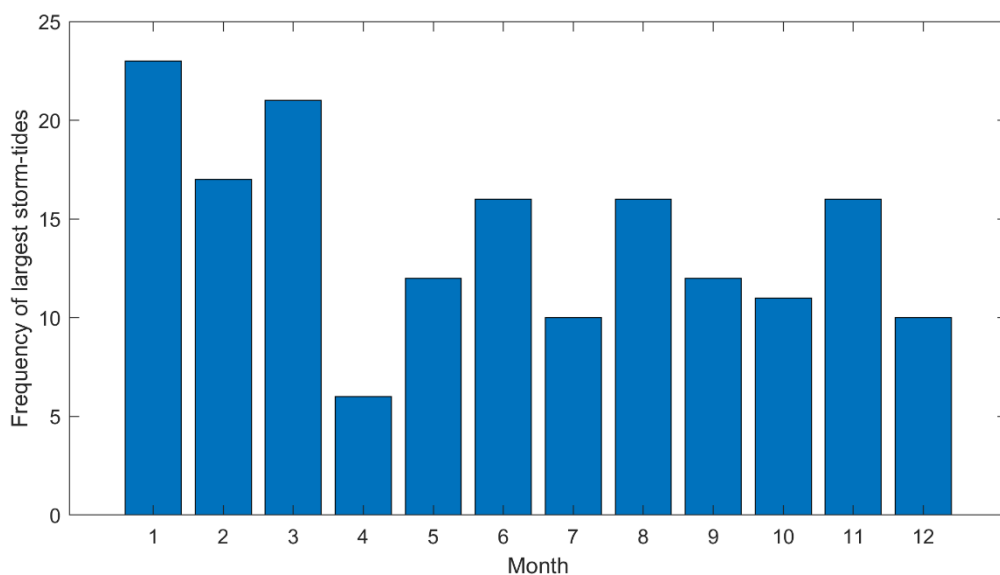
**Figure 7-12: Frequency of the five largest storm-tides each year sorted by month at Whitianga.** The mean annual sea-level cycle has been removed.

### 7.3.2 Tararu

There is no clear seasonal trend in the *height* of the largest storm-tides at Tararu (Figure 7-13). The storm-tide *frequency* distribution shows a distinct quiescent period in April when fewer storm tides occur (Figure 7-14)—April was also a relatively quiet month at Whitianga.



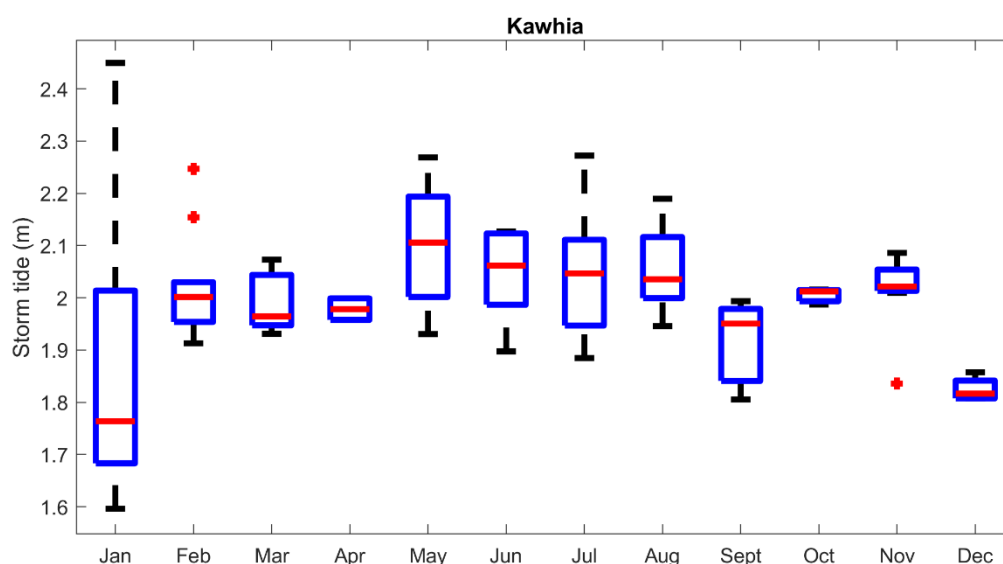
**Figure 7-13: Monthly boxplot of the five largest storm tide events per year at Tararu.** The mean annual sea-level cycle has been removed. Median (red line), top and bottom of boxes represent 3<sup>rd</sup> and 1<sup>st</sup> quartiles respectively. Maximum and minimum (excluding outliers) (black lines), outliers (red dots) correspond to values greater than  $Q3 + 1.5(Q3-Q1)$  or less than  $Q1 - 1.5(Q3-Q1)$ .



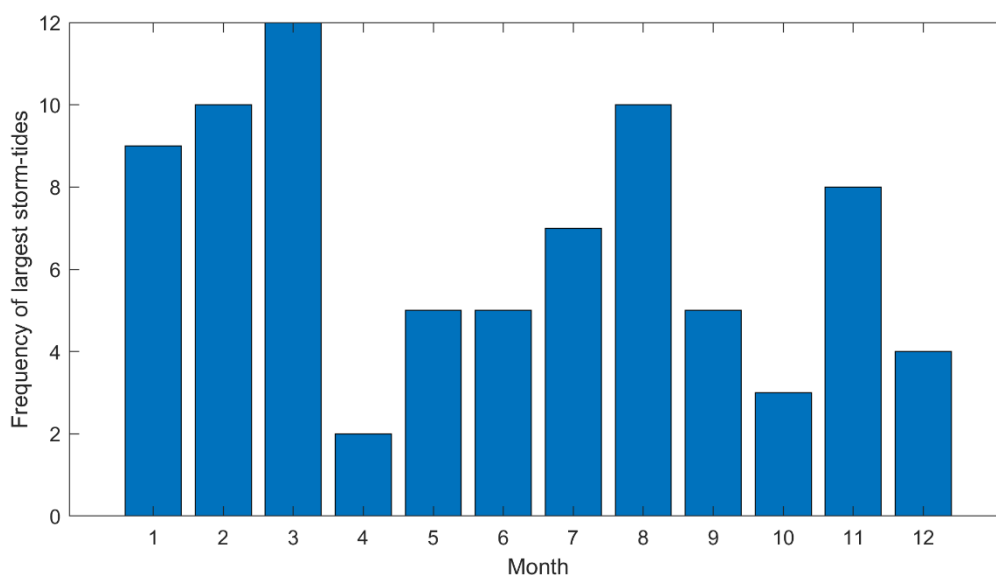
**Figure 7-14: Frequency of the five largest storm-tides each year sorted by month at Tararu.** The mean annual sea-level cycle has been removed.

### 7.3.3 Kawhia

At Kawhia, the largest storm tides tend to be larger on average in the winter (Figure 7-15) but are more common in the summer (Figure 7-16). Again, April is a relatively quiet month (Figure 7-16).



**Figure 7-15: Monthly boxplot of the five largest storm tide events per year at Kawhia.** The mean annual sea-level cycle has been removed. Median (red line), top and bottom of boxes represent 3rd and 1st quartiles respectively. Maximum and minimum (excluding outliers) (black lines), outliers (red dots) correspond to values greater than  $Q3 + 1.5(Q3-Q1)$  or less than  $Q1 - 1.5(Q3-Q1)$ .



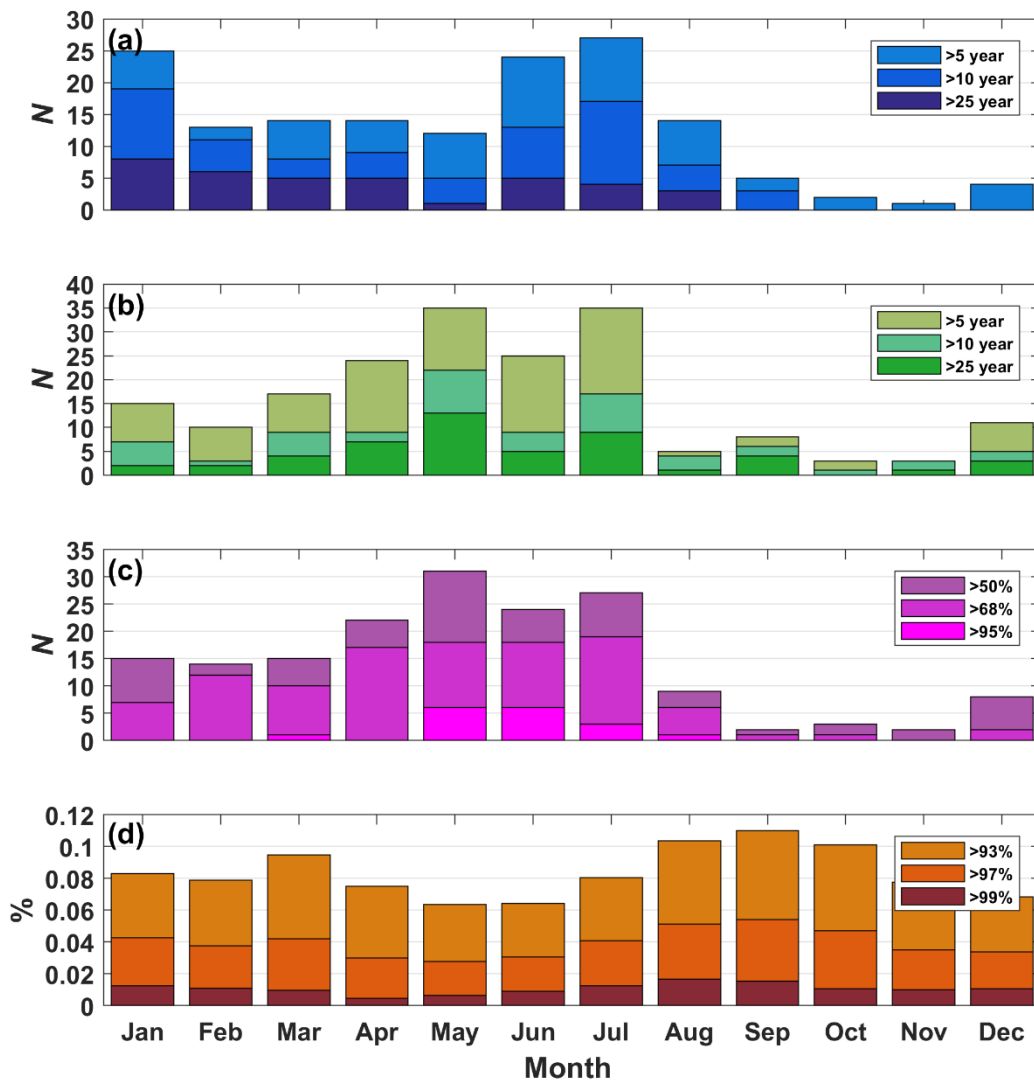
**Figure 7-16: Frequency of the five largest storm-tides each year sorted by month at Kawhia.** The mean annual sea-level cycle has been removed.

### 7.3.4 Raglan & Manu Bay

The sea-level records at Raglan and Manu Bay are too short to meaningfully examine the seasonality of storm tides.

### 7.3.5 Summary

The observed seasonality patterns in the Waikato sea-level records are similar to those observed in a national analysis of extreme sea levels by Stephens et al. (2020)—the national analysis considered only storm tides and skew surges with a return period of > 5 years (Figure 7-17). In the national analysis, winter is an energetic time, as is January, but spring and early summer is a quiescent period.



**Figure 7-17: Seasonal distribution of sea-level components associated with extreme storm-tide and skew-surge events around NZ (source, Stephens et al. 2020).** (a) extreme storm tide, (b) extreme skew surge, (c) MSLA and (d) high tide  $\geq 93$ rd percentile (includes all high tides, not just those associated with extreme storm-tide events). N denotes number of occasions.

## 8 Sea level anomaly

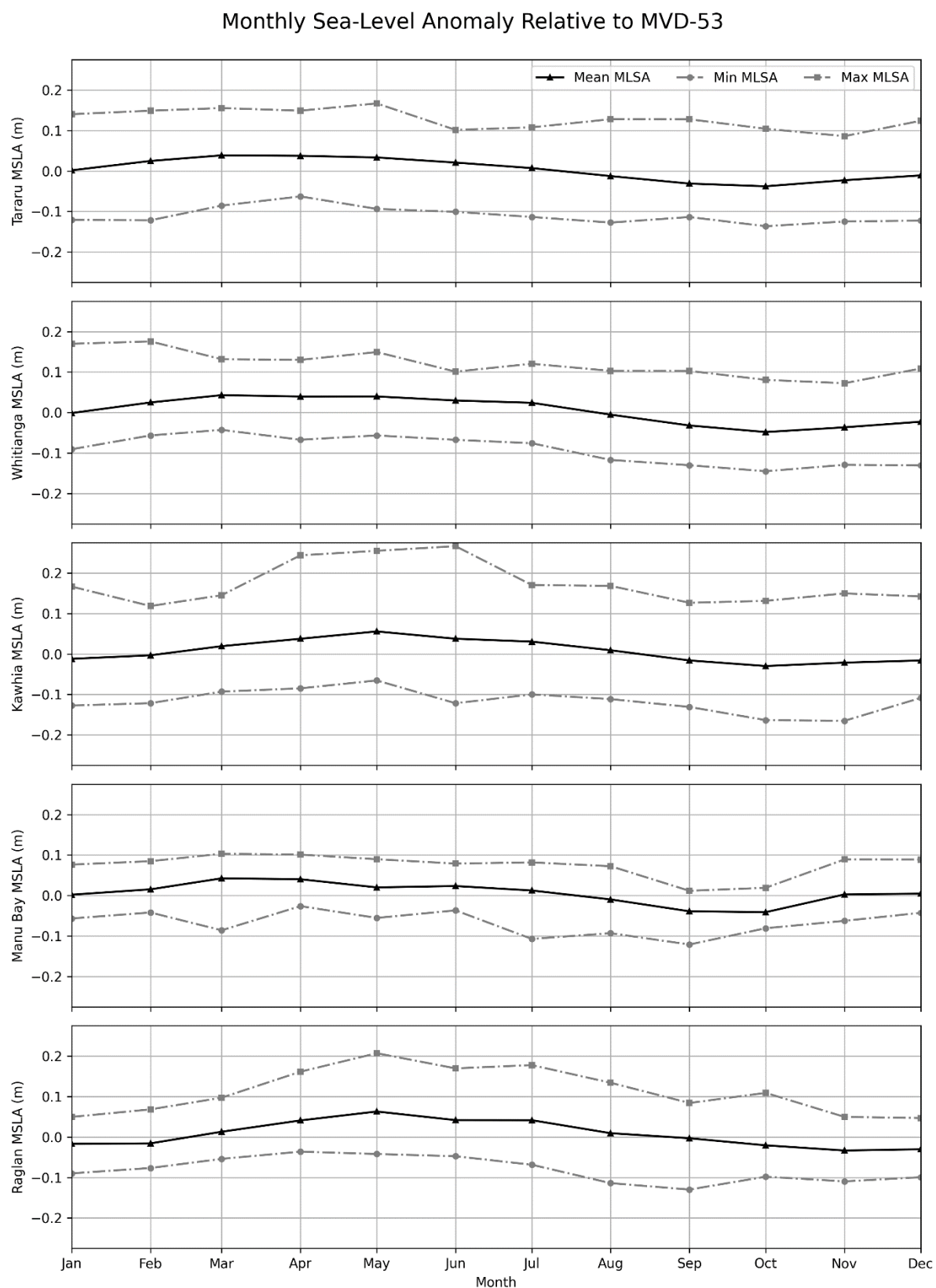
The sea level anomaly (SLA) is the variation of the non-tidal sea level about the longer term MSL on time scales ranging from a monthly basis to decades, due to climate variability. This includes ENSO and IPO patterns on sea level, winds and sea temperatures, and seasonal effects.

At each site, the mean, minimum and maximum SLA was calculated for each month of the year (Figure 8-1) - the results are presented in Table 8-1 to Table 8-5. This is done by applying 31-day running average to the detrended NTR then calculating the mean, minimum and maximum for each month of the year. Similar to the earlier work by Stephens, S. A. et al. (2015) with the now longer records there is a clear seasonal trend in the SLA. SLA tends to rise in the summer and peak in April/May and decline to its lowest during October/November. This is a well-known pattern of behaviour (Bell, 1998) noted the dominant influence on the annual cycle of sea level on the North-east Coast of New Zealand (mean amplitude=378 mm) is associated with thermo-steric sea-level adjustments, which explains 50–80% of the variance in the annual frequency band. Sea levels generally peak at the end of April (austral autumn), lagging the SST cycle by around 2 months.

The maximum sea-level anomaly at Whitianga was 0.176 m, occurring in February (Table 8-1). At Tararu, the highest sea-level anomaly occurred in May at 0.167 m relative (Table 8-2). At Kawhia, the highest sea-level anomaly occurred in June at 0.266 m relative to (Table 8-3). At Raglan and Manu Bay, the highest anomalies were 0.207 m (in May) and 0.103 m (in March), respectively (Table 8-4 and Table 8-5).

The Raglan and Manu Bay SLA curves are less smooth and contain more monthly variability because the records are of short duration.





**Figure 8-1: Mean, minimum and maximum monthly sea-level anomaly.**

**Table 8-1: Minimum, mean and maximum SLA for each month of the year at Whitianga.** The elevations presented here are given relative to a zero MSL. To calculate the elevations relative to MVD-53, add the present-day MSL datum offsets in Table 4-2

Month	Minimum SLA (m)	Mean SLA (m)	Maximum SLA (m)
Jan	-0.091	-0.001	0.170
Feb	-0.057	0.025	0.176
Mar	-0.043	0.043	0.132
Apr	-0.067	0.040	0.130
May	-0.057	0.040	0.149
Jun	-0.067	0.030	0.101
Jul	-0.076	0.024	0.121
Aug	-0.117	-0.005	0.103
Sep	-0.130	-0.032	0.103
Oct	-0.145	-0.048	0.081
Nov	-0.129	-0.037	0.072
Dec	-0.131	-0.023	0.109

**Table 8-2: Minimum, mean and maximum SLA for each month of the year at Tararu.** The elevations presented here are given relative to a zero MSL. To calculate the elevations relative to MVD-53, add the present-day MSL datum offsets in Table 4-2.

Month	Minimum SLA (m)	Mean SLA (m)	Maximum SLA (m)
Jan	-0.121	0.002	0.140
Feb	-0.122	0.025	0.149
Mar	-0.085	0.039	0.156
Apr	-0.063	0.038	0.149
May	-0.094	0.034	0.167
Jun	-0.101	0.021	0.102
Jul	-0.114	0.007	0.108
Aug	-0.127	-0.012	0.128
Sep	-0.114	-0.031	0.128
Oct	-0.136	-0.038	0.104
Nov	-0.125	-0.023	0.086
Dec	-0.123	-0.011	0.124

**Table 8-3: Minimum, mean and maximum SLA for each month of the year at Kawhia.** The elevations presented here are given relative to a zero MSL. To calculate the elevations relative to MVD-53, add the present-day MSL datum offsets in Table 4-2

Month	Minimum SLA (m)	Mean SLA (m)	Maximum SLA (m)
Jan	-0.127	-0.012	0.167
Feb	-0.121	-0.003	0.119
Mar	-0.093	0.019	0.145
Apr	-0.085	0.038	0.244
May	-0.065	0.056	0.255
Jun	-0.122	0.038	0.266
Jul	-0.100	0.031	0.171
Aug	-0.111	0.009	0.168
Sep	-0.131	-0.016	0.127
Oct	-0.163	-0.030	0.131
Nov	-0.165	-0.021	0.150
Dec	-0.108	-0.016	0.142

**Table 8-4: Minimum, mean and maximum SLA for each month of the year at Raglan.** The elevations presented here are given relative to a zero MSL. To calculate the elevations relative to MVD-53, add the present-day MSL datum offsets in Table 4-2.

Month	Minimum SLA (m)	Mean SLA (m)	Maximum SLA (m)
Jan	-0.090	-0.017	0.050
Feb	-0.077	-0.016	0.068
Mar	-0.054	0.013	0.097
Apr	-0.036	0.041	0.161
May	-0.042	0.063	0.207
Jun	-0.048	0.042	0.170
Jul	-0.069	0.042	0.178
Aug	-0.114	0.009	0.134
Sep	-0.130	-0.003	0.084
Oct	-0.098	-0.021	0.109
Nov	-0.110	-0.033	0.050
Dec	-0.099	-0.030	0.047

**Table 8-5: Minimum, mean and maximum SLA for each month of the year at Manu Bay.** The elevations presented here are given relative to a zero MSL. To calculate the elevations relative to MVD-53, add the present-day MSL datum offsets in Table 4-2.

Month	Minimum SLA (m)	Mean SLA (m)	Maximum SLA (m)
Jan	-0.057	0.002	0.076
Feb	-0.042	0.015	0.085
Mar	-0.086	0.042	0.103
Apr	-0.026	0.040	0.101
May	-0.055	0.020	0.090
Jun	-0.037	0.023	0.079
Jul	-0.107	0.012	0.082
Aug	-0.093	-0.010	0.072
Sep	-0.121	-0.039	0.012
Oct	-0.081	-0.041	0.019
Nov	-0.063	0.003	0.089
Dec	-0.043	0.005	0.089

## 9 Whitianga and Tararu Tsunami

Of the five sea level gauges, Whitianga and Tararu are the only locations with consistent 1-minute sampling. A sample frequency of 1-minute or less is desirable for the assessment of tsunami signals in sea-level data. To ensure the reliability of our data, we apply a filter allowing only periods of 2 to 48 minutes to be considered (Section 2.3). Because we have observed evidence of meteorological tsunamis in the sea-level records, we focus solely on measured data records that are correlated to known tsunami events.

In Table 9-1 and Table 9-2, we have documented the three largest tsunamis at Whitianga and Tararu.

The most significant tsunami recorded at Whitianga is attributed to the Tohoku (Japan) Tsunami on 12 March 2011. In this event, the highest wave peak reached 0.68 meters, and the lowest trough measured -0.68 meters. The approximate wave period during this tsunami was 40 minutes. Notably, due to the of resonance of long-waves in Mercury Bay at Whitianga, the measured tsunamis are considerably larger when compared to those recorded at Tararu (Gegar et al. 2011).

On the other hand, the largest tsunami observed in the available sea-level record at Tararu originated from the Tonga Volcano Eruption on 15 January 2022. During this event, the highest wave peak was 0.11 meters, and the lowest trough measured -0.12 meters. The approximate wave period during this tsunami was 28 minutes.

**Table 9-1: There largest Tsunami event measured at Whitianga.** Date represents when the first wave arrives at tide gauge.

Source	Date	Highest Peak (m)	Lowest Trough (m)	Largest Crest to Trough (m)	Period (minutes)
Tohoku (Japan)	12-Mar-2011 06:53:00	0.68	-0.68	1.29	~40
Tonga Eruption	15-Jan-2022 19:17:00	0.58	-0.68	1.27	~43
Chile	28-Feb-2010 07:29:00	0.35	-0.50	0.74	~59

**Table 9-2: There largest Tsunami event measured at Tararu.** Date represents when the first wave arrives at tide gauge.

Source	Date	Highest Peak (m)	Lowest Trough (m)	Largest Crest to Trough (m)	Period (minutes)
Tonga Eruption	15-Jan-2022 21:32:00	0.11	-0.12	0.23	~28
Tohoku (Japan)	12-Mar-2011 06:53:00	0.09	-0.09	0.18	~45
Chile	28-Feb-2010 10:45:00	0.06	-0.07	0.11	~20

## 10 Review of sea-level gauge network

As outlined in Section 1.1, sea-level records provide vital information for coastal management purposes. Important questions are:

Q1: Do the current gauge locations cover the main populated coastal areas in the Waikato?

- The distribution of gauge locations covers most of the populated coastal areas in the Waikato Region.
- Ideally, sea-level gauges would be added at an open-coast location on the east coast. This is because gauges in open-coast locations measure tides before they have to pass through the narrow and shallow tidal inlet throat, as is the case at Whitianga. Tides measured on the open coast are therefore representative of a longer coastline. Tidal measurements are important because tides are the largest component of sea-level variability.

Q2: Are the sea level gauges accurately measuring RSLR?

- The Tararu (32 years), Whitianga (23 years) and Kawhia (14 years) gauges are sufficiently established to provide valuable historical sea-level records that could be maintained and extended to improve extreme sea level estimates and measure changing MSL and rates of SLR.
- All of the gauges appear to be collecting data that is robustly surveyed to datum. This is enabling robust tracking of RSLR.
- The Manu Bay and Raglan gauge records are still relatively short and will become more valuable in time, for tracking MSL or calculating extreme sea-level analyses.
- Several decades of sea level record are required to distinguish statistically significant sea-level rise trends from the effects of climate variability. Nevertheless, there is visual consistency between the MSL trends being measured by the Waikato gauges when compared to the Auckland and Moturiki records, relative to their local vertical datums. Sea-level gauges by themselves measure relative SLR (SLR relative to the local landmass). Fitting of GNSS or other technology to measure vertical land motion would enable absolute SLR to be calculated.
- All the gauges should remain at 1-minute sampling intervals, sufficient to measure the effects of tsunamis and seiche and is also the maximum NEMS sampling frequency (Baddock 2019).

Q3: is VLM being measured at the gauge locations?

- Land vertical tectonic movements (VLM) could be recorded at all sea-level gauge locations to enable absolute MSL to be determined in the future. According to recommendations from Denys (2018), a minimum of once-yearly VLM surveys should be conducted, with surveys scheduled at the same time each year. Consistent timing is particularly important in locations like the Firth of Thames, which experiences seasonal land deformation (Swales et al. 2016). VLM is already being recorded at Tararu and continues to provide valuable data. Waikato Regional Council (WRC) also conducts annual VLM surveys to monitor vertical land movement at the other sea-level gauge sites. At the time of writing,



LINZ has an open tender for a GNSS deployment campaign at locations across New Zealand.

Q4: are there notably compromised data, like datum survey issues, drifts or large gaps?

- The Manu Bay gauge experienced reliability issues in the past, including occasional failures due to sediment contamination within the bubbler and unresolvable datum offset issues. However, since its last installation in 2019 with a modified aperture, these problems have been resolved, and the gauge has operated without failure. The large percentage (~50%) of missing data in the record is primarily due to initial bubbler issues, as well as damage and modifications to the breakwater prior to 2019. Despite these improvements, the temporal coverage of the Manu Bay record remains shorter than that of other Waikato gauge sites.
- All gauges require regular maintenance and servicing to minimise down time due to failure.

Q5: Are there any problematic sites?

- It is hard to collect sea level data on very wave-exposed coasts. The Manu Bay gauge is clearly impacted by waves but it's hard to think of a better spot. A different gauge type, or an improved stilling well. Good alternative locations would be on the lee side of small offshore islands (e.g., Gannet Island), or on the lee side of a peninsula with relatively deep water adjacent, away from breaking waves and outside of estuaries. A good location on the east of the Coromandel Peninsula would be at or northward of Mercury Bay, as this is approximately halfway between the Tararu gauge, and the Moturiki Island gauge operated by NIWA. For the purpose of measuring tides and mean sea level, sea-level gauges would ideally be located in an open-water location where tidal amplitudes represent the adjacent coastline well, and outside of the wave breaking zone, since waves are known to degrade the quality of "still-water" sea level measurements.

## 11 Conclusions

The Waikato Regional Council (WRC) has established operational sea-level measurement stations at Tararu, Whitianga, Kawhia, Raglan, and Manu Bay. Commencing in 1990, 1999, 2008, 2008, and 2008 respectively, these stations have digitally recorded sea-level data. WRC collaborated with NIWA to conduct a comprehensive analysis of these sea-level records. The primary focus was on examining mean sea level change, tidal elevations, and extreme events within the sea-level records to elucidate the localised dynamics of storm-tides in relation to tidal patterns, meteorological conditions, and wave activity. This report offers diverse sea-level analyses pertinent to coastal planning, regulatory efforts, hazard assessment, and is applicable across the five-gauge locations.

As of the time of compiling this report, all five sea-level gauges demonstrate robust data collection capabilities. The data obtained is of satisfactory quality, facilitating accurate extraction of various sea-level components, determination of mean sea-level, and computation of extreme sea-level values. Discrepancies in the vertical reference point at Manu Bay and Raglan have now been incorporated in the WRC live data feed. However, at Kawhia offset issues still appear to exist attributed to unrecorded datum offsets in the NIWA data, unrelated to gauge performance or data quality. The corrections for an observed datum drift at Kawhia, alongside the ongoing data feed to NIWA, remain unadjusted.

For the period spanning 2009 to 2024, mean sea levels were computed relative to Moturiki vertical datum 1953 as 0.20 m for Auckland, 0.14 m for Moturiki, 0.18 m for Whitianga, 0.19 m for Tararu, 0.20 m for Kawhia, and 0.21 m for Raglan. Annual mean sea level variability exhibited comparable behaviour across the various sites.

Mean high-water spring (MHWS) elevations were derived using multiple definitions from the gauge records, and MHWS elevations were also extended to other locations along the Waikato region's coastline. MHWS measurements captured at the Whitianga gauge within its harbour environment were approximately 10 cm lower compared to those outside the Harbour, based on comparisons with the NIWA tide forecaster model and comparison of that model with other Coromandel sea-level records (not analysed here see Stephens et al. 2015).

The distribution of skew surge events in terms of frequency and magnitude was computed for each gauge. Whitianga, Tararu, Kawhia, Raglan and Manu Bay yielded 1% Annual Exceedance Probability (AEP) skew surge estimates of 0.67 m, 0.73 m, 1.07 m, 1.18 and 0.6 respectively. These estimates were accompanied by typical uncertainty, particularly evident at Raglan and Manu Bay due to their relatively short durations of 14 and 6 years respectively. Distinct surge drivers were observed between the eastern (Whitianga) and western (Kawhia, Raglan) coastlines of New Zealand. The east coast gauges have a proportionately larger inverse barometer (MSLP) component compared to the west coast gauges where surge is strongly dominated by wind setup. The east coast surges tend to be driven by tight, fast moving low-pressure weather systems, whereas the largest west coast surges are driven by prolonged strong north-westerly winds generated by weather fronts. These persistent winds resulted in surges nearly twice the magnitude of those at Whitianga, with some exceeding 1 m.

Similarly, storm tide distribution was examined, revealing 1% AEP storm tide estimates of 1.47 m for Whitianga, 2.37 m for Tararu, and 2.7 m for Kawhia. Tidal influence was identified as the predominant component within storm tides, however the two most recent storm tides at Whitianga (Tropical cyclone Hale and Gabrielle) the surge component was larger than the tide. All of the largest storm tides included a moderate surge component.

There was a clear annual cycle in the sea-level anomaly at all sites with mean SLA peaking between March and May, reaching a minimum in October, and lagging the SST cycle by approximately two months. Investigation of storm tide seasonality was conducted for Whitianga Tararu and Kawhia. In Whitianga the winter months witnessed a greater number of substantial storm tides but at Kawhia and Tararu the Summer months tended to generate more storm tides.

In summary, the sea-level gauges have collected reliable data, and with ongoing maintenance, these records will remain valuable for forthcoming analyses of sea-level trends, skew surges, and storm-tide anomalies. The historical records from Tararu (32-years) and Whitianga (25- years) are especially significant and warrant continued investment to enhance extreme sea level estimations, assess shifting mean sea levels, and gauge rates of sea-level rise. While the Kawhia gauge's record is relatively short (16-years), its long-term value can be substantial if maintained. The Raglan (15-years but with a ~3-year gap) and Manu Bay (~6-years total) records are both short and contain large periods of missing data but have still contributed meaningfully to our understanding of sea level behaviour and will grow in value with time. Expanding (east coast) and maintaining (west coast) the sea-level network to encompass open-coast locations on the east coast of the Waikato region would avoid the susceptibility of small estuaries to morphological changes impacting tidal dynamics. A considered effort must be given to minimizing downtime during sea-level gauge failures.

If future determination of absolute Mean Sea Level (MSL) is a goal, then vertical land motion would need to be measured at the sea-level gauge sites—a once yearly measurement collected at the same time of the year would suffice.

## 12 Glossary of abbreviations and terms

AEP	Annual exceedance probability – The probability of a given (usually high) sea level or wave height being equalled or exceeded in elevation, in any given calendar year. AEP can be specified as a fraction (e.g., 0.01) or a percentage (e.g., 1%).
ARI	Average recurrence interval – The average time interval (averaged over a very long time period and many “events”) that is expected to elapse between recurrences of an infrequent event of a given large magnitude (or larger). A large infrequent event would be expected to be equalled or exceeded in elevation, once, on average, every “ARI” years, but with considerable variability.
ENSO	El Niño Southern Oscillation. A natural global climate phenomenon involving the interaction between the tropical Pacific and the atmosphere, but has far-reaching effects on the global climate, especially for countries in the Pacific rim. ENSO is the strongest climate signal on time scales of one to several years. The quasi-periodic cycle oscillates between El Niño (unusually warm ocean waters along the tropical South American coast) and La Niña (colder-than-normal ocean waters off South America).
Epoch	A particular period of history that is selected as a point of reference – used in connection with developing a baseline sea level.
Equilibrium Tide	The elevation of the sea surface that would be in equilibrium with the tidal forces if the earth were covered with water and the response of the water to the tidal forces were instantaneous.
HF	High-frequency sea-level component – a product of wavelet filtering of the non-tidal residual sea level.
IPO	Interdecadal Pacific Oscillation – a long timescale oscillation in the ocean–atmosphere system that shifts climate in the Pacific region every one to three decades.
Joint probability	The probability of two separate processes occurring together (e.g., large waves and high storm-tide).
MHWPS	Mean high-water perigean springs – this occurs when MHWs coincides with the moon being closest to the Earth in its elliptical orbit (in perigee). MHWPS includes the sum of twice daily lunar $M_2$ tide, the twice daily solar $S_2$ tide, and the elliptic semi-diurnal $N_2$ tide: $MHWPS = M_2 + S_2 + N_2$ .
MHWS	Mean high-water springs – The high tide height associated with higher-than-normal high tides that result from the beat of various tidal harmonic constituents. The high tide exceeds the mean high water springs elevation every 2 weeks approximately, at both new and full moon, when the gravitational forces of the Sun and the Earth’s moon align to produce higher than normal tides. Thus the nautical definition of MHWS (MHWSn) includes the sum of twice daily lunar $M_2$ tide and the twice daily solar $S_2$ tide: $MHWSn = M_2 + S_2$ . MHWS can be defined in various ways, and the MHWS elevation varies according to definition.
MHWS-10	the elevation equalled or exceeded by the largest 10% of all high tides.
MHWS-6	the elevation equalled or exceeded by the largest 6% of all high tides.

MHWAN	mean apogean neap
MSL	Mean sea level – obtained by averaging the sea level, relative to a local vertical datum, over a defined epoch.
MSLA	Mean sea-level anomaly – Also referred to as SLA – the variation of the non-tidal sea level about the longer term MSL on time scales ranging from a monthly basis to decades, due to climate variability. This includes ENSO and IPO patterns on sea level, winds and sea temperatures, and seasonal effects.
NEMS	National Environmental Monitoring Standards
NTR	Non-tidal residual – The difference between observed sea level and the predicted tidal level, encompassing all non-tidal influences on sea level such as atmospheric pressure changes, wind setup, and seasonal variation.
NZVD2016	New Zealand vertical datum 2016
skew surge	Skew surge is the height difference between a sea-level (storm-tide) peak and the nearest predicted astronomical high tide. It may occur at a different time to the tide peak, hence the term <i>skew surge</i> —skewed in time.
SLA	Sea-level anomaly – Also referred to as MSLA – the variation of the non-tidal sea level about the longer term MSL on time scales ranging from a monthly basis to decades, due to climate variability. This includes ENSO and IPO patterns on sea level, winds and sea temperatures, and seasonal effects.
SS	Storm surge – The rise in sea level due to storm meteorological effects. Low-atmospheric pressure relaxes the pressure on the ocean surface causing the sea-level to rise, and wind stress on the ocean surface pushes water down-wind (onshore winds) and to the left up against any adjacent coast (alongshore winds). Storm surge has timescales of sea-level response that coincide with typical synoptic weather motions; typically 1–3 days.
SSJPM	Skew-surge joint-probability technique. A technique to model extreme sea-level. Suitable for short data records and provides the flexibility to mix measured and modelled sea-level components.
Storm surge	The rise in sea level due to storm meteorological effects. Low-atmospheric pressure relaxes the pressure on the ocean surface causing the sea-level to rise, and wind stress on the ocean surface pushes water down-wind (onshore winds) and to the left up against any adjacent coast (alongshore winds). Storm surge has timescales of sea-level response that coincide with typical synoptic weather motions; typically 1–3 days.
Storm tide	The sea-level peak around high tide reached during a storm event, resulting from a combination of SLA + tide + storm surge.
tide	The tides are caused by the gravitational attraction of solar-system bodies, primarily the Sun and the Earth’s moon, which then propagate as forced long waves in the ocean interacting in a complex way with continental shelves. In New Zealand the astronomical tides have by far the largest influence on sea level, followed by storm surge (in most locations).

Wave runup	The maximum vertical extent of wave “up-rush” on a beach or structure above the still water level, and thus constitutes only a short-term upper-bound fluctuation in water level relative to wave setup.
Wave setup	The average temporary increase in mean still-water sea level at the coast, resulting from the release of wave energy in the surf zone as waves break.



## 13 References

- Baddock, E. (2019) National Environmental Monitoring Standards (NEMS). *Water level (Water Level Field Measurement Standard)*. <https://www.nems.org.nz/>
- Batstone, C., Lawless, M., Tawn, J., Horsburgh, K., Blackman, D., McMillan, A., Worth, D., Laeger, S., Hunt, T. (2013) A UK best-practice approach for extreme sea-level analysis along complex topographic coastlines. *Ocean Engineering*, 71: 28-39. <http://dx.doi.org/10.1016/j.oceaneng.2013.02.003>
- Bell, R.G. (2010) Tidal exceedances, storm tides and the effect of sea-level rise. *Proceedings of the 17th Congress of the Asia and Pacific division of the IAHR*, Auckland, New Zealand, 21-24 February 2010.
- Boon, J.D. (2013) *Secrets of the tide: tide and tidal current analysis and predictions, storm surges and sea level trends*. Elsevier.
- Brown, J.M., Morrissey, K., Knight, P., Prime, T.D., Almeida, L.P., Masselink, G., Bird, C.O., Dodds, D., Plater, A.J. (2018) A coastal vulnerability assessment for planning climate resilient infrastructure. *Ocean & Coastal Management*, 163: 101-112. <http://nora.nerc.ac.uk/id/eprint/520361/>
- Chen, Y., Rojas, M., Samset, B.H., Cobb, K., Fesenfeld, L., Hawkins, E., Hegerl, G., Payne, M., Ranasinghe, R., Ruane, A.C., Schwingshackl, C., Vautard, R., Zaaboul, R. (2021) Chapter 12: Climate Change Information for Regional Impact and for Risk Assessment. In: V. Masson-Delmotte, P. Zhai, A. Pirani et al. (Eds). *Climate Change 2021: The Physical Science Basis. Contribution of Working Group I to the Sixth Assessment Report of the Intergovernmental Panel on Climate Change*. Cambridge University Press, Cambridge, United Kingdom and New York, NY, USA. <https://www.ipcc.ch/report/ar6/wg1/chapter/chapter-12/>
- Codiga, D.L. (2011a) Unified Tidal Analysis and Prediction Using the UTide Matlab Functions: 59.
- Codiga, D.L. (2011b) Unified Tidal Analysis and Prediction Using the UTide Matlab Functions. Technical Report 2011-01. Graduate School of Oceanography, University of Rhode Island, Narragansett, RI. 59pp.
- Coles, S. (2001) *An introduction to statistical modeling of extreme values*. Springer-Verlag, London.
- Costa, W., Bryan, K.R., Stephens, S.A., Coco, G. (2023) A regional analysis of tide-surge interactions during extreme water levels in complex coastal systems of Aotearoa New Zealand. *Frontiers in Marine Science*, 10. 10.3389/fmars.2023.1170756
- Denys, P. (2018) Monitoring vertical land motion at tide gauge stations: Recommended procedures. *Waikato Regional Council Internal Series Report*.
- Denys, P. (2024) The establishment of benchmarks in the Firth of Thames: The new tide gauge platform (TAR2) and Thames Air Quality site (THAQ).
- Dong, B., Dai, A. (2015) The influence of the Interdecadal Pacific Oscillation on Temperature and Precipitation over the Globe. *Climate Dynamics*, 45(9): 2667-2681. 10.1007/s00382-015-2500-x

Gegar, P., Healy, T., de Lange, W. (2011) Hydrodynamic modelling of tsunami inundation in Whitianga.

Godin, G. (1973) *The analysis of tides*. <https://ui.adsabs.harvard.edu/abs/1973anti.book.....G>

Goring, D.G. (1999) Whitianga sea-level recorder: Preliminary analysis.

Goring, D.G., Stephens, S.A., Bell, R.G., Pearson, C.P. (2011) Estimation of Extreme Sea Levels in a Tide-Dominated Environment Using Short Data Records. *Journal of Waterway Port Coastal and Ocean Engineering-Asce*, 137(3): 150-159. 10.1061/(asce)ww.1943-5460.0000071

Greer, D., Borrero, J., McIntosh, R. (2017) Tsunami Hotspots: Analysis of New Zealand Tide Gauge Data: 445.

Haigh, I.D., Nicholls, R., Wells, N. (2010) A comparison of the main methods for estimating probabilities of extreme still water levels. *Coastal Engineering*, 57(9): 838-849.  
<https://doi.org/10.1016/j.coastaleng.2010.04.002>

Hunt, S. (2021) Optimisation of the Waikato Regional Council tide gauge network, 21790189.

IOC-UNESCO (2016) Global Sea Level Observing System (GLOSS). In: I.O. Commission (Ed).  
<http://www.gloss-sealevel.org/>

Kilonsky, B.J., Caldwell, P., Ilee (1991) *In the pursuit of high-quality sea-level data*: 669-675. <Go to ISI>://WOS:A1991BV11J00135

Merrifield, M.A., Genz, A.S., Kontoes, C.P., Marra, J.J. (2013) Annual maximum water levels from tide gauges: Contributing factors and geographic patterns. *Journal of Geophysical Research: Oceans*, 118(5): 2535-2546. <https://doi.org/10.1002/jgrc.20173>

MfE (2024) Te Ahukaramū Charles Royal, 'Waikato tribes - Waikato landmarks', Te Ara - the Encyclopedia of New Zealand. <http://www.TeAra.govt.nz/en/photograph/1716/river-mouth-at-port-waikato>

Perez-Gomez, B., de Alfonso, M., Huess, V., Rickards, L. (2010) Near Real Time Quality Control and validation of Sea Level in-situ data within MyOcean. 10.13155/74307

Perez, B.a., de Alfonso Alonso-Muñozoyerro, M., Huess, V., Rickards, L. (2010) Near Real Time Quality Control and validation of Sea Level in-situ data within MyOcean. 10.13155/74307

Pugh, D.T. (1987) *Tides, Surges and Mean Sea-Level*.

Pugh, D.T. (2004) *Changing sea levels. Effects of Tides, Weather and Climate*. Cambridge University Press, New York: 265.

Stephens, S.A., Bell, R.G., Haigh, I.D. (2020) Spatial and temporal analysis of extreme storm-tide and skew-surge events around the coastline of New Zealand. *Nat. Hazards Earth Syst. Sci.*, 20(3): 783-796. 10.5194/nhess-20-783-2020

Stephens, S.A., Bell, R.G., Ramsay, D., Goodhue, N. (2014) High-Water Alerts from Coinciding High Astronomical Tide and High Mean Sea Level Anomaly in the Pacific Islands Region. *Journal of Atmospheric and Oceanic Technology*, 31(12): 2829-2843. 10.1175/JTECH-D-14-00027.1

Stephens, S.A., Robinson, B., Bell, R.G. (2015) Analysis of Whitianga, Tararu and Kawhia sea-level records to 2014, HAM2015-046: 98.

Swales, A., Denys, P., Pickett, V.I., Lovelock, C.E. (2016) Evaluating deep subsidence in a rapidly-accreting mangrove forest using GPS monitoring of surface-elevation benchmarks and sedimentary records. *Marine Geology*, 380: 205-218. <https://doi.org/10.1016/j.margeo.2016.04.015>

Tawn, J.A., Vassie, J.M. (1989) Extreme sea-levels: the joint probabilities method revisited and revised. . *Proceedings of the Institute of Civil Engineering Part 2*.

Walters, R.A., Goring, D.G., Bell, R.G. (2001) Ocean tides around New Zealand. *New Zealand Journal of Marine and Freshwater Research*, 35(3): 567-579. 10.1080/00288330.2001.9517023

Williams, J., Horsburgh, K.J., Williams, J.A., Proctor, R.N.F. (2016) Tide and skew surge independence: New insights for flood risk. *Geophysical Research Letters*, 43(12): 6410-6417. <https://doi.org/10.1002/2016GL069522>

## Appendix A MHWS elevations from tide model

Mean high-water springs elevations in the Waikato region, output from NIWA's tide model, are presented in Table A-1.

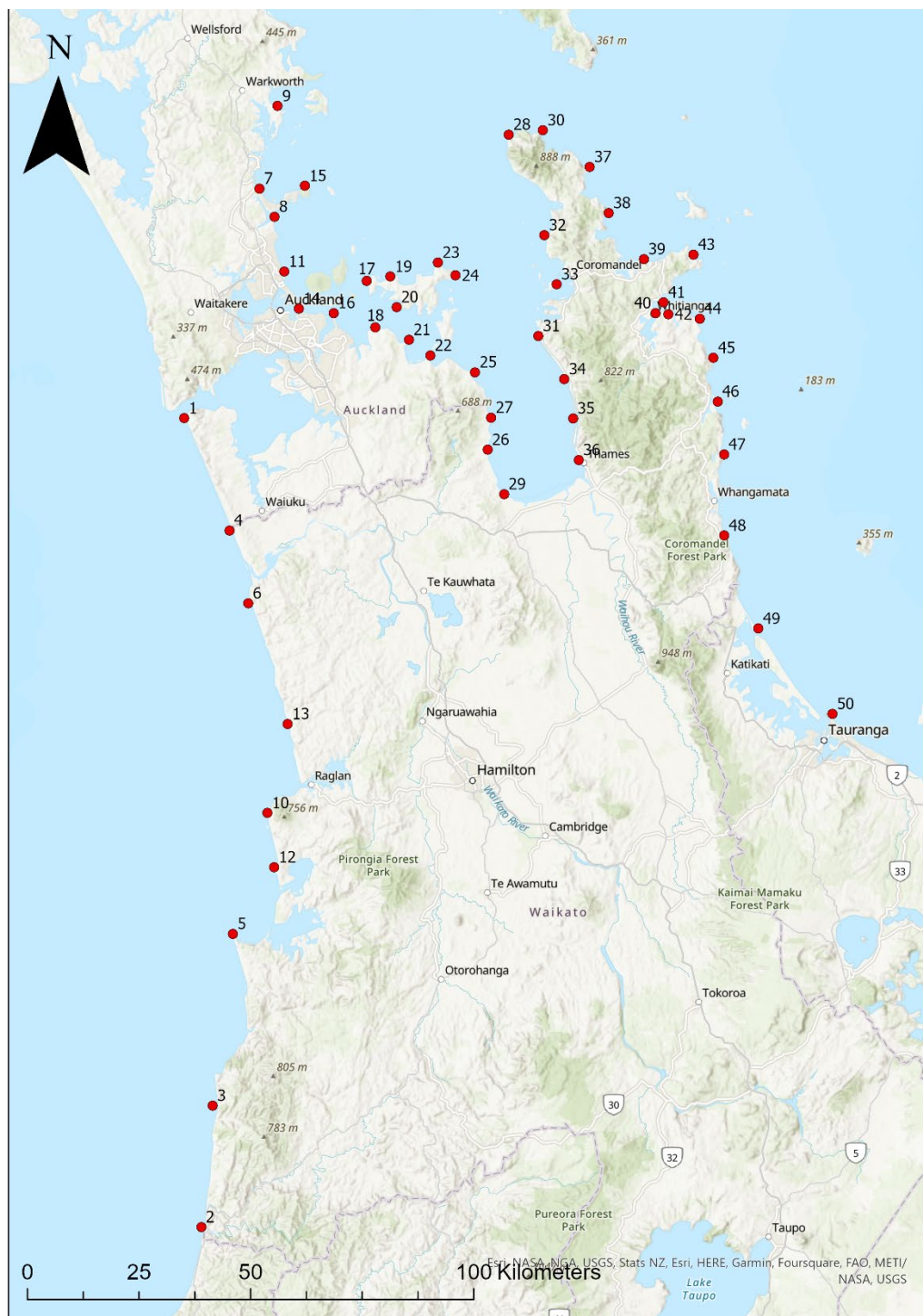


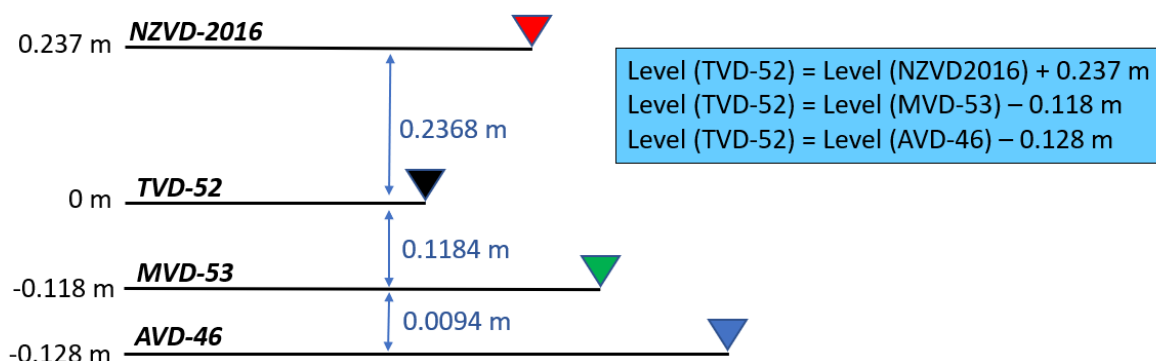
Figure A-1: Locations for MHWS elevations shown in Table A-1.

**Table A-1: Mean high-water springs elevations around the Waikato region, from NIWA's tide model.**  
 MHWS-10, MHWS-6 and MHWPS values have been locally adjusted where needed from the EEZ tide model output. Vertical "datum" is MSL=0, i.e., relative to still water level locally.

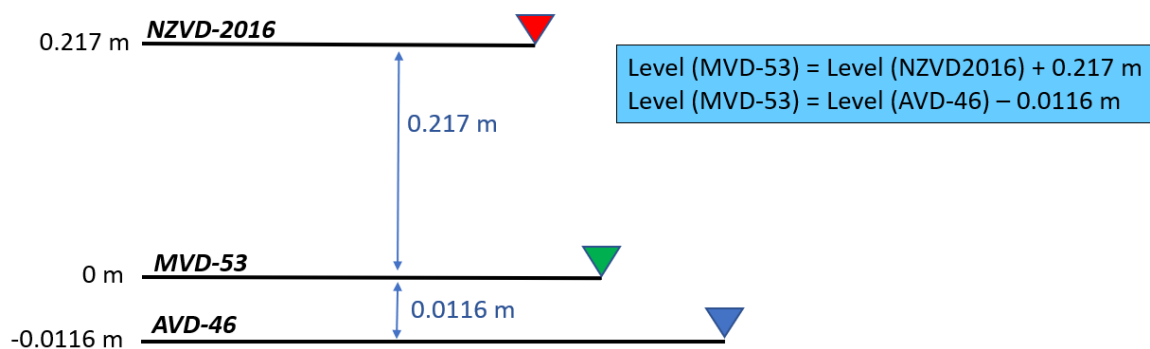
Site	NZTM_easting	NZTM_northing	HAT	MHWS10	MHWS6	MHWSP
1	1736036	5896835	1.86	1.52	1.59	1.64
2	1739880	5715676	2.03	1.65	1.73	1.77
3	1742437	5742856	1.99	1.62	1.69	1.73
4	1746202	5871714	1.86	1.51	1.58	1.62
5	1747000	5781341	1.94	1.57	1.65	1.69
6	1750438	5855383	1.87	1.52	1.59	1.63
7	1752951	5948294	1.60	1.30	1.33	1.35
8	1756317	5942007	1.65	1.34	1.38	1.39
9	1757008	5966784	1.58	1.28	1.32	1.33
10	1754683	5808423	1.91	1.56	1.63	1.67
11	1758461	5929712	1.73	1.41	1.48	1.47
12	1756250	5796293	1.93	1.57	1.64	1.68
13	1759265	5828375	1.91	1.55	1.62	1.66
14	1761739	5921374	1.82	1.48	1.54	1.56
15	1763084	5948905	1.60	1.30	1.34	1.35
16	1769530	5920425	1.76	1.44	1.49	1.50
17	1776936	5927599	1.68	1.36	1.41	1.42
18	1778882	5917209	1.75	1.42	1.47	1.48
19	1782252	5928586	1.64	1.34	1.38	1.39
20	1783649	5921763	1.75	1.43	1.47	1.49
21	1786415	5914401	1.78	1.45	1.50	1.51
22	1791195	5910891	1.79	1.46	1.51	1.52
23	1792913	5931706	1.64	1.34	1.37	1.39
24	1796833	5928873	1.69	1.38	1.42	1.43
25	1801222	5907155	1.81	1.48	1.52	1.54
26	1804043	5889793	1.95	1.59	1.65	1.67
27	1804823	5896959	1.89	1.54	1.60	1.61
28	1808793	5960394	1.47	1.19	1.22	1.24
29	1807735	5879870	1.99	1.63	1.70	1.71
30	1816452	5961340	1.37	1.11	1.13	1.15
31	1815416	5915278	1.79	1.46	1.50	1.52
32	1816776	5937885	1.68	1.36	1.41	1.42
33	1819538	5926847	1.76	1.43	1.48	1.49
34	1821238	5905591	1.87	1.52	1.58	1.59
35	1823189	5896801	1.92	1.57	1.63	1.64
36	1824437	5887507	1.99	1.63	1.70	1.71

Site	NZTM_easting	NZTM_northing	HAT	MHWS10	MHWS6	MHWS10
37	1826926	5953129	1.29	1.04	1.07	1.08
38	1831226	5942802	1.26	1.02	1.04	1.05
39	1839047	5932503	1.25	1.01	1.04	1.05
40	1841698	5920369	1.01	0.84	0.87	0.88
41	1843460	5922793	1.16	0.94	0.98	0.98
42	1844557	5920153	1.16	0.94	0.98	0.98
43	1850153	5933518	1.18	0.96	0.98	0.99
44	1851566	5919153	1.15	0.94	0.96	0.97
45	1854647	5910360	1.15	0.93	0.96	0.97
46	1855601	5900603	1.15	0.93	0.96	0.96
47	1857027	5888722	1.14	0.93	0.95	0.96
48	1857077	5870559	1.14	0.93	0.95	0.96
49	1864726	5849733	1.16	0.94	0.97	0.98
50	1881304	5830611	1.17	0.95	0.97	0.98

## Appendix B Vertical Datums

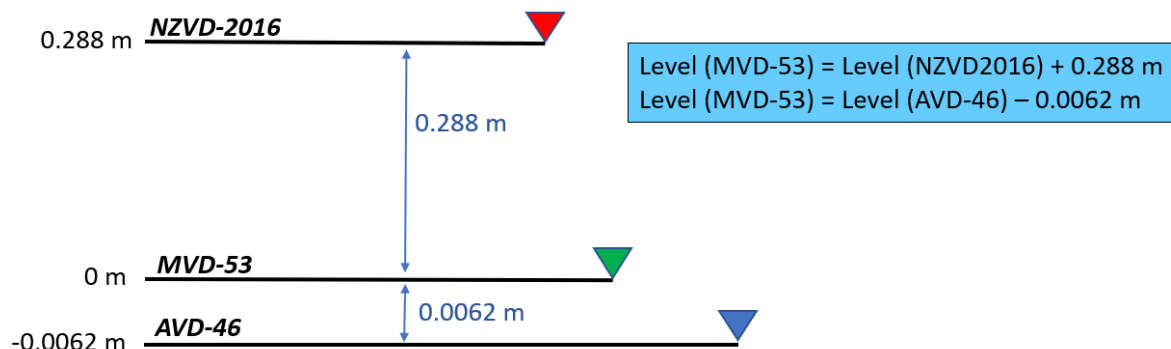


**Figure B-1: Relationships and conversions between LVDs at Tararu: Auckland (AVD-46), Moturiki (MVD-53), Tararu (TVD-52) and New Zealand Vertical Datum (NZVD2016).** Note: That NZVD2016 varies spatially so the offset is specific to the tide gauge at Tararu.

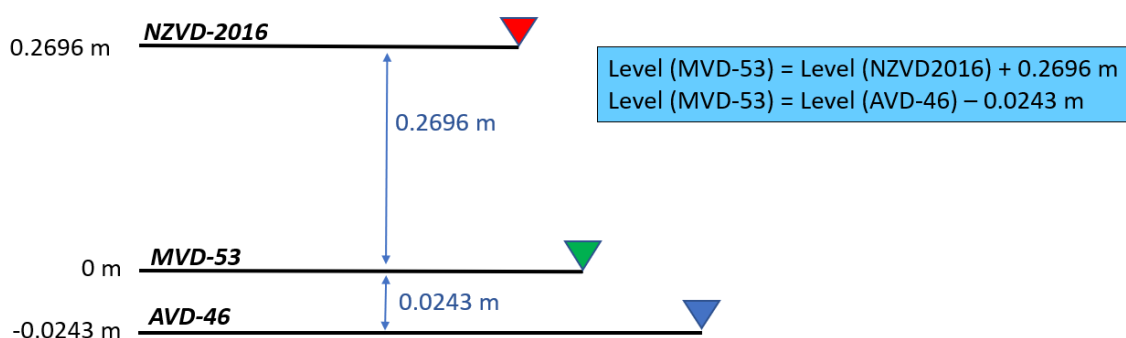


**Figure B-2: Relationships and conversions between LVDs at Whitianga: Auckland (AVD-46), Moturiki (MVD-53) and New Zealand Vertical Datum (NZVD2016).** Note: That NZVD2016 varies spatially so the offset is specific to the tide gauge at Whitianga.

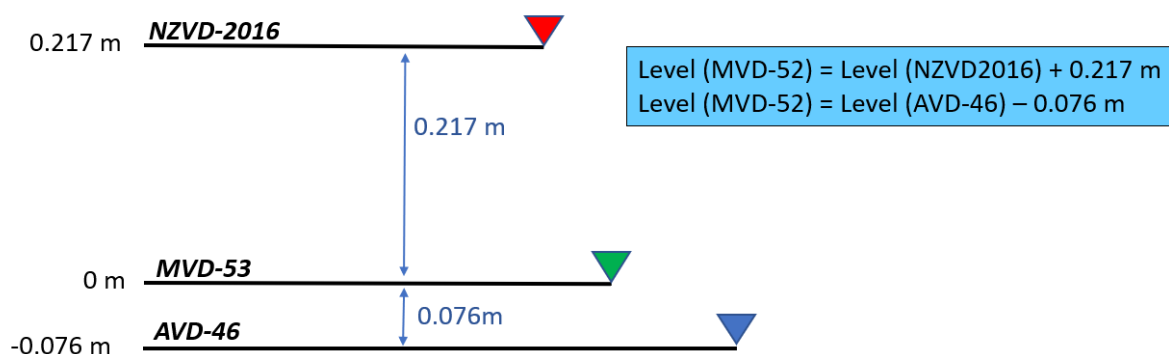




**Figure B-3: Relationships and conversions between LVDs at Kawhia: Auckland (AVD-46), Moturiki (MVD-53) and New Zealand Vertical Datum (NZVD2016).** Note: That NZVD2016 varies spatially so the offset is specific to the tide gauge at Kawhia.



**Figure B-4: Relationships and conversions between LVDs at Manu Bay: Auckland (AVD-46), Moturiki (MVD-53) and New Zealand Vertical Datum (NZVD2016).** Note: That NZVD2016 varies spatially so the offset is specific to the tide gauge at Manu Bay.



**Figure B-5: Relationships and conversions between LVDs at Raglan: Auckland (AVD-46), Moturiki (MVD-53) and New Zealand Vertical Datum (NZVD2016).** Note: That NZVD2016 varies spatially so the offset is specific to the tide gauge at Raglan.

## Appendix C Tide, storm tide and projected sea-level rise tables

The following tables are a collation of tide and storm-tide elevations from elsewhere in the report. The MHWPS and Maximum tide definitions from Table 5-1 was applied. The lower storm-tide range estimate uses the median 2-year (39% AEP) ARI and the upper range estimate uses the upper 95% confidence interval for the 200-year ARI (0.5% AEP), for Whitianga (Table 7-1), Kawhia (Table 7-2), Tararu (Table 7-3), Raglan (Table 7-4) and Manu Bay (Table 7-5). All elevations presented in the tables below have been adjusted to include the 2013–2023 MSL offset to MVD-53, with the exception of Manu Bay, where data availability is limited to records from 2018 onward. These MSL offsets have been added to the tide and storm-tide elevations.

### Whitianga Harbour

Sea Level Scenario		Sea Level (MVD-53) MSL = 0	Sea Level (MVD-53) + MSL (2013- 2023)	Sea Level (NZVD- 2016) + MSL (2013-2023)
Present Day	MHWPS	0.89	1.05	0.76
	Max Tide	1.03	1.19	0.90
	Lower Storm Tide Range (Estimate)	1.19	1.35	1.06
	Upper Storm Tide Range (Estimate)	1.61	1.77	1.48
Future Projected +0.5m Sea Level Rise	MHWPS	1.39	1.55	1.26
	Max Tide	1.53	1.69	1.40
	Lower Storm Tide Range (Estimate)	1.69	1.85	1.56
	Upper Storm Tide Range (Estimate)	2.11	2.27	1.98
Future Projected +1.0m Sea Level Rise	MHWPS	1.89	2.05	1.76
	Max Tide	2.03	2.19	1.90
	Lower Storm Tide Range (Estimate)	2.19	2.35	2.06
	Upper Storm Tide Range (Estimate)	2.61	2.77	2.48

### Tararu (Firth of Thames)

Sea Level Scenario		Sea Level (MVD-53) MSL = 0	Sea Level (MVD-53) + MSL (2013- 2023)	Sea Level (NZVD- 2016) + MSL (2013-2023)
Present Day	MHWPS	1.74	1.93	1.58
	Max Tide	1.93	2.12	1.77
	Lower Storm Tide Range (Estimate)	2.08	2.27	1.91
	Upper Storm Tide Range (Estimate)	2.47	2.66	2.30
Future Projected +0.5m Sea Level Rise	MHWPS	2.24	2.43	2.08
	Max Tide	2.43	2.62	2.27
	Lower Storm Tide Range (Estimate)	2.58	2.77	2.41
	Upper Storm Tide Range (Estimate)	2.97	3.16	2.80
Future Projected +1.0m Sea Level Rise	MHWPS	2.74	2.93	2.58
	Max Tide	2.93	3.12	2.77
	Lower Storm Tide Range (Estimate)	3.08	3.27	2.91
	Upper Storm Tide Range (Estimate)	3.47	3.66	3.30

## Kawhia Harbour

Sea Level Scenario		Sea Level (MVD-53) MSL = 0	Sea Level (MVD-53) + MSL (2013- 2023)	Sea Level (NZVD- 2016) + MSL (2013-2023)
Present Day	MHWSP	1.70	1.92	1.63
	Max Tide	1.97	2.19	1.90
	Lower Storm Tide Range (Estimate)	2.21	2.43	2.14
	Upper Storm Tide Range (Estimate)	2.88	3.10	2.81
Future Projected +0.5m Sea Level Rise	MHWPS	2.20	2.42	2.13
	Max Tide	2.47	2.69	2.40
	Lower Storm Tide Range (Estimate)	2.71	2.93	2.64
	Upper Storm Tide Range (Estimate)	3.38	3.60	3.31
Future Projected +1.0m Sea Level Rise	MHWPS	2.70	2.92	2.63
	Max Tide	2.97	3.19	2.90
	Lower Storm Tide Range (Estimate)	3.21	3.43	3.14
	Upper Storm Tide Range (Estimate)	3.88	4.10	3.81

## Raglan Harbour

Sea Level Scenario		Sea Level (MVD-53) MSL = 0	Sea Level (MVD-53) + MSL (2013- 2023)	Sea Level (NZVD- 2016) + MSL (2013-2023)
Present Day	MHWPS	1.63	1.85	1.62
	Max Tide	1.86	2.08	1.85
	Lower Storm Tide Range (Estimate)	2.14	2.36	2.13
	Upper Storm Tide Range (Estimate)	3.05	3.27	3.04
Future Projected +0.5m Sea Level Rise	MHWPS	2.13	2.35	2.12
	Max Tide	2.36	2.58	2.35
	Lower Storm Tide Range (Estimate)	2.64	2.86	2.63
	Upper Storm Tide Range (Estimate)	3.55	3.77	3.54
Future Projected +1.0m Sea Level Rise	MHWPS	2.63	2.85	2.62
	Max Tide	2.86	3.08	2.85
	Lower Storm Tide Range (Estimate)	3.14	3.36	3.13
	Upper Storm Tide Range (Estimate)	4.05	4.27	4.04

## Manu Bay

Sea Level Scenario		Sea Level (MVD-53) MSL = 0	Sea Level (MVD-53) + MSL (2018- 2023)	Sea Level (NZVD- 2016) + MSL (2018-2023)
<b>Present Day</b>	MHWS	1.66	1.88	1.61
	Max Tide	1.88	2.10	1.83
	Lower Storm Tide Range (Estimate)	2.02	2.24	1.97
	Upper Storm Tide Range (Estimate)	2.37	2.59	2.32
<b>Future Projected +0.5m Sea Level Rise</b>	MHWS	2.16	2.38	2.11
	Max Tide	2.38	2.60	2.33
	Lower Storm Tide Range (Estimate)	2.52	2.74	2.47
	Upper Storm Tide Range (Estimate)	2.87	3.09	2.82
<b>Future Projected +1.0m Sea Level Rise</b>	MHWS	2.66	2.88	2.61
	Max Tide	2.88	3.10	2.83
	Lower Storm Tide Range (Estimate)	3.02	3.24	2.97
	Upper Storm Tide Range (Estimate)	3.37	3.59	3.32

## Appendix D Data Processing and Quality Assurance

### E.1 - Background

National environmental monitoring standards for sea level measurement are set by governments and other organisations to ensure data are collected, managed, and used accurately and reliably. These standards specify the methods and tools used to collect, store, and analyse sea level data, as well as the requirements for data quality and accuracy (Perez et al. 2010; IOC-UNESCO 2016; Baddock 2019). For instance, the Intergovernmental Oceanographic Commission (IOC) of UNESCO has established a global sea level observing system that provides a framework for consistent and comparable sea level data across different regions and timeframes. The system specifies guidelines for instrument calibration, data processing, and quality control to ensure data accuracy and consistency. New Zealand has the National Environmental Monitoring Standards (NEMS), which are a series of environmental monitoring standards, prepared by the NEMS steering group on authority from the Regional Chief Executive Officers (RCEOs) and the Ministry for the Environment (MfE) (Baddock 2019). NEMS has guidelines and recommendations for sea level data to ultimately meet a NEMS standard of QC=600, achieving data of high quality is the outcome of multiple activities, processes and decisions that all form part of "monitoring" (Baddock 2019). These include, but are not limited to:

- site selection,
- equipment selection,
- equipment deployment,
- data acquisition,
- data archiving, and
- quality assurance of field stations.

However, to date no guidelines exist for the purpose of sea level data quality assurance (QA). QA is a process of ensuring that the data used to measure sea levels is accurate, reliable, and up to date. This includes verifying the accuracy of the data, performing tests to detect potential errors or discrepancies, estimating measurement uncertainty, and ensuring the data is stored securely and cannot be deleted, corrupted, or altered. QA also includes ensuring the data is properly documented and stored in a way that makes it easy to access and use. QA is important to ensure that sea level data is used correctly and accurately to make decisions, inform policy, provide long-term relative sea level trends, tidal datums, coastal boundaries, emergency management and navigation information. The objective of this section of the report is to compile "best practices" and processes that may routinely be applied to tide gauge data to achieve data of a consistent standard. Once documented and applied, these practices and processes may be updated so that improvements in technology and refinements in knowledge may be incorporated to further improve the quality of data.

We make no comment on the site or instrument selection, we expect that any instrument installation meets the criteria outlined by the relevant National Environmental Monitoring Standard (NEMS), such as site selection and calibration of sensors. Because NIWA is not involved with the site selection, data storage, gauge maintenance and calibration we cannot comment on these elements of the NEMS. This document is solely for the purpose of detailing the QA process for sea level data.

## E.2 - In this Section

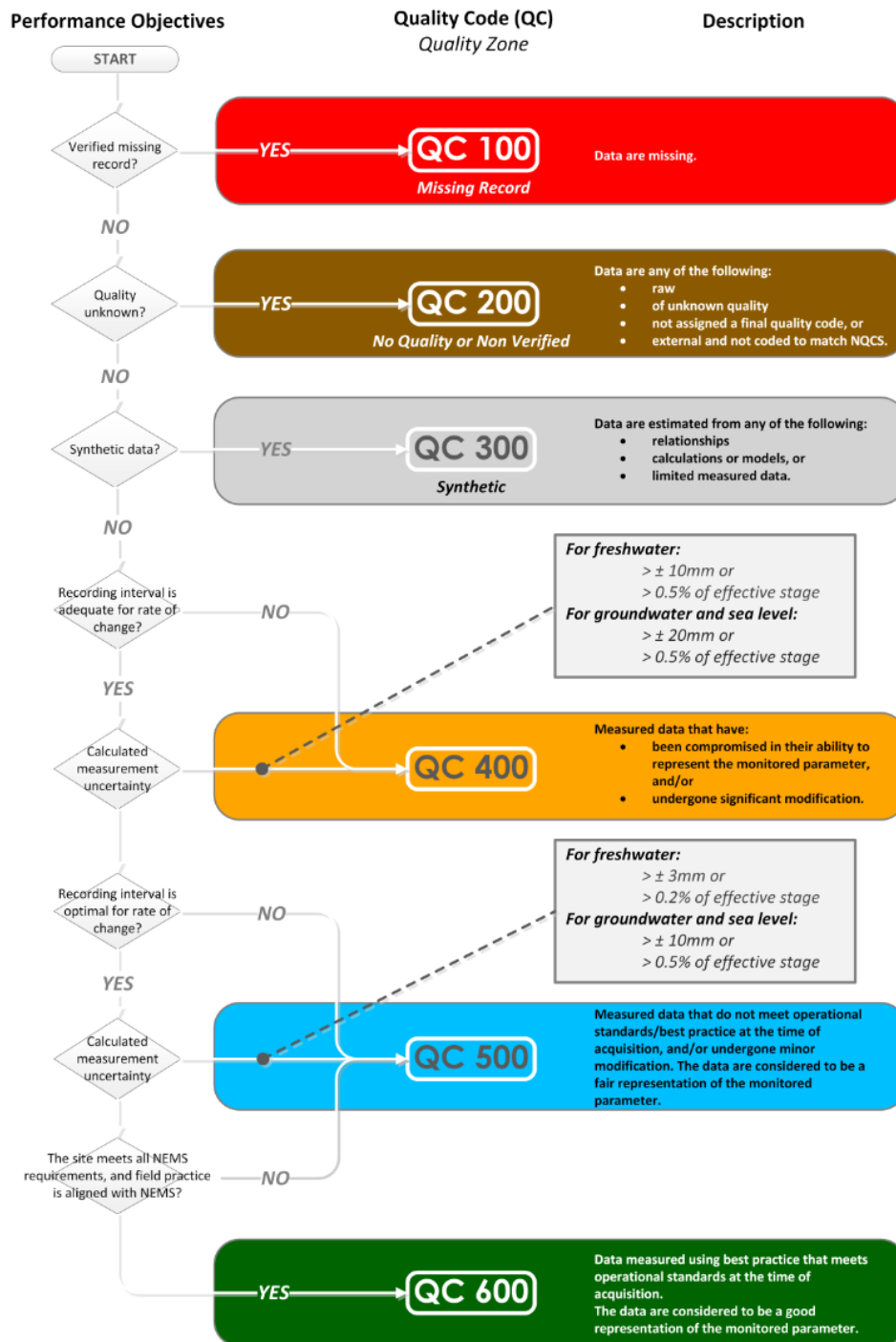
The aim of this section is to document the quality analysis process for sea-level records. This analysis draws on recommendations from the University of Hawaii Sea Level Center (UHSLC) (Kilonsky et al. 1991) and takes some of the processing methodology and architecture from the MyOcean project (Perez-Gomez et al. 2010) and the Global Sea Level Observing System (GLOSS) programme. A suggested list of actions at each step is documented, along with code written to accomplish those actions.

MyOcean is an online platform that provides access to real-time ocean-related data and information, such as sea level, sea surface temperature, currents, waves, tides, and more. While MyOcean does not provide the same level of quality assurance as national standards, it does provide access to a range of data that can be used to inform decisions about the ocean environment.

Global Sea Level Observing System (GLOSS) is a voluntary, international network of sea level monitoring stations that measure sea level and related variables. GLOSS provides access to a range of data about sea level, as well as data about sea surface temperature, currents, waves, and tides. GLOSS also assists agencies to achieve data quality by providing guidance about how the accuracy of data may be verified, and suggesting processes that help ensure that data are properly documented and stored.

The NEMS requirements differ from that of the global standards outlined by GLOSS and MyOcean – neither GLOSS nor MyOcean require a quality assurance code. NEMS has a recommended sampling frequency of 1-minute for water level data (Baddock 2019). Whereas prior to 2004 GLOSS suggests a 5-minute sampling interval. Raw data are normally registered at time intervals between 1-minute and 1 hour. Before 2004 waves, seiches or tsunamis were not the main priority for GLOSS stations, as the focus was then on tides and mean sea levels. For this reason, the most common sampling for stations before then was 5, 6, 10 or 15 minutes. However, now the GLOSS recommendation aligns with NEMS to use a lower sampling (at 1 min or less) in those regions where higher frequency oscillations such as infragravity waves, meteotsunamis, seiches or tsunamis are to be detected. Nonetheless, there is still no requirement that the data be QA'd at 1-minute resolution. The recommended approach still allows that the data can be sub-sampled to a coarser temporal resolution (for example, 10 minutes) and QA'd at that level. This is where our recommendation based on NEMS differs. We recommend all data be QA'd at 1-minute intervals if available.

In addition, NEMS requires that the data must be quality coded in accordance with the National Quality Coding Schema. The schema permits valid comparisons within and across multiple data series. NEMS supply the flow chart shown in Figure D-1 to illustrate how quality codes should be assigned to water level records.



**Figure D-1: National Environmental Monitoring Standards (NEMS) quality code schema flow chart.** Schema flow chart data requirements for assigning a quality code (QC). Flow chart from (Baddock 2019).

### E.3 - Data types

Data associated with water level monitoring can be split into two main types:

- Metadata.
- Water level measurements.



## E.4 - Metadata and comments

In accordance with NEMS, “metadata” describe the type of data, where it has been measured, length of the record, sampling interval and information relevant to the data being recorded at the site.

NEMS recommend metadata comments are captured to explain unusual features or events in the record of which users of the data should be aware. In addition, routine comments are required for key site information. The NEMS document recommends that this metadata should include, but not be limited to the information outlined in Table D-1.

**Table D-1: Metadata requirements for National Environmental Monitoring Standards (NEMS) data processing.**

Metadata	NEMS suggested details	Raglan sea level recorder example												
Site details	<ul style="list-style-type: none"> <li>– site purpose</li> <li>– recording agency</li> <li>– site location in coordinate system supported by Land Information NZ<sup>4</sup></li> <li>– site name and past and present aliases</li> <li>– names and/or indices of relevant environmental features (river, lake, coast)</li> </ul>	<ul style="list-style-type: none"> <li>– Sea level gauge</li> <li>– Waikato Regional Council</li> <li>– latitude: -37.794521</li> <li>– longitude: 174.880279</li> <li>– 857-Raglan Harbour</li> <li>– 23 Raglan Wharf</li> </ul>												
Site history details	start and end data of site record	– 01/07/2008 13:10:00 - present												
Sensor and recorder details including media	<ul style="list-style-type: none"> <li>– chart</li> <li>– tape</li> <li>– data logger</li> <li>– memory capacity</li> <li>– storage card, and</li> <li>– telemetry capability.</li> </ul>	– Bubbler 01/07/2008 13:10:00, Radar 06/11/2012 00:49:00												
Instrument relocation dates		– Reinstall after fire damage 04/11/2019												
Data capture and/or retrieval method	<ul style="list-style-type: none"> <li>– digitised</li> <li>– manual CSV import, or</li> <li>– telemetered</li> </ul>	– telemetered												
Calibration results		– Site survey date: 03/02/2021												
Information about	<ul style="list-style-type: none"> <li>– legal requirements</li> <li>– confidentiality agreements,</li> <li>– intellectual property, and</li> <li>– any other restrictions related to data access</li> </ul>	<p>“All environmental data is subject to the terms and conditions outline here:  <a href="http://waikatoregion.govt.nz/terms">http://waikatoregion.govt.nz/terms</a>”</p>												
Sampling interval		<table> <tr> <td>01/07/2008 13:05:00</td><td>5</td><td>mins</td></tr> <tr> <td>14/07/2008 15:54:00</td><td>1</td><td>mins</td></tr> <tr> <td>06/11/2012 00:49:00</td><td>5</td><td>mins</td></tr> <tr> <td>24/06/2021 08:46:00</td><td>1</td><td>mins</td></tr> </table>	01/07/2008 13:05:00	5	mins	14/07/2008 15:54:00	1	mins	06/11/2012 00:49:00	5	mins	24/06/2021 08:46:00	1	mins
01/07/2008 13:05:00	5	mins												
14/07/2008 15:54:00	1	mins												
06/11/2012 00:49:00	5	mins												
24/06/2021 08:46:00	1	mins												

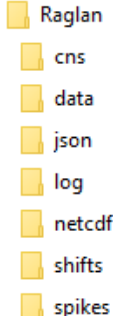
<sup>4</sup> Note: Latitude/longitude coordinates, must be expressed to a minimum of 6 decimal places.

## E.5 - Quality coding

GLOSS, SELENE and JASL are publicly available software tools suitable for processing sea level data. However, these software don't meet the requirements for data processing to NEMS standards – NEMS recommends that data be processed at 1-minute sampling intervals, contain metadata and have a quality code. None of these three software products provide all this functionality. To achieve the data processing steps to enable a user to QA the data to NEMS requirements, I have written Python modules that provide the required functionality. The Python modules outline in Table D-2 draw upon the methodologies from GLOSS, JASL and SELENE, but have been modified to satisfy the requirements of a NEMS. In particular:

- We adopt a similar metadata approach to SELENE, where site specific metadata is passed into the code via a JSON (JavaScript Object Notation) file.
- We use a similar running window filtering approach as used by GLOSS, JASL and SELENE – this allows the automatic identification data outliers.

**Table D-2: List of steps for carrying out the quality assurance data processing.**

Step	Code
1. Create a working folder ("Raglan"). This can be done by formatting and running the Python script <i>make_subdirectory_structure.py</i> or manually. Within the main working folder ("Raglan"), the site-specific harmonic constituents file needs to be placed in the "cns" folder, raw timeseries data ("data"), a metadata *.json file ("json"), output log and NetCDF files ("log", "netcdf"). Optionally, files which control the manual removal of spikes and datum shifts can be added.	<i>make_subdirectory_structure.py</i> 
2. main processing code (which calls the following scripts)	<i>sea_level_qa.py</i>
3. check for model time step and changes in timestep.	At present part of <i>sea_level_qa.py</i>
4. look for timing errors	<i>phase_shifts.py</i>
5. filter of raw sea level and NTR data	<i>qc_sealevel.py</i>
6. calculate non-tidal residual (NTR)	<i>cnstide.py, ut_solve.py</i>
7. gap fill missing data up to 24 hours	<i>backfill_data.py</i>
8. apply NEMS QA coding	<i>nems_qa_code.py</i>
9. write netCDF output	<i>nc_out.py</i>

**Step 1:** For each sea-level recorder the user needs to set-up data processing folders described in Table D-2. These folders can be generated manually or by modifying and running the Python script "*make\_subdirectory\_structure.py*". The raw sea level data (saved as \*.txt or \*.csv) is placed in the "data" folder, tidal harmonic constituents are put in the "cns" folder and site metadata is written as a \*.json file (explained in step 2) and placed in the "json" folder. The log and NetCDF folders are where the code writes the log file and saves output NetCDF files. The "shift" and "spike" folders are optional and are used if datum offsets are required or when additional spike removal is required. Note: the radar style water level sensors often require a manual/visual inspection and some additional de-spiking.

**Step 2:** create a metadata \*.json file. NEMS suggests that metadata must include but is not limited to the items outlined in Table D-1. Here we have chosen to store the metadata in a JSON file. JSON files are commonly used in web development for transferring data between the server and client-side applications and are supported by many programming languages and platforms. JSON is a lightweight data interchange format that is easy for humans to read and write, and easy for machines to parse and generate. In the JSON file displayed in Figure D-2, data is represented using two basic structures: objects and arrays (Table D-3).

**Table D-3: JSON file structure and formatting.**

JSON Structures	Format
Objects	<p>Objects are enclosed in curly braces “{ }” and contain a set of key-value pairs, where the keys are strings and the values can be strings, numbers, booleans, null, other objects, or arrays. In</p> <pre> {   "bad_data_fn": "2022-12-19 17:10:00",   "bad_data_st": "2022-09-06 09:10:00",   "data_capture": "telemetered",   "easting": 1765551,   "Gauge zero": "Moturiki Vertical Datum 1953 (MVD-53)",   "latitude": -37.794521,   "longitude": 174.880279,   "legal information": "All environmental data is subject to the terms and conditions outline here: <a href="http://waikatoregion.gov">http://waikatoregion.gov</a>",   "maxlevel": 3.000,   "maxsurge": 1.500,   "minlevel": -2.500,   "minsurge": -1.500,   "name": "Raglan",   "northing": 5815318,   "qc_level_nsigma": 4,   "qc_level_splinedegree": 2,   "qc_level_winsize": 200,   "qc_stucklimit": 10,   "qc_surge_nsigma": 5,   "qc_surge_splinedegree": 3,   "qc_surge_winsize": 3600,   "sensor": "Bubbler 01/07/2008 13:10:00, Radar 06/11/2012 00:49:00",   "sensor accuracy (mm)": [     {       "Dates": "01/07/2008 13:10:00",       "accuracy": 3     },     {       "Dates": "06/11/2012 00:49:00",       "accuracy": 3     },     {       "Dates": "04/11/2019 17:00:00",       "accuracy": 3     }   ],   "shortname": "Rag",   "Site": "857_Raglan_Harbour",   "Site Number": "857_23",   "Station": "23_Raglan_Wharf",   "time_step": [     {       "Dates": "01/07/2008 13:05:00",       "step": 5     },     {       "Dates": "14/07/2008 15:54:00",       "step": 1     },     {       "Dates": "06/11/2012 00:49:00",       "step": 5     },     {       "Dates": "24/06/2021 08:46:00",       "step": 1     }   ] }</pre>

Figure D-2 the Object has key-value pairs, where the keys are “name”, “Gauge zero”, “sensor accuracy”, “shortname”, “time\_step”, “latitude”, “longitude” etc. The values can be a string (name and gauge zero), a number (sensor accuracy), a Boolean (true, false).

JSON Structures	Format
-----------------	--------

## Arrays

Arrays are enclosed in square brackets “[ ]” and contain an ordered list of values, which can be any valid JSON data type. In

```

{
  "bad_data_fn": "2022-12-19 17:10:00",
  "bad_data_st": "2022-09-06 09:10:00",
  "data_capture": "telemetered",
  "easting": 1765551,
  "Gauge zero": "Moturiki Vertical Datum 1953 (MVD-53)",
  "latitude": -37.794521,
  "longitude": 174.880279,
  "legal information": "All environmental data is subject to the terms and conditions outline here: http://waikatoregion.gov",
  "maxlevel": 3.000,
  "maxsurge": 1.500,
  "minlevel": -2.500,
  "minsurge": -1.500,
  "name": "Raglan",
  "northing": 5815318,
  "qc_level_nsigma": 4,
  "qc_level_splinedegree": 2,
  "qc_level_winsize": 200,
  "qc_stucklimit": 10,
  "qc_surge_nsigma": 5,
  "qc_surge_splinedegree": 3,
  "qc_surge_winsize": 3600,
  "sensor": "Bubbler 01/07/2008 13:10:00, Radar 06/11/2012 00:49:00",
  "sensor accuracy (mm)": [
    {
      "Dates": "01/07/2008 13:10:00",
      "accuracy": 3
    },
    {
      "Dates": "06/11/2012 00:49:00",
      "accuracy": 3
    },
    {
      "Dates": "04/11/2019 17:00:00",
      "accuracy": 3
    }
  ],
  "shortname": "Rag",
  "Site": "857_Raglan_Harbour",
  "Site Number": "857_23",
  "Station": "23_Raglan_Wharf",
  "time_step": [
    {
      "Dates": "01/07/2008 13:05:00",
      "step": 5
    },
    {
      "Dates": "14/07/2008 15:54:00",
      "step": 1
    },
    {
      "Dates": "06/11/2012 00:49:00",
      "step": 5
    },
    {
      "Dates": "24/06/2021 08:46:00",
      "step": 1
    }
  ]
}

```

Figure D-2 the Array example would be “time\_step” and “sensor accuracy (mm)”.

```

{
  "bad_data_fn": "2022-12-19 17:10:00",
  "bad_data_st": "2022-09-06 09:10:00",
  "data_capture": "telemetered",
  "easting": 1765551,
  "Gauge zero": "Moturiki Vertical Datum 1953 (MVD-53)",
  "latitude": -37.794521,
  "longitude": 174.880279,
  "legal information": "All environmental data is subject to the terms and conditions outline here: http://waikatoregion.govt.nz/terms",
  "maxlevel": 3.000,
  "maxsurge": 1.500,
  "minlevel": -2.500,
  "minsurge": -1.500,
  "name": "Raglan",
  "northing": 5815318,
  "qc_level_nsigma": 4,
  "qc_level_splinedegree": 2,
  "qc_level_winsize": 200,
  "qc_stucklimit": 10,
  "qc_surge_nsigma": 5,
  "qc_surge_splinedegree": 3,
  "qc_surge_winsize": 3600,
  "sensor": "Bubbler 01/07/2008 13:10:00, Radar 06/11/2012 00:49:00",
  "sensor accuracy (mm)": [
    {
      "Dates": "01/07/2008 13:10:00",
      "accuracy": 3
    },
    {
      "Dates": "06/11/2012 00:49:00",
      "accuracy": 3
    },
    {
      "Dates": "04/11/2019 17:00:00",
      "accuracy": 3
    }
  ],
  "shortname": "Rag",
  "Site": "857_Raglan_Harbour",
  "Site Number": "857_23",
  "Station": "23_Raglan_Wharf",
  "time_step": [
    {
      "Dates": "01/07/2008 13:05:00",
      "step": 5
    },
    {
      "Dates": "14/07/2008 15:54:00",
      "step": 1
    },
    {
      "Dates": "06/11/2012 00:49:00",
      "step": 5
    },
    {
      "Dates": "24/06/2021 08:46:00",
      "step": 1
    }
  ]
}

```

**Figure D-2: Site specific metadata contained in the \*.json file.** Metadata for Raglan used by the sea level quality assurance Python code.

**Step 3:** Check that data is collected at 1-minute intervals (recommended by NEMS for tidal data). If the sampling interval is less than 1-minute, cannot attain a QC value of 500, regardless of data quality (Figure D-1). The data is resampled to 1-minute intervals this is required because the variable as “qc\_level\_winsize” and “stuck\_limit” (discussed in Step 6) are parameterised to around the NEMS 1-minute requirement. We found that it was difficult to auto QA data when the data was collected at greater than 1-minute resolutions, because it was difficult to clearly identify as extreme events such as infragravity waves, meteotsunamis, seiches or tsunamis from outlier values.

**Step 4:** Check for repeated or overlapping dates and remove repeated data.

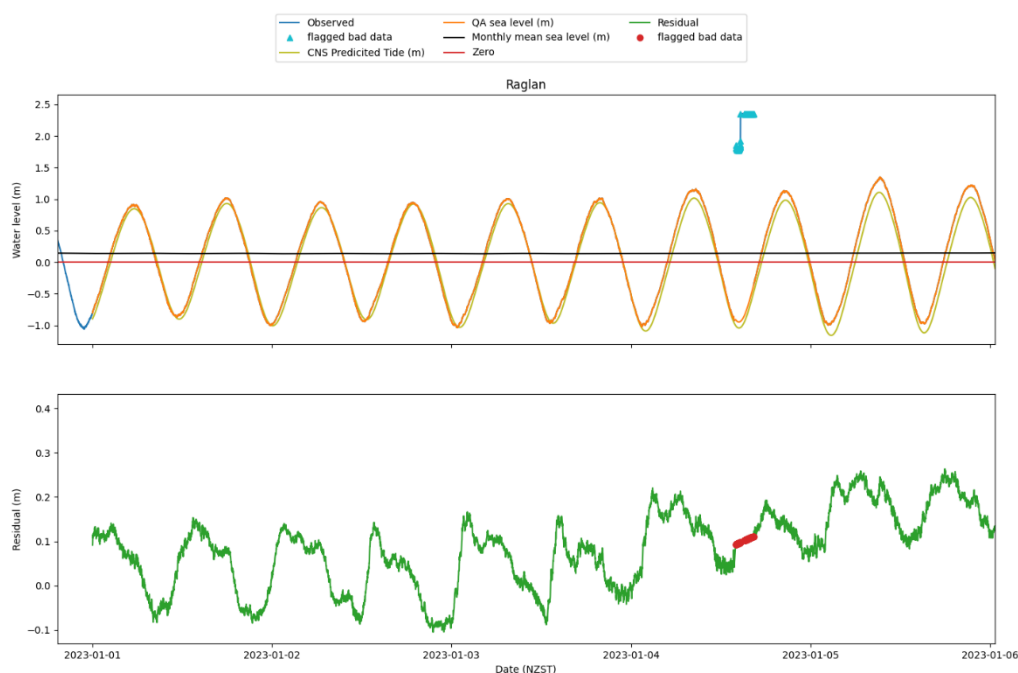
**Step 5:** Check for and flag out-of-range values (based on predefined upper and lower limits, dependent on the station and included in the metadata for each station).

**Step 6:** Initial raw data spike filtering and flagging. The algorithm for detection of spikes is the main component of the qc code: it is based on the fit of a spline to a moving window. This running window filter draws filtering parameters from the predefined settings stored in the site-specific \*.json file. These filtering variables include the size of the window to fit the spline, the degree of the spline, the number of standard deviations used to identify outliers, and the number of individual counts used to identify a “stuck value” (Figure D-4, Figure D-5). This is a quality flag value used when there is no change in the magnitude of sea level after a defined number of time steps. The number of similar consecutive data points allowed depends on the location of the gauge, the point within the tidal cycle and the sampling interval of the data. Figure D-3 illustrate an example of stuck data from the Raglan sea-level record where we use a stuck limit of 10 minutes (“qc\_stucklimit”).



**Figure D-3: Stuck values automatically identified between 31/08/2008 and 02/09/2008 in the Raglan raw sea level data.** Top pane: yellow line is the predicted tide, orange line QA sea level data, blue dots show the “stuck” raw sea level data. Second pane: green line shows the non-tidal residual (NTR). Third pane: grey line shows the NEMS values. Bottom pane: pink line representing the difference/change in the NTR.





**Figure D-4: Outlier values automatically identified between 04/01/2023 and 05/01/2023 in the Raglan raw sea level record.** Top pane: yellow line is the predicted tide, orange line QA sea level data, blue dots show the “stuck” raw sea level data. Second pane: green line shows the non-tidal residual (NTR), red dots show the data removed from the NTR.

The filter adopts the Python NumPy modules polyfit and polyval. The polyfit is a function that fits a polynomial of a specified degree to a set of data using a least-squares approach. It takes three arguments as input:

1. x: a 1D array-like object containing the independent variable values.
2. y: a 1D array-like object containing the dependent variable values.
3. Degree of the spline: an integer specifying the degree of the polynomial to fit.

The function returns an array containing the coefficients of the polynomial that best fits the data in a least-squares sense.

The degree of the spline (usually 2 or 3) “qc\_level\_splinedegree” and the size of the window “qc\_level\_winsize” can be selected and determined depending on the characteristics of the tide, the data sampling, etc. It is configured in \*.json. The algorithm flags as spikes the values that differ more than  $n$  standard deviations from the fit “qc\_level\_nsigma” (usually larger than 3, this can also be defined in the \*.json file). When the sampling frequency is greater than 1-minute we increase the value for the variables “qc\_level\_splinedegree”, “qc\_level\_winsize” and “qc\_level\_nsigma” are increased to not incorrectly flag and remove data.

**Step 7:** Undertake a harmonic analysis using the U-Tide Python module and calculate the non-tidal residual (NTR) (Codiga, D.L 2011a). Forecasting the tides means that we can de-tide the record. De-tiding is the process of calculating the NTR ( $\text{NTR} = \text{measured sea level} - \text{predicted sea level}$ ). This is a useful diagnostic tool for identifying errors in the data. Note: at present the processing script can be switched to either use a harmonic constituent file, or to calculate harmonic constituent by undertaking a harmonic fit from the raw water level data. The switching process is automatic: if a

\*.cns file is present in the folder, the script automatically switches to generate tides from the \*.cns file. In the instance where there is either less than 12-months of data or the data record is very long, we recommend using the option of the \*.cns file approach. This is because with short records there isn't enough data to produce a reliable tidal harmonic analysis and with very long records the code becomes computationally very expensive and slow.

**Step 8:** Inspect and undertake manual spike removal. Here we difference the NTR to check for spikes which represent unrealistically rapid changes in the measured sea-level data. The difference in the NTR exaggerates these changes in water level and makes it easier to identify them (see Figure D-5). When an unrealistic data spike is identified, the date of the spike can be added to the \*.cns file which is placed in the optional “spike” folder; when an unrealistic change in sea level is identified and an offset in sea-level is required (see Figure D-6), the date of the shift can be added to the “shifts” folder which exists in the main directory.



**Figure D-5: Spike in Tararu sea-level record which was not detected by the running window filter.** Top Pane: Blue raw sea-level data, yellow predicted tide from CNS harmonic fit, orange processed QA sea level. Second Pane: Green non-tidal residual (NTR). Third Pane: grey NEMS QA code. Bottom Pane: Pink, difference in NTR used to identify data spikes.



**Figure D-6: Datum offset issue identified in the Kawhia sea-level record.** Top Pane: Blue raw sea-level data, yellow predicted tide from CNS harmonic fit, orange processed QA sea level. Second Pane: Green non-tidal residual (NTR). Third Pane: grey NEMS QA code. Bottom Pane: Pink, difference in NTR used to identify data spikes.

**Step 9:** Having identified large spikes, these should be either deleted, or interpolated over, and the changes documented in the log file. The procedure for filling gaps is to replace the missing data flags (e.g., NaN) with quality-controlled data from an auxiliary sea level gauge that is linked to the same datum. Typically, in New Zealand redundant sensors which generate auxiliary data suitable for this purpose are not available. An alternate method is linear interpolation via the predicted-tide method. The predicted-tide method for filling gaps requires yearly files of observed and corresponding predicted data (Godin 1973). To perform linear interpolation, high-quality annualised tidal-harmonic prediction is required. The module is configured to allow the user to switch between a harmonic fit to the raw data or reading and reconstructing tides from a pre-made constituents file which can be placed in the “cns” folder. Note: undertaking a harmonic fit to the raw data requires at least 1-year of data and is computationally demanding and time consuming. The predicted tides are shifted in time to match the timing characteristics of the observed series. The residuals between the predicted tides and the observed data are calculated. Then, a linear interpolation between the end points of the gap in the (NTR) residual series is performed, and each interpolation constant is added to the shifted (predicted) tides over the span of the gap. UHSLC and GLOSS recommend using this procedure for gaps less than or equal to 24 hours, and we have adopted this convention. The Python code *backfill\_data.py* is used to fill gaps using the predicted tide method.

**Step 10:** The Python code *nems\_qa\_code.py* is to assign the quality codes (QC). The methodology used in *nems\_qa\_code.py* to apply NEMS QC to processed sea-level data are outlined below:

- Raw data with no data jumps: **QC=600** unless collected at greater than 1-minute intervals and with an accuracy of less than 10 mm. Note: currently NIWA does not quality code data to a QC=600 standard. This is because QC=600 requires an

assessment of the operational standards of a sea level gauge. This requires instrument installation, calibration, data storage and site maintenance assessments, which are beyond the scope of this project.

- Gaps up to 5 minutes, data contains no data jumps: **QC=500** where a simple linear fit to the NTR is used to fill missing data. We find that gaps of this magnitude don't significantly impact the longer term MSLO calculations.
- Where gaps are greater than 5 minutes, but less than 10-minutes: **QC=400**.
- Gaps that are greater than 10 minutes but less than 24 hours: **QC=300**. We use tidal fit approach, which uses the mean from the peaks and troughs 5 days either of the missing data.
- Where uncertain datum shifts are applied or if data has required a trend to be removed: **QC=200**.
- Gaps greater than 24 hours: **QC=100**.

**Step 11:** The final step in the analysis is to write the processed data to NetCDF files. NetCDF (Network Common Data Form) is a data format that is commonly used in the scientific community for storing and sharing large, multidimensional datasets. Some of the benefits of using NetCDF include:

- Portability: NetCDF files can be read and written on many different computing platforms, making it easy to share data across different systems.
- Self-Describing: NetCDF files contain metadata that describes the contents of the file, including the structure of the data and the units used, making it easier to understand and work with the data. NetCDF metadata also have global attributes that provide information about the data as a whole, such as the creation date, author, and project. These global attributes can be expanded to contain the metadata described in Table D-1.
- Efficiency: NetCDF files are designed to be efficient for both reading and writing large datasets, which is important for many scientific applications.
- Interoperability: NetCDF is supported by a wide range of software tools and programming languages, making it easy to work with data stored in this format.
- Scalability: NetCDF supports large, multidimensional datasets and can handle data of varying sizes and types.
- Compression: NetCDF supports compression of data, which can help reduce file size and make it easier to store and transfer large datasets.

Overall, NetCDF is a versatile and powerful format that can be used for a wide range of scientific applications, including climate modelling, oceanography, and meteorology. Its benefits make it a popular choice for storing and sharing large, complex datasets in the scientific community.